Progress in Energy and Combustion Science 104 (2024) 101174

Contents lists available at ScienceDirect

Progress in Energy and Combustion Science

journal homepage: www.elsevier.com/locate/pecs

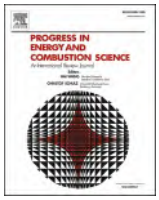

Premixed flame ignition: Theoretical development

Dehai Yu [a,b], Zheng Chen [a,*]

[a] SKLTCS, HEDPS, CAPT, Department of Aeronautics and Astronautics, College of Engineering, Peking University, Beijing, 100871, China
[b] State Key Laboratory of High Temperature Gas Dynamics, Institute of Mechanics, Chinese Academy of Sciences, Beijing, 100190, China

ARTICLE INFO

Handling editor: Hai Wang

Keywords:
Ignition
Premixed flame
Minimum ignition energy
Flame propagation

ABSTRACT

Premixed flame ignition is a fundamental issue in combustion. A basic understanding of this phenomenon is crucial for fire safety control and for the development of advanced combustion engines. Significant efforts have been devoted to understanding the mechanisms of ignition and determining critical ignition conditions, such as critical flame radius, minimum ignition energy, and minimum ignition power, which have remained challenging research topics for centuries. This review provides an in-depth investigation of the forced-ignition of laminar premixed flames in a quiescent flammable mixture, with emphasis on theoretical developments, particularly those based on activation energy analysis. First, the fundamental concepts are overviewed, including spark ignition, characteristic time scales, and critical ignition conditions. Then, the chronological development of premixed flame ignition theories is discussed, including homogeneous explosion, thermal ignition theory, flame ball theory, quasi-steady ignition theory, and, more importantly, transient ignition theory. Premixed flame ignition consists of three stages: flame kernel formation, flame kernel expansion, and transition to a self-sustaining flame. These stages are profoundly affected by the coupling of positive stretch with preferential diffusion, characterized by the Lewis number. Specifically, positive stretch makes the expanding ignition kernel weaker at larger Lewis numbers, consequently increasing the critical ignition radius and MIE. The premixed flame ignition process is dominated by flame propagation dynamics. Both quasi-steady and transient ignition theories demonstrate that the critical flame radius for premixed ignition differs from either flame thickness (by thermal ignition theory) or flame ball radius (by flame ball theory). Particularly, the transient ignition theory appropriately acknowledges the "memory effect" of external heating, offering the most accurate description of the evolution of the ignition kernel and the most sensible evaluation of minimum ignition energy. In addition, the effects of transport and chain-branching reactions of radicals, finite droplet vaporization, and repetitive heating pulses on premixed flame ignition are discussed. Finally, a summary of major advances is provided, along with comments on the applications of premixed flame ignition theory in ignition enhancement. Suggested directions for future research are presented.

1. Introduction

1.1. Background

Ignition is one of the most fundamental and important problems in combustion [1–3]. Understanding ignition is important not only for fundamental combustion research but also for fire safety control and the development of advanced combustion engines. The fundamental mechanisms of ignition and the determination of critical ignition conditions, such as the critical flame radius and minimum ignition energy (MIE), have been the most challenging research topics over the last hundred years. Therefore, tremendous efforts, including experimental investigations (e.g., Refs. [4–6]), theoretical studies (e.g., Refs. [7–9]) and numerical simulations (e.g., Refs. [10–13]) have been devoted to ignition.

Ignition in combustion science refers to the progress by which a fuel-air mixture is brought to conditions that allow for spontaneous combustion without continuous external energy input [14]. This critical phase transition is characterized by the fuel's reaction rate with an oxidizer, which, upon reaching a certain energy threshold, leads to self-sustaining combustion. In favorable conditions with high temperature and pressure, ignition may occur spontaneously, known as auto-ignition. Nevertheless, in order to precisely control combustion in engines, the ignition in practical combustion facilities is in general induced by energy deposition from external sources, which is termed as

* Corresponding author.
E-mail address: cz@pku.edu.cn (Z. Chen).

https://doi.org/10.1016/j.pecs.2024.101174
Received 5 July 2023; Received in revised form 25 June 2024; Accepted 26 June 2024
Available online 6 July 2024

Nomenclature

Alphabetic symbols

a_{acoustic}	Acoustic speed
B	Collision frequency factor of global reaction
c_p	Heat capacity of combustible mixture at constant pressure
D	Mass diffusivity
d_L	Thickness of laminar premixed flame
d_L^0	Thickness of adiabatic planar premixed flame
d_D	Induction length of normal detonation
d_{spark}	Gap distance between two electrodes
E_{burnt}	Internal energy within ignition kernel
$E_{\text{detonation}}$	detonation initiation energy
E_{flame}	Ignition energy of laminar premixed flame
E_{ignition}	Energy deposition from ignition source
E_{min}	Minimum ignition energy by transient ignition theory
E'_{min}	Minimum ignition energy by quasi-steady ignition theory
E_{release}	Energy release from ignition source
E_{unburnt}	Internal energy outside ignition kernel
h	Heat transfer coefficient
k_B	Rate coefficient of chain-branching reaction
k_R	Rate coefficient of recombination reaction
L	Normalized heat loss of flame ball
$\overrightarrow{n}$	Normal direction to the flame front
n_p	Pulse number for multi-stage central heating
p_e	Uniform pressure in hot pocket due to energy deposition
p_N	Pressure behind shock wave
p_{kernel}	Ignition kernel pressure
q_c	Chemical heat release per unit mass of reactant
$Q_{\text{ca-diss}}$	Cathode-anode fall dissipation of discharge energy
$Q_{\text{conduction}}$	Conductive dissipation of discharge energy due to thermal boundary layer
Q_{chemical}	Minimum power for chemical runaway
$Q_{cr,\text{runaway}}$	Critical heating power for thermal runaway
$Q_{cr,\text{front}}$	Critical heating power for reaction front formation
$Q_{cr,\text{kernel}}$	Critical heating power for flame kernel formation
Q_m	Heating power of external source
$Q_{m,cr}$	Critical heating power
Q_{min}	Minimum heating power for premixed flame ignition
$Q_{\text{radiation}}$	Radiation loss of discharge energy
r	Radial coordinate
r_e	Edge of the hot pocket due to energy deposition
r_N	Radial distance of shock wave
r_s	Radial coordinate relative to the ignition kernel front
r_v	Vaporization front
R	Dimensional radial distance of the ignition kernel/ detonation front from the origin
R_0	Domain of external heating during flame kernel formation
R_{cr}	Critical radius of ignition kernel
R_{kernel}	Ignition kernel radius
R_Z	Radius of Zel'dovich flame ball
$R_{Z,p}$	Perturbation of flame ball radius
S_L^0	Propagation speed of adiabatic planar premixed flame
t	Dimensional time
t_0	Time of external heating during flame kernel formation
t_{arc}	Characteristic time for arc stage during spark discharge
$t_{\text{blastwave}}$	Characteristic time for blast wave induced by spark discharge
$t_{\text{breakdown}}$	Formative time lag for breakdown
t_{cr}	Instant of ignition kernel arriving at the critical state
t_{chemical}	Characteristic time scale for chemical reaction
$t_{\text{conduction}}$	Characteristic time scale for conduction
$t_{\text{consumption}}$	Delay time for reactant consumption at heating center
$t_{\text{convection}}$	Characteristic time for convective transport during spark discharge
$t_{\text{deformation}}$	Characteristic time for flame kernel deformation during spark discharge
$t_{\text{diffusion}}$	Characteristic time for mass diffusion during spark discharge
$t_{\text{evolution}}$	Characteristic time during flame kernel evolution
$t_{\text{explosion}}$	Delay time for thermal runaway
t_{front}	Delay time for establishing reaction front at heating center
t_{glow}	Characteristic time for glow stage during spark discharge
t_{ignition}	Delay time for autoignition
$t_{\text{ignition},0}$	Delay time for adiabatic autoignition
t_{kernel}	Delay time for formation of ignition kernel
$t_{\text{propagation}}$	Delay time for reaction front propagation towards the edge of heating domain
$t_{\text{radiation}}$	Characteristic time scale for radiation
t_s	Scaled time for transient evolution of ignition kernel
t_{spark}	Duration of spark discharge
T_a	Activation temperature of global
$T_{a,B}$	Activation temperature for chain-branching reaction
T_{ad}	Adiabatic temperature of laminar premixed flame
T_b^0	Initial temperature of the ignition kernel
T_{center}	Temperature at the heating center
$T_{\text{crossover}}$	Crossover temperature for chain-branching reaction
T_f	Temperature at flame front
T_{FK}	Temperature at the edge of Frank-Kamenetskii region
T_H	Critical ignition temperature of homogeneous explosion
T_{kernel}	Ignition kernel temperature
T_p	Temperature perturbation of flame ball
T_u	Temperature of unburnt mixture
T_v	Reference temperature for vaporization
u_N	Propagation speed of shock wave
U	Propagation speed of ignition kernel front
U_{cr}	Propagation speed of ignition kernel front at the critical state
v_N	Moving speed of fluid behind shock wave
Y_F	Mass fraction of the deficient reactant in combustible mixture
$Y_{F,\text{center}}$	Mass fraction of the deficient reactant at the heating center
Y_F^o	Initial mass fraction of the deficient reactant
Y_Z	Mass fraction of radical species
Y_{FV}	Mass fraction of fuel vapor
Y_{FD}	Mass fraction of droplet

Greek letters

α	Thermal conductivity of combustion mixture
δ_D	Initial droplet load
φ	Global equivalence ratio
λ_{tm}	Intermittent factor of adjacent heating pulse
ρ_0	Density of the unburnt mixture
ρ_N	Fluid density behind shock wave
σ	Expansion ratio
σ_s	Scaled radial coordinate for transient evolution of ignition kernel
θ	Temperature perturbation
ω	Rate of chemical reaction
ω_v	Rate of vaporization
ϖ	Burning rate of droplet
Ω	Complex frequency of flame ball radius perturbation
χ	Stretched coordinate representing flame structure
ξ_{uT}	Transformed coordinate for temperature in the unburnt region
ξ_{uc}	Transformed coordinate for concentration in the unburnt region
ξ_{bT}	Transformed coordinate for temperature in the burnt

region

Nondimensional parameters

Ar	Arrhenius number
Ar_B	Arrhenius number for chain-branching reaction
Da	Damköhler number
Kn	Kndusen number
Le	Lewis number of combustible mixture
Le_F	Lewis number of fuel
Le_Z	Lewis number of radical
Ze	Zel'dovich number
Ze_B	Zel'dovich number for chain-branching reaction
Δ	modified Damköhler number

Acronyms and abbreviations

DDT	Deflagration to detonation transition
ICE	Internal combustion engine
CCV	Cycle-to-cycle variation
PCI	Pre-chamber ignition
SWACER	Shock wave amplification by coherent energy release
DE	Discharge energy
FK	Frank-Kamenetskii region

Subscripts

0	Initial state of combustible mixture
u	Unburnt state
$+$	Unburnt region separated by the ignition kernel
$-$	Burnt region separated by the ignition kernel

Overheads

$\sim$	Nondimensional quantities for ignition kernel propagation
$\wedge$	Nondimensional quantities for flame kernel formation
$\vee$	Nondimensional quantities for thermal wave propagation

forced-ignition. Differentiating between various ignition mechanisms is essential for implementing combustion processes in various applications, ranging from internal combustion engines to industrial furnaces.

In practical combustion devices, ignition is initiated by spark discharge. Spark ignition is widely applied in internal combustion engines (ICEs). Dale et al. [15] reviewed the progress on high-energy ignition systems with emphasis on the process of high-energy breakdown, the physicochemical properties of igniters, and the effects of exhaust gas recirculation in assisting ignition. Energy and environmental concerns impose increasingly stringent regulations on efficiency improvement and emission control. To increase thermal efficiency and reduce NOx formation, advanced ICEs tend to operate at ultra-lean conditions [16–19]. Due to lower combustion temperatures than that at the stoichiometric condition, the heat transfer loss at ultra-lean conditions is greatly alleviated [6,20] and thereby the thermal efficiency increases. Besides, the combustion chamber of the engine can operate at higher compression ratios under fuel-lean conditions, which further improves the thermal efficiency [21,22]. However, as approaching the fuel-lean operation limit, misfire and partial burning might cause cycle-to-cycle variation (CCV), which affects the engine performance adversely [16,23]. Suitable forced-ignition systems must be implemented to ensure reliable ignition in such limiting situations. For example, the Pre-Chamber Ignition (PCI) strategy has been developed [6,20,24–26]. The combustible mixture in the pre-chamber is first ignited by spark discharge, issuing hot turbulent jets into the main chamber through the small holes and inducing ignition at multiple locations in the homogeneous fuel-lean mixture. The turbulent jets from the pre-chamber also enhance the turbulence and, thereby, the burning rate in the main chamber. Therefore, the PCI strategy exhibits superior performance for forced-ignition in extremely fuel-lean situations.

Ignition also plays a crucial role in air-breathing aviation propulsion systems. The relight of an aircraft gas-turbine at high altitudes is a significant issue. Modern civilian aircrafts cruise at high altitude (~9 km), where the combustion chambers receive inflow at relative low temperature (~200 K) and pressure (~0.4 atm) [27,28]. Under such conditions, a sufficient amount of ignition energy must be provided in order to achieve reliable initiation of an ignition kernel. Otherwise, relight may fail due to the decrease in fuel vapor pressure and flow rate [3,29]. For hypersonic flight, the aircraft is usually driven by the air-breathing scramjet, whose operation requires stable and reliable combustion at high-speed flow conditions [30–34]. An oblique shock wave forms at the leading edge of the inlet, which increases the volumetric internal energy of the inflow into the combustion chamber. The resident time of both injected fuel and mainstream airflow is exceedingly short. Moreover, the high speed inflow conditions in the combustion chamber cause severe heat loss, jeopardizing the survival of the ignition kernel [35]. Consequently, it is challenging to achieve successful ignition in scramjet engines [36]. In addition, the intensive flow stretch effect causes strong deformation of the ignition kernel, which brings great difficulty in its transition to a self-sustained flame [8,37]. Therefore, robust forced-ignition systems must be equipped in order to achieve successful ignition and stable combustion, which provide reliable thrust over a broad range of flight conditions [33,34].

Fire accidents are one of the primary threats to human lives and social properties [38,39]. Recently, fire safety issues occurring in industry (e.g., coal mine explosion [40] and ignition by mechanical spark [41]), transportation (e.g., traffic accident [42] and battery fires [43,44]) and the environment (e.g., urban and forest fires [45,46]) have drawn increasing attention. Fires in urban and wild spaces are usually initiated by unexpected ignition [47]. For example, spot ignition of a combustible mixture or material by hot particles is one of the important routes leading to urban and wild spot fires [47]. Besides, unexpected ignition is one of the prime concerns for spacecraft fire safety issues and for inhabited space exploration [48]. Understanding ignition mechanisms and critical ignition conditions is of pivotal importance for fire control and safety management [49,50].

Fundamentally, ignition is characterized by the onset of thermal runaway, followed by three sequential stages [2,3,51]: (1) creation of the ignition kernel, (2) expansion of reaction fronts, and (3) generation of a self-sustained premixed flame or stabilized non-premixed flame. It is well known that chemical reactions take place only when the fuel and oxidizer are mixed at the molecular level [14]. In practical combustion devices, stages (1) and (2) can proceed only at regions where fuel and oxidizer are mixed, which highlights the significance of ignition in premixed combustible mixtures. Non-premixed flame ignition refers to the emergence of a non-premixed flame, initiated from and stabilized by a local premixed region, where a triple flame structure forms [2,3]. Therefore, premixed flame ignition characterizes the birth of non-premixed flames. In this paper, we shall present a review on elementary understandings of premixed flame ignition with emphasis on the advancement of fundamental ignition theory. The ignition of non-premixed flame is not covered in this review.

1.2. Classification of ignition

The ignition phenomenon can be understood from different aspects, which are categorized as follows:

Thermal runaway. A premixed flame is initiated by the onset of thermal runaway. It can be comprehensively understood by analyzing the relationship between the heat release rate and temperature, or by an equivalent controlling parameter determining the rate of chemical reaction, i.e., the Damköhler number Da [14]. Plotting temperature (or

burning rate) versus *Da* results in either a regular, S-shaped folded curve or a stretched S-shaped unfolded curve, as first studied by Fendell [52] and Linán [53]. In general, the folded S-curve, consisting of three branches, corresponds to the situation of thermal runaway during premixed flame ignition. By increasing Da along the lower branch, the combustible mixture exhibits weakly reactive, nearly frozen states, which in physics, represents the accumulation of both heat and radicals. Beyond a critical Damköhler number Da_I, the lower branch transitions to the middle branch through a turning point, which represents the extrema, delineate regions of stable and unstable characteristics of the ignition process. At the critical value Da_I, the change in the reaction intensity, T_f, with respect to the change in the system's reactivity, *Da*, becomes infinite. The system consequently "jumps" to the upper branch for higher Damköhler numbers and faster reaction rates, and therefore represents all the intensely burning states the system can have. It is then reasonable to identify point I as the state of ignition and Da_I as the ignition Damköhler number. Physically, the existence of turning points implies that there exist states for which the chemical reaction rate cannot balance the heat transport rate in a steady state. Thus, for the lower branch, beyond Da_I, the chemical heat is generated so fast in the reaction zone that it cannot be transported away in a steady manner, i.e., thermal runaway occurs accordingly. The S-curve curve provides crucial insights into the stability and multiplicity of steady-state solutions in combustion systems.

Autoignition and forced-ignition. Depending on the presence of an external igniter, ignition can be classified into two types: autoignition and forced-ignition [14,54]. Autoignition, also known as self-ignition or spontaneous ignition, is caused by chain branching or thermal feedback in a homogeneous mixture without the input of either an external source of thermal energy or active radicals into the system. For homogeneous premixed reactants, autoignition occurs throughout the whole spatial domain after an induction time, known as the ignition delay time, t_{ignition}. The ignition delay time is one of the most prominent parameters in the autoignition process. It can be measured in a shock tube [55] or a rapid compression machine [56,57]. The ignition delay time is very sensitive to the temperature and pressure. At room temperature and atmospheric pressure, the ignition delay time for typical hydrocarbon fuels is exceedingly long, and thereby forced-ignition is required to achieve successful ignition. Unlike autoignition, forced-ignition is a result of electrical discharge (spark), heated surface, shock wave, or pilot flame, with the locally initiated flame front subsequently reaching a self-propagating state so that the ignition source can be removed without extinguishing the combustion process. In forced-ignition, the deposition of energy/radicals from the external igniter rapidly accelerates the reaction rate among the reactant mixture in the vicinity of the igniter, providing suitable conditions for autoignition to proceed. The external igniter creates local inhomogeneity in temperature or radical concentration in the reactant mixture, which induces loss of heat and active radicals via heat conduction and mass diffusion respectively. The result of the forced-ignition depends on the competition between the loss and production rates of both heat and radicals through the chemical process. Nevertheless, it is important to recognize that there is no definite boundary between autoignition and forced-ignition. This review aims to provide a conceptual framework that aids in understanding these complex processes rather than to assert rigid classification. The broad spectrum of ignition phenomena highlights the separate roles of spontaneous heat and radical generation due to chemical reactions and the deposition of heat and radicals from an external source in the ignition process. This review focuses on the forced-ignition of premixed flames, and thereby, the following ignition is equivalent to forced-ignition unless otherwise indicated.

Spark ignition and laser ignition. The primary effect of an external igniter is to accelerate autoignition nearby [58,59]. There are many types of external igniters. In spark ignition, thermal energy deposition from electric breakdown increases the local temperature of the reactant and induces local autoignition [60–68]. Sher et al. [66] presented a theoretical model that underlines the breakdown mechanisms and provides a parametric description of the breakdown phase. Unfortunately, a large amount of energy in spark ignition is utilized to heat the electrodes, resulting in relatively low ignition efficiency [69,70]. Plasma-assisted ignition, in particular the non-equilibrium plasma, helps to improve the ignition efficiency by forming a large number of active radicals due to collisions between high energy electrons and the reactant molecules [71,72]. The accumulation of active radicals accelerates the chain-branching reactions and thereby facilitates the chemical runaway process during autoignition [73,74]. Both spark and plasma ignition require the presence of an igniter, which is intrusive to the reactive flow field. Besides, the installation of the igniter is restricted by the geometric design of the combustor and cannot be freely placed to optimize the ignition performance. Because of non-intrusive nature, laser-induced ignition exhibits great potential in advanced propulsion systems [75–77]. Ronney [78] reviewed the fundamental process of laser-induced ignition and made a critical comparison between laser and conventional ignition. According to Phuoc [79,80], laser ignition can be divided into four categories, i.e., laser thermal ignition, non-resonant breakdown, resonant breakdown and photochemical ignition, depending on the wavelength and intensity of the laser source. Compared with conventional ignition, laser ignition has advantages in the ability to choose the ignition location(s) in the combustion chamber and the accurate timing control of ignition events [75,79,81]. In addition, it was found that laser ignition could expand the fuel-lean ignition limit and significantly shorten ignition time [82,83].

Ignition of premixed and non-premixed flames. There are mainly two types of flames: premixed and non-premixed flames. Premixed combustion occurs when the fuel and oxidizer are mixed on molecular scales before they enter the reaction zone, e.g., Bunsen flames [84]. By consuming reactants, the premixed flame behaves as a wave propagating into the unburned mixture. Stabilization of a premixed flame is mainly determined by the balance between the local flow speed and the laminar flame speed. Non-premixed combustion takes place when the fuel and oxidizer are separately transported to the reaction zone from different directions. In contrast to the premixed flame, the non-premixed flame has the advantage in flame stabilization since its location is mainly determined by the local mixture fraction rather than the flow speed. In general, the edge of a non-premixed flame is enveloped by a branch of a partially premixed flame, which helps anchor the non-premixed flame in a flowing environment [85]. Despite the difference in the outcome of premixed and non-premixed ignition (i.e., the appearance of the self-sustained propagating premixed flame and the growth and stabilization of the non-premixed flame, respectively), their ignition processes share some common features [2,3]. For example, local mixing of fuel and oxidizer is the prerequisite for the creation and subsequent development of the ignition kernel, which are necessary stages in both premixed and non-premixed ignition.

Ignition of premixed flame and detonation. Depending on the propagation speed, the premixed combustion wave exhibits in two forms, i.e., flame and detonation. The laminar flame speeds of various fuels are much smaller than the sound speed, and thereby the premixed flame is usually assumed to propagate under isobaric conditions [14]. The premixed flame structure consists of a preheat zone and a much thinner reaction zone. The preheat zone is a bridge that, by means of convection and diffusion, supplies the fresh mixture to the reaction zone, and in the meanwhile, transports heat from the reaction zone to warm up the fresh mixture. In the reaction zone, reactant consumption and heat generation are respectively balanced by mass diffusion and heat conduction, which implies that the rate of molecular transport plays the decisive role in premixed flame. Particularly, the diffusion of radicals back into the unburnt gas can significantly influence the flame propagation speed and stability, exhibiting more profound impacts than thermal back diffusion [86].

In contrast to premixed flame, detonation is a supersonic wave [87],

which consists of a leading shock wave followed by a reaction front [88]. For detonation initiation, there are two possible ways: direct detonation initiation [89,90] and deflagration-to-detonation transition (DDT) [91,92]. In direct detonation initiation, the leading shock results from the blast wave created by the rapid release of energy. In the region swept by the leading shock, the reaction front propagates at the rate determined by the gradient of autoignition delay time [93,94]. According to the reactivity gradient theory of Zel'dovich [93,94] and the SWACER (shock wave amplification by coherent energy release) mechanism of Lee et al. [95], the coherent coupling between the propagating reaction front and pressure wave leads to the development of the detonation structure. In detonation, the distance between the leading shock and the subsequent reaction front is defined as the induction length, d_D, which is in general considerably longer than the thickness of a premixed flame, d_L, i.e., $d_D \gg d_L$ [96]. Dimensional analysis suggests that the minimum energies for premixed flame ignition, $E_{F,min}$ and detonation initiation $E_{D,\min}$ are respectively proportional to the cubic of their characteristic length scales [12,97], i.e., $E_{L,\min} \sim d_L^3$ and $E_{D,\min} \sim d_D^3$. Therefore, we have $E_{D,\min} \gg E_{F,\min}$, which interprets the fact that detonation initiation is much more difficult than premixed flame ignition. The underlying mechanism responsible for DDT is more involved [92,98]. Phenomenologically, DDT can be understood as detonation initiation resulting from the acceleration of premixed flames, which is driven by various flame instabilities and turbulence. However, the essential mechanism responsible for DDT is still unclear, and many fundamental questions remain to be answered [91,99,100].

The essential stage for both premixed flame ignition and detonation initiation is the establishment of their inner structures. In premixed flame ignition, it is the evolution of explosive autoignition to the expanding ignition kernels that yields the transport-controlled flame structure [51,101]. While the structure of detonation is much more complex than that of a premixed flame. The Zel'dovich-von Neumann-Döring (ZND) theory presents a simplified detonation structure, consisting of a leading shock followed by reaction fronts [88]. The ZND theory suggests that the overall thickness of the detonation process, including the shock and subsequent reaction zones, can be much larger than that of a premixed flame under normal conditions [88]. However, the inherent instability of the ZND detonation structure implies that the actual detonation wave is multi-dimensional. The size of the cellular structure of detonation is influenced by the thermochemical characteristics of the premixed combustible. The boundary of the individual cellular structure comprises the shock and subsequent reaction front, and thus the span of the cellular structure is much larger than the thickness of the premixed flame.

1.3. Scope of the present review

Ignition is one of the most complicated problems in combustion research. It is a formidable task to present a comprehensive review on all aspects of the ignition phenomenon. In the literature, several reviews have been conducted for special aspects of ignition. Fundamentally, Mastorakos [2] gave an in-depth review on the autoignition and spark ignition of turbulent non-premixed combustion of gaseous fuels. Emphasis was placed on the essential understandings of the associated turbulent-chemistry interactions, which helps to reveal the stochastic nature of the flame kernel onset and the subsequent flame establishment following spark ignition. For spray combustion, Mastorakos [3] consolidated the existing knowledge on the spark-induced ignition kernel and subsequent flame development in the presence of both spatially distributed droplets and turbulent flow. A variety of primary parameters that distinguish spray ignition from gaseous flame ignition, e.g., fuel voidability, droplet size, overall fuel-to-air ratio, and the degree of pre-evaporation were highlighted. Shy [102] proposed a solid review of the dynamic process of premixed turbulent spark ignition, in which the variation of turbulent minimum ignition energies against the laminar minimum ignition energy over wide ranges of turbulence fluctuation velocities has been thoroughly analyzed. It was found that at a sufficiently large Lewis number and small spark gap, turbulence can promote ignition, yielding a lower minimum ignition energy than that in laminar situation, which is then interpreted as a non-monotonic minimum ignition energy transition. The underlying mechanism of turbulence-facilitated ignition was attributed to the coupling effects of differential diffusion, heat losses to electrodes, and turbulence on the spark kernel. Babrauskas [103] conducted a systematic review of the literature on ignition over the past century as well as an insightful interpretation of the current status, covering ignition properties of ignitable materials, characteristics of ignition sources, and behaviors of self-heating in ignition. Ronney [78] gave a critical review on the initiation of the combustion process, with emphasis on comparison between the conventional electric spark and laser igniting sources, whose main advantages could be attributed to the precise timing control and freedom of placement in the ignition system. Morsy [83] reviewed innovative techniques of laser-induced ignition and discussed the feasibility of adopting such technique in practical applications, especially the ICE. It was concluded that most incident laser energy could be utilized in laser-indued cavity ignition, leading to significant enhancements to the combustion process. Patane and Nandgaonkar [104] presented a thorough review on a variety of techniques utilized for multi-point laser ignition, underlying its effect on combustion performance in a constant volume chamber. For ICE, it was demonstrated that laser-induced ignition contributes substantial improvements in engine efficiency and operation stability without flame quenching. Starikovskiy and Aleksandrov [105] and Ju and Sun [106] gave comprehensive reviews on the plasma-assisted ignition and combustion and discussed the possibility for generation of the chemically active discharge plasma with desirable parameters as well as the effect of nonequilibrium plasma upon ignition and combustion processes in various practical conditions. Li et al. [107] provided a wide review on the recent developments in plasma-assisted ignition and combustion in the fields of aerospace engines with emphasis on experimental investigations covering ignition, emission, lean blow-out, combustion efficiency and stability. Practically, Toulson et al. [26] presented a review on the pre-chamber initiated jet ignition combustion system, highlighting its high efficiencies with jet ignition and simplicity of mechanical system, which suggests promising potential to be adopted in advanced ICE operating at ultra-lean conditions. Yu and Zheng [108] gave a review on recent progress of ignition improvement with emphasis on fundamental understandings in ignition improvements and working principles of primary categories of advanced ignition systems, including high-energy spark ignition, pulsed nanosecond discharge ignition, radio-frequency plasma ignition, laser-induced plasma ignition, and pre-chamber ignition.

Unlike previous reviews, this review focuses on forced-ignition of laminar premixed flames with the emphasis on the recent progress in fundamental theories of ignition. The present review will not cover homogeneous autoignition [57,78], non-premixed flame ignition, spray flame ignition, or detonation initiation [87,92]. Besides, the emphasis of the present review is on the chronological development of theory on premixed flame ignition in a quiescent flammable mixture. The progress in the numerical simulation and experiments on premixed flame ignition will not be included in the present review.

The rest of the paper is organized as follows. In section 2 the fundamentals of premixed flame ignition are reviewed, including the process of spark ignition, the various time scales involved in the creation of premixed flame by spark and critical ignition conditions, such as critical radius of ignition kernel and the minimum ignition energy. In section 3, the progressive development of ignition theory is presented, in which the key mechanisms leading to premixed flame ignition in a quiescent combustible mixture, i.e., exothermic chemical reaction, diffusive and conductive transport of reactant and heat respectively, the flame front expansion of the ignition kernel, and the transient effects involved in ignition energy deposition and flame propagation are sequentially

incorporated as the ignition theory advances. In section 4, the concluding remarks are presented in association with suggested future research directions.

2. Basics of premixed flame ignition

Forced-ignition in a combustible mixture is a very complex process, consisting of three stages: flame kernel formation, flame kernel expansion, and transition to a self-sustained flame [51,109]. The spark discharge process plays an essential role in generating the flame kernel and has wide-spread applications, particularly in internal combustion engines [63,65,110,111], motivating us to place deserves special attention. A brief review on the spark discharge process is presented in section 2.1. The forced-ignition involves various physical mechanisms, characterized by different time scales [51,112,113]. Those time scales are discussed in depth in section 2.2. The key parameters dominating the transition from an expanding flame kernel to a self-sustained flame are the critical ignition radius, minimum ignition energy, and minimum ignition power, which are introduced in section 2.3.

2.1. The spark ignition process

Spark ignition represents a critical mechanism by which a controlled ignition process can be achieved. This section is focused on spark ignition by thoroughly examining the pre-breakdown, breakdown, arc, and glow discharge phases, which provides essential insights into the initiation and sustaining of the flame kernel in premixed combustible.

According to previous studies [110,114], there are four phases during spark discharge, i.e., the pre-breakdown, the breakdown, the arc, and the glow discharge. The durations and voltages on the corresponding electrodes in the process of spark discharge are given in Fig. 1. It shows that the characteristic times for each stage are apparently separated, implying different mechanisms dominating individual stages.

The pre-breakdown phase refers to the transition from insulated gas between the electrodes to an active plasma channel connecting the anode and cathode [116,117]. When the voltage applied to the anode, ranging from 50 to 100 kV/cm, is much higher than the threshold value of around 30 kV/cm, the formative time lag for the breakdown $t_{breakdown}$, tends to be exceedingly short, i.e., $t_{breakdown} \sim 1$ ns [66,68]. The establishment of plasma channel is achieved by means of electron avalanches. The electrons are accelerated to high speed by the strong electric field, and they collide with atoms nearby, producing ions and new electrons.

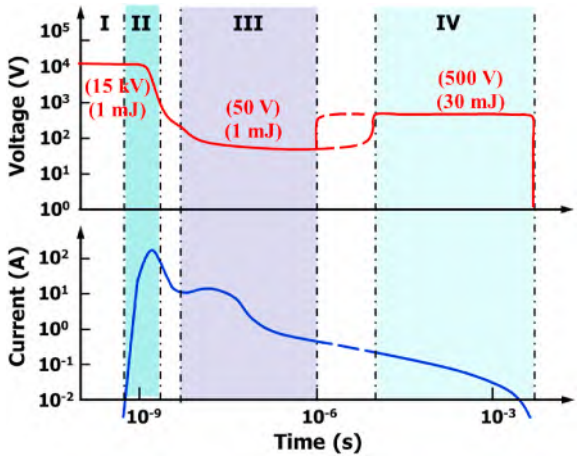

Fig. 1. The temporal evolution of voltage and current in a typical spark ignition process. Typical values of energy deposition for each phase are given in parentheses. Four phases are shown: I, the pre-breakdown phase; II, the breakdown phase; III, the arc phase; and IV, the glow discharge phase. There are two transition regions (in grey) between II and III and between III and IV. Figure reprinted from Ref. [115] with permission from Elsevier.

Consequently, the number of freely moving electrons grows exponentially [66].

The breakdown phase starts at the onset of the plasma channel, which connects the electrodes by current [98]. A schematic of breakdown phase is shown in Fig. 2 from Ref. [111]. Strong current through the plasma channel is characterized by substantial motion of electrons. Because of the drastic mass difference, the electrons acquire much higher kinetic energy than the other heavy particles, such as atoms, ions, and molecules, during the pre-breakdown phase, indicating that the plasma channel is in a thermal non-equilibrium state [118–120]. In general, the process of achieving thermal equilibrium between the electrons and the gas, i.e., the conversion of potential energy to thermal energy via collisions and recombination reactions, lasts for tens of nanoseconds, which is thereby defined as the lapse of the breakdown stage. The end state of breakdown provides a suitable initial condition based on which the spark ignition analysis is conducted.

The arc phase proceeds in the plasma channel after thermal equilibrium is established [66]. Willems and Sierens [121] developed a model to interpret the growth of the initial plasma channel in spark ignition engines. The model takes into account the detailed properties of the ignition system (e.g., the electrical power, geometry of the spark plug, and the cylinder wall), the flammable mixture (e.g., the pressure, temperature, and equivalence ratio), and the flow (e.g., turbulence intensity, stretch, and characteristic time/length scales). Thermal equilibrium is characterized by a substantially lower concentration of freely moving electrons and ions than in the breakdown phase and, thus, a higher impedance in the plasma channel [98]. At the end of the breakdown phase, the plasma temperature reaches around thousands of kelvins [110]. Such a high temperature is considerably higher than the melting point of the material comprising the electrodes, resulting in electron emission from the spot on the electrode surface. Such an effect is known as thermionic emission, which is the dominant mechanism responsible for the discharge in the arc phase [110,122]. Moreover, dissociation of gas molecules profoundly affects the thermal dynamics of an arc, particularly lowering the arc temperature [123]. This process significantly influences the energy balance of the arc and affects its characteristics and behavior. By absorbing thermal energy, the dissociation of gas molecules cools the arc, impacting the birth of the ignition kernel and the subsequent ignition process.

The glow is the final phase of spark discharge. The temperature in the plasma channel falls due to the conductive heat transfer to the surroundings, which leads to a decrease in current in the gap provided by thermionic emission [124]. The transition from the arc to the glow phase takes place when the current is below a threshold, at which the melting on the electrode surface no longer sustains and thereby the thermionic emission is switched off [63,125]. Accordingly, the current in the gap can only be sustained by the positive ion bombardment mechanism, according to which freely moving electrons are produced during collisions among heavy positive ions on the cathode surface.

The loss of plasma energy during spark ignition can be understood as heat transfer to the surroundings. The energy distribution during different phases of spark discharge is shown in Fig. 1, and the proportion of plasma energy and energy loss to electrodes in each stage is given in Table 1. The breakdown phase is associated with a shock wave originating from the plasma channel [18]. Propagation of the shock wave leads to the convective transfer of ignition energy from the plasma channel. The intensity of the shock wave depends on the amount of ignition energy deposited during the breakdown phase [111]. For conventional spark ignition, this convective loss of plasma energy appears to be negligible. Because of the short duration and relatively small voltage fall on the cathode, it was estimated that the energy loss associated with the breakdown stage is less than 5 % [15]. As shown in Fig. 1, the arc phase is much longer than the breakdown phase and it usually lasts for tens of microseconds [115]. Compared to the breakdown phase, the arc phase has a relative longer duration and a higher temperature of the plasma channel, implying that the heat loss through

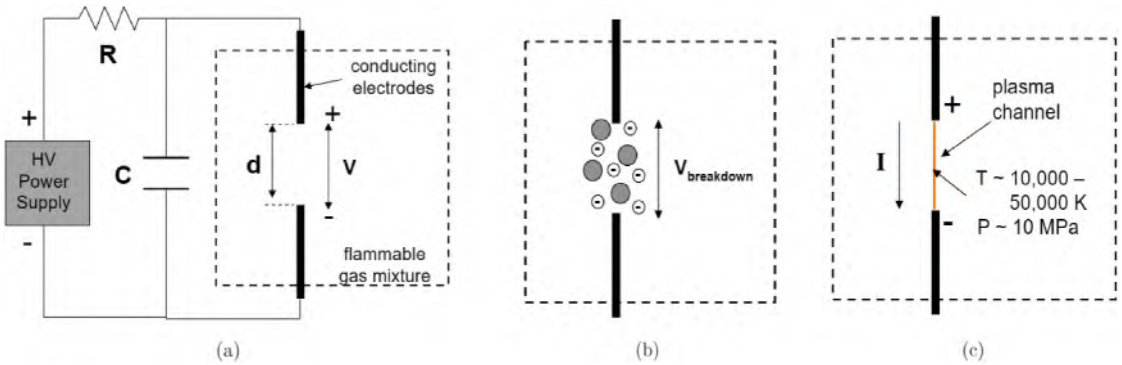

Fig. 2. Schematics of the spark breakdown process: (a) a circuit is connected to two conductors at a distance with increasing voltage across the gap; (b) the breakdown voltage is reached, causing the gap to ionize through the "electron avalanche"; (c) a high-temperature, high-pressure, electrically conductive plasma channel forms across the gap. Reprinted from Ref. [111] with permission from Dr. Sally Bane.

Table 1
Energy distribution for breakdown, arc, and glow phases [15].

	Breakdown	Arc	Glow, %
Radiation loss	<1 %	5 %	<1 %
Heat loss to electrodes	5 %	45 %	70 %
Total loss	6 %	50 %	70 %
Plasma energy	94 %	50 %	30 %

heat transfer should be more pronounced. During the glow phase, the loss of plasma energy can be attributed to the voltage fall on the cathode and thermal conduction to the electrodes [110]. In general, the loss of plasma energy in the glow phase is much more significant than that in the arc phase. Maly and Vogel [115] demonstrated that the effectiveness of breakdown discharge in ignition is higher than that of arc discharge, which is in turn more efficient than glow discharge.

The formation of flame kernel is a very complex process, which profoundly affects the performance of engines [126–130]. Eisazadel-Far et al. [129] conducted experimental and theoretical work on the spark discharge-induced flame kernel formation and propagation in premixed gas, and examined the effects of various parameters, including discharged energy, radiation loss, and the initial condition of the plasma kernel. Song and Sunwoo [128] proposed a one-dimensional simulation model for the flame kernel growth induced by a spark in a gasoline-air mixture, in which the heat transfer to both the cylinder wall and electrodes, the environmental turbulent flow of the combustible mixture, and the effect of residual gas were taken into account.

Spark discharge creates a plasma channel, which involves an expanding flame kernel and subsequently leads to a premixed flame. There are three major steps of ignition kernel formation induced by spark ignition: (1) plasma channel formation; (2) transition from plasma channel to flame kernel; and (3) flame kernel development into propagating flame [98]. During the first step, the plasma channel is characterized by an exceedingly high electron temperature, and accordingly, the expansion of the plasma kernel is dominated by strong thermal conduction and an expanding shock wave induced by breakdown. Therefore, the chemical reaction can hardly be initiated during a period of nanoseconds [125,131]. Entering the arc and glow phases, the temperature of the plasma channel decreases over longer time scales, during which the chemical reactions make an increasing contribution to the plasma kernel expansion. By the end of the breakdown phase, the created plasma channel consists of a large amount of high-temperature ions [124]. As the spark discharge proceeds, the high-temperature plasma channel expands and finally transitions into a flame kernel at the end of the second step. In the third step, the flame kernel develops into a propagating flame, which is dominated by chemical reactions and the transport of heat and species. The chemical reaction at the flame front must be sufficiently intensive in order to balance various effects leading to heat loss without supplementary energy supply, and meanwhile, the flame kernel should be of comparable size so that the flame stretch can be sustained without local quenching.

Fig. 3 further shows the sequential process of flame kernel formation. The shock wave, flow entrainment, and vortex development are clearly depicted in Fig. 3. The shock wave originating from the spark plays a crucial role during flame kernel formation. Arpaci et al. [132] examined the development of ignition kernels in propane-air mixtures and found that the early radius of the kernel exhibits similarity behavior, i.e., $R \sim t^{1/5}$. Subsequent analysis showed that the shock wave from the spark kernel induces a strong detonation and that the temperature variation within the kernel can be obtained based on the 1/5-power law [133]. At initial states, the 1/5-scaling relation implies that such a flow structure accelerates more rapidly than the Sedov-Taylor blast wave, which satisfies $R \sim t^{2/5}$ [134]. This strong blast wave refers to the high-energy wave front emanating from the spark channel and is characterized by rapid expansion and high pressure. Bradley et al. [135]

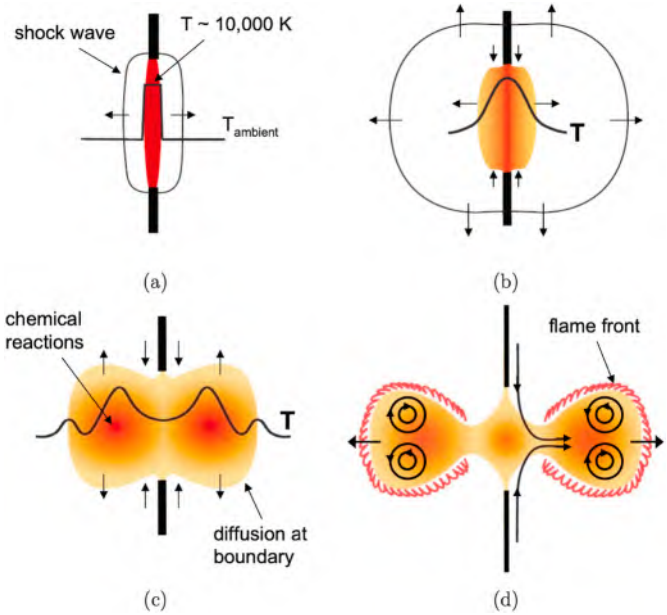

Fig. 3. Schematics of the flame formation process. (a) A blast wave is emitted due to the high temperature, high pressure spark channel; (b) the hot gas kernel expands rapidly following the blast wave and fluid is entrained along the electrodes; (c) chemical reactions produce heat inside the gas kernel and diffusion of heat and species occurs at the boundary; (d) if the proper conditions exist, a self-sustaining flame forms after approximately 10–100 μs. Reproduced from Ref. [111] with permission from Dr. Sally Bane.

conducted an experimental and theoretical study on the characteristics and underlying mechanisms of high-energy laser ignition. They demonstrated that the strong shock wave has a complex impact on the ignition process. On one hand, the shock wave takes away a substantial amount of thermal energy, which increases the MIE for laser ignition. On the other hand, the rarefaction wave associated with the strong shock wave creates a favorable condition that enhances the flame spread and thus facilitates the ignition process [135].

The flame front indicated in Fig. 3(d) refers specifically to the formation of the flame front at the initial phase of ignition. This phase is characterized by rapid chemical kinetics, especially in environments with high-energy initiation methods or highly reactive fuel mixtures, allowing for the very fast establishment of an autoignition-dominated reaction zone after an approximate duration of 10–100 μs. This time scale differs from that of transport, which affects the subsequent propagation of the flame front through the combustible mixture and is typically on the order of milliseconds. This transport time scale is determined by the rates of heat and mass transfer that sustain the flame front as it moves through the unburnt mixture. The distinction between these two phases—rapid ignition and subsequent steady-state propagation—resolves the apparent discrepancy. The microsecond time scale refers to the very initial establishment of a chemically active zone, while the millisecond time scale reflects the broader process of flame front propagation and stabilization in the combustible mixture. These differences between the phases of flame kernel development are crucial for understanding flame dynamics.

The ignitability of spark discharge can be evaluated based on an energy budget analysis. According to Eisazadel-Far et al. [129], radiation is an important source of energy loss in plasma, particularly in situations with high temperatures. This is demonstrated by Fig. 4, which shows the temporal evolution of the energy deposition rate from the spark and the rates of energy loss due to various mechanisms. However, when a self-sustained flame establishes itself, radiation is not an important source of energy loss. In addition, Song and Sunwoo [128] found that increasing breakdown energy enlarges the plasma kernel radius and thereby yields faster development of the ignition kernel. Therefore, efficient spark ignition should avoid significant energy loss during the arc and glow phases.

Despite widespread practical applications, spark ignition has some limitations, such as electrode erosion over time and low reliability in limiting situations. Particularly for the ignition of a lean mixture or ignition at high pressure conditions, the ignition energy deposited by the spark might be insufficient. To overcome these limitations and enhance ignition efficiency, alternative advanced ignition techniques have been developed, including laser ignition and plasma jet ignition. Available techniques to develop advanced ignition approaches include laser [135–137] and plasma jet [138,139]. In spite of the similarities in dominant mechanism and evolution process shared between conventional spark ignition and laser-induced ignition, the latter exhibits several advantages, such as an extremely high rate of energy transfer from the beam and freedom in selecting a location for breakdown. In laser ignition, unless tuned for resonant excitations of particular species [140], the absorption of laser energy causes electrical breakdown through multiphoton ionization and electro-ion bremsstrahlung [79]. It leads to a substantial increase in both temperature and pressure and, thereby, the emission of a strong shock wave. Subject to a sufficiently strong igniter, the initial shock wave can be treated as a blast wave that rapidly decays to an acoustic wave followed by a growing diffusion boundary layer [141,142]. The laser-induced ignition offers high precision and control over the spark ignition process and is able to target specific locations within the combustible mixture. However, its drawbacks include the high cost of laser equipment, the complexity of integrating laser systems into combustion, and potential safety concerns with laser operation. In addition, the effectiveness of laser-induced ignition can be influenced by the optical properties of the fuel mixture, which might limit its applicability across different combustion scenarios.

The plasma jet igniter includes two spark energy delivery systems, whose operation process can be interpreted as follows: A high voltage, low current discharge is initially imposed to break down or ionize the gap, which is followed by a low voltage, high current discharge that adds the dominant part of the spark energy. The second spark discharge rapidly heats the flammable mixture to a high temperature and high pressure, which subsequently produces a high-speed jet of high temperature ions and free electrons [107,143]. Plasma jet ignition offers advantages in igniting lean mixtures and can improve combustion efficiency and stability. The challenges associated with this method include the complexity of the ignition system, higher energy requirements compared to conventional spark ignition, and the need for specialized equipment to generate and deliver the plasma jet to the combustion zone. Additionally, long-term durability and deploying plasma jet systems into existing engine designs pose significant engineering challenges.

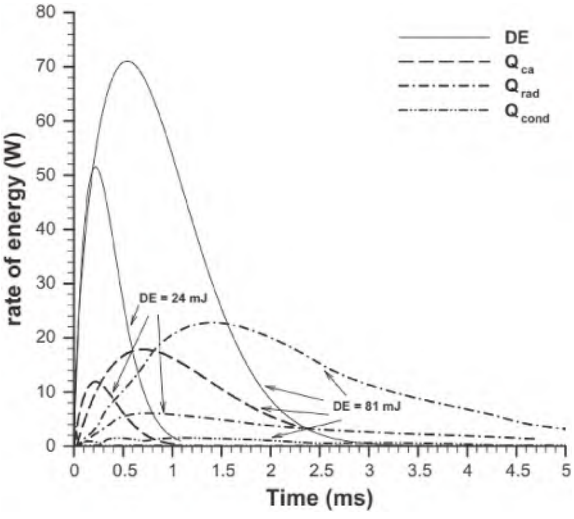

Fig. 4. Rate of variation of discharge energy (DE), cathode-anode fall dissipation $Q_{ca-diss}$, radiation loss $Q_{radiation}$, and conduction dissipation by thermal boundary layer $Q_{conduction}$ for air. The ignition radius is $r_i = 0.5$ mm and the distance between electrodes is $d_e = 0.38$ mm. Reprinted from Ref. [129] with permission from Elsevier.

2.2. Different characteristic times in premixed flame ignition

As indicated by Fig. 1, various time scales are involved in different phases during premixed flame ignition. For sufficiently high overvoltage, the breakdown time is in nanoseconds (10^{-9} s), during which electron avalanches open the plasma channel connecting the electrodes [63]. Subsequent to the breakdown phase, a thermal equilibrium plasma channel forms. The arc phase lasts for tens of microseconds (10^{-5} s), within which a shock wave is created by the rapid thermal energy addition since strong current flows through the plasma channel by means of thermionic emission [66]. The plasma region spreads due to both shock wave propagation and thermal expansion, which cools the plasma kernel over time. At a period comparable to the mixture's autoignition delay time, the chemical reaction becomes pronounced and tends to dominate the expansion of the plasma kernel at a relatively large distance, which creates the flame kernel. The glow phase is much longer, typically in milliseconds (10^{-3} s) [124]. Despite huge losses to the electrodes, the ignition energy deposited in the glow phase supports the expansion of the flame kernel. The expansion of the flame kernel is due to the outward propagation of the flame front at the edge. The motion of the flame front is driven by chemical reactions and is meanwhile subject to heat transfer caused by various effects, such as radiation, conduction, and expansion waves [8,144]. Specifically, the

radiation time scale can be evaluated based on temperature and size of the spark channel. At high temperatures, the radiation time scale may be exceedingly short and efficiency of radiation in transferring energy in such scenarios is significantly enhanced due to the T^4-dependence of radiative emission according to Stefan-Boltzmann law [145]. The flame kernel development time is usually in the range of 1–10 ms (10^{-3}~10^{-2} s) and the subsequent flame propagation takes much longer time in the range of 10–1000 ms (10^{-2}~1 s). These time-scaling analyses suggest that radiative energy transfer is an important mechanism, in association with conduction and convection, in the brief duration of the spark to initiate combustion.

Numerical and experimental efforts have been devoted to unveiling the range of timescales involved in each process of premixed flame ignition [81,136,146,147]. The schematics of the primary characteristics and associated time scales of different phases of laser induced ignition are shown in Fig. 5.

The inverse of reaction rate defines the characteristic time scale for chemical reactions t_{chemical}, which is very sensitive to temperature and is affected by the ambient pressure and equivalence ratio of the mixture [14]. Each heat loss mechanism is characterized by a time scale as well. In general, radiation time scale $t_{\text{radiation}}$ is much larger than t_{chemical}. This indicates that radiative heat loss cannot balance the heat generation from reaction and thereby has marginal influence during flame kernel expansion [148,149]. The heat conduction time is evaluated as $t_{\text{conduction}} \sim R_{\text{kernel}}^2/\alpha$, in which R_{kernel} is the flame kernel radius and α the thermal conductivity of the mixture. The expansion wave propagates at the speed of sound, a_{acoustic}. Accordingly, the time scale for the cooling induced by expansion wave is $t_{\text{acoustic}} \sim R_{\text{kernel}}/a_{\text{acoustic}}$. The time ratio $t_{\text{acoustic}}/t_{\text{conduction}} \sim \alpha/(a_{\text{acoustic}}R_{\text{kernel}})$ is of the same order as the Knudsen number Kn, which is the ratio of mean-free-path to the flame kernel size and is in general considerably small, i.e., $t_{\text{acoustic}}/t_{\text{conduction}} \sim Kn$. According to physics kinetics [150], the Knudsen number separates the continuum regime and the kinetics-dominated regime of free molecular flow. Regarding the specific flame kernel size in practical combustion problems, we noticed that the Knudsen number is significantly less than unity, i.e., $Kn \ll 1$. It implies that the smallest flame kernel size, determined by the spark plug gap of the order of 1 mm, is substantially larger than the mean free path in typical conditions. It solidifies that the gas behavior in the vicinity of the flame kernel can be appropriately interpreted within the continuum regime.

In general, spark discharge time scales in ignition systems range from a few nanoseconds to several hundred microseconds, depending on the energy level, spark gap, and electrical characteristics of the ignition system. For instance, a typical automotive spark ignition system operates with discharge times on the order of tens to hundreds of microseconds, with the initial high-energy discharge phase lasting approximately 1–2 μs, followed by a long, lower-energy tail. These time scales are crucial for ensuring sufficient energy transfer to initiate combustion. Thus, it is difficult to specify a unique time scale characterizing the spark discharge process because of its multi-stage nature. Table 2 provides a summary of the primary characteristic time scales involved in the forced-ignition of premixed flames. This table also presents the dimensional relationships of these time scales as well as their dependence on state variables.

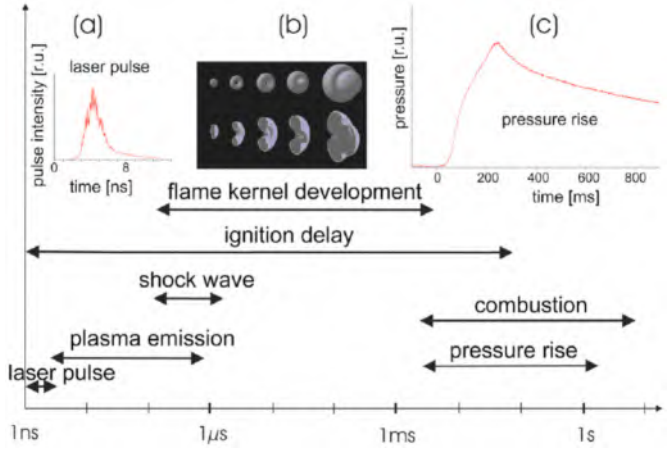

Fig. 5. Range of timescales for various processes involved in laser-induced ignition: the lengths of the box indicate the durations of the indicated process. Reprinted from Ref. [146] with permission from SAE International.

Depending on the flame front propagation speed, the primary mechanism of heat loss differs. Vázquez-Espí and Liñán [151,152] defined two ignition regimes by comparing characteristic times describing the dominant mechanism and chemical reaction respectively. In the regime satisfying $t_{\text{chemical}} \sim t_{\text{acoustic}} \ll t_{\text{conduction}}$, i.e., the reaction time being comparable with the acoustic time, the reaction heat release is balanced by heat loss due to thermal expansion, and thereby ignition exhibits to be a fast, non-diffusive process, during which the heat conduction can hardly respond. In the other regime with $t_{\text{acoustic}} \ll t_{\text{conduction}} \sim t_{\text{chemical}}$, the heat conduction turns out to be the primary cooling mechanism that controls the ignition process. Before ignition takes place, the expansion wave would have propagated to far distance and thereby cannot be perceived by the flame kernel. Since the expansion of the flame kernel is determined by the reaction rate, the propagation speed of the flame front shall be correlated to $t_{\text{conduction}}$. In the non-diffusive ignition regime, the flame kernel grows at the speed comparable with local sound speed, which may induce detonation initiation according to gradient theory of Zel'dovich [93]. In real-world scenarios, the flame kernel growth in the non-diffusive ignition regime involves complex hydrodynamic and chemical processes. Particularly, the growth speed of the flame kernel in non-diffusive regime is significantly influenced by the propagation of acoustic waves induced by the flame kernel expansion. These acoustic waves can collapse into a shock wave, holding the potential to transition to detonation and playing more crucial role in the dynamics of the flame kernel development [153]. A thorough review of denotation and deflagration-to-detonation transition (DDT) can be found in Refs. [91,112,154] and it is beyond the scope of this review. In the thermal-diffusive ignition regime, the equilibrium

Table 2
List of primary characteristic time scales involved in forced-ignition of premixed flame

Spark discharge	Breakdown	$t_{\text{breakdown}} \sim$ ns
	Arc (electric discharge)	$t_{\text{arc}} \sim$ μs
	Glow (electric discharge)	$t_{\text{glow}} \sim$ ms
Ignition kernel formation	Acoustic	$t_{\text{acoustic}} \sim t_{\text{acoustic}}(T_{\text{kernel}})$
	Blast wave	$t_{\text{blastwave}} \sim t_{\text{blastwave}}(T_{\text{kernel}}, P_{\text{kernel}})$
	Chemical reaction	$t_{\text{chemical}} \sim t_{\text{chemical}}(T_{\text{kernel}}, P_{\text{kernel}})$
	Thermal conduction	$t_{\text{conduction}} \sim R_{\text{kernel}}^2/\alpha$
	Kernel deformation	$t_{\text{deformation}} \sim R_{\text{kernel}}/U_{\text{front}}$
Ignition kernel propagation	Chemical reaction	$t_{\text{chemical}} \sim t_{\text{chemical}}(T_{\text{kernel}}, P_{\text{kernel}})$
	Thermal conduction	$t_{\text{conduction}} \sim R_{\text{kernel}}^2/\alpha$
	Radiation	$t_{\text{radiation}} \sim t_{\text{radiation}}(T_{\text{kernel}}, R_{\text{kernel}})$
	Mass diffusion	$t_{\text{diffusion}} \sim R_{\text{kernel}}^2/D$
	Convection	$t_{\text{convection}} \sim R_{\text{kernel}}/U_{\text{front}}$
Key parameters	Ignition kernel temperature	T_{kernel}
	Ignition kernel pressure	P_{kernel}
	Ignition kernel radius	R_{kernel}
	Speed of kernel front	U_{front}
	Thermal diffusivity	α
	Mass diffusivity	D

between chemical reaction and heat conduction indicates the definite flame structure at the edge of flame kernel [155,156] and suggests that the flame kernel shall evolve into a self-sustained spherical flame [144,157]. This process introduces one more essential time scale, whose interpretation involves critical ignition radius R_{cr} and flame front propagation speed U.

Nevertheless, it shall be noted that the physicochemical process of flame kernel development in real-world situations would be more complex [130,158]. For instance, as the flame kernel temperature increases, it significantly influences the rates of chemical reactions and sound speeds in highly dynamic environments of the gas mixture. This interplay suggests that a simple balance between these time scales is unlikely to be stable, and additionally, their interplay is subject to the evolving conditions within the flame kernel. The early development of the flame kernel involves complex and highly transient physio-chemical processes, characterized by rapid changes in temperature, pressure, and species concentrations [159].

In the next subsection, we shall briefly look into the definition of critical ignition radius. The dynamic behavior of flame kernel development will be thoroughly reviewed in section 3.

2.3. Critical ignition radius and minimum ignition energy

Successful ignition is characterized by the setup of a flame kernel that is able to propagate outwardly in a self-sustained manner. Studies on the evolution of the ignition kernel showed that there is a critical radius R_{cr}, corresponding to the marginal state that separates the growth (i.e., transition to an ever-expanding spherical flame) and collapse (i.e., shrink of the flame kernel leading to extinction) of the flame kernel [160,161]. Utilizing a high-speed laser schlieren system, Ko et al. [142], recorded the temporal growth of the ignition kernel from a spark near the MIE in a propane/air mixture and showed the existence of a critical ignition radius, beyond which the flame front can propagate outwardly in a self-sustained manner.

The flame kernel initiated by the spark discharge is very small and thereby subject to a very large positive stretch, which is inversely proportional to the flame radius. Consequently, flame stretch substantially affects the developing procedure of the flame kernel and thus plays a decisive role in determining the outcome of the ignition process [8,144]. According to the coupling of positive stretch with preferential diffusion between heat and mass (i.e., the Lewis number, Le, which is the ratio between heat diffusivity of the mixture and mass diffusivity of the deficient reactant), the temperature and propagation speed of the flame kernel are increased (decreased) in mixtures with Lewis number less (greater) than unity, which accordingly promotes (inhibits) the ignition process [157,162,163]. This is consistent with the fact that successful ignition can always be achieved once the flame kernel is created in a combustible mixture with $Le < 1$ [12,164].

Nevertheless, it is difficult to ignite a mixture with $Le > 1$ because of the inhibiting effect induced by the positive stretch [12,17]. For a flame kernel expanding in a quiescent mixture, the flame stretch is proportional to the flame curvature. Correspondingly, the threshold intensity of stretch is interpreted in terms of the critical ignition radius, and it implies that R_{cr} increases with Lewis number [12,157]. When the flame curvature is greater than $2/R_{cr}$, the flame front propagation needs to be supported by external energy supply, i.e., the ignition energy. Considering flame kernel growth as a two-step process consisting of an instantaneous blast followed by a diffusion penetration into the surrounding area, Ko et al. [141] developed a theoretical model to interpret the temporal evolution of the flame kernel and to evaluate the critical ignition radius. However, the structure and the dynamic propagation of the flame kernel were not appropriately considered in the formulation of Ko et al. [141]. Such issues were addressed by later ignition theories [109,144], on which a detailed review is presented in the next section. In practical combustion, there exists turbulence in the combustible mixture, which alters the transport rate of both heat and radicals. While, except for extremely strong turbulence, the turbulent eddies may not significantly damage the fundamental structure of the flame kernel [165], which is exceedingly small at the ignition stage. Despite a turbulent Lewis number close to unity, the dynamic behavior of the ignition kernel is profoundly affected by local stretch and differential diffusion defined by the molecular Lewis number in turbulent flows.

In experiments, ignition energy is provided by a capacitive spark with variable power levels and discharge durations [114]. For a mixture at given initial temperature and pressure, there exists a transition band of the spark energy level between ignition and non-ignition [166–168], which can be attributed to the perturbation in various aspects, such as the breakdown energy, the subsequent discharge, and the location of the spark channel. In practice, ignition is usually considered a statistical rather than a threshold phenomenon. Accordingly, the concept of ignition probability is widely adopted [167,169,170]. The ignition probability grows monotonically as the spark energy level increases from the lower to the upper bound within this transition band. In general, the middle point within this transition band corresponding to 50 % ignition probability defines the MIE [166–168]. It is noted that a slight variation in fuel concentration may significantly change the ignition probability and thereby the MIE [111].

The MIE changes non-monotonically with the gap distance between two electrodes, d_{spark}. It reaches the smallest value at some optimal distance $d_{spark,optimal}$, which is in the same order as the quenching distance [171–173]. Ono et al. [174,175] measured the MIE of hydrogen/air mixtures, for which the quenching distance increases with hydrogen concentration. Similarly, the MIE changes non-monotonically with the discharge duration t_{spark}, and there exists an optimum spark duration $t_{spark,optimal}$ that leads to the smallest value of MIE at a given electrode gap distance [69,176]. Combining the effects of electrode gap distance and spark duration, the absolute (least) MIE can be determined by satisfying the conditions $d_{spark} = d_{spark,optimal}$ and $t_{spark} = t_{spark,optimal}$. In flow environments, experimental studies [5,116,177] found that the severe stretch imposed on the ignition kernel renders the ignition process more difficult, and accordingly, the MIE becomes higher. In addition to the increase in MIE, the optimal spark duration for a flowing mixture tends to be smaller than that for the corresponding stagnant mixture [178]. This indicates that a stronger ignitor must be adopted to initiate flame in a flowing mixture. Moreover, Sloane and Ronney [179] found that the MIE predicted based on a one-step chemical model is substantially lower than those calculated using detailed chemical mechanisms. This suggests that the detailed chemistry needs to be taken into account for a qualitative evaluation of the MIE.

The dynamic evolution of the flame kernel changes drastically for ignition near the MIE [5,69,180]. Initially, the spark-induced flame kernel expands exceedingly rapidly. As depicted in Fig. 6, the propagation speed of the flame front falls in the course of time as it approaches the critical radius. The origin of Fig. 6 does not start at $r = 0$, which

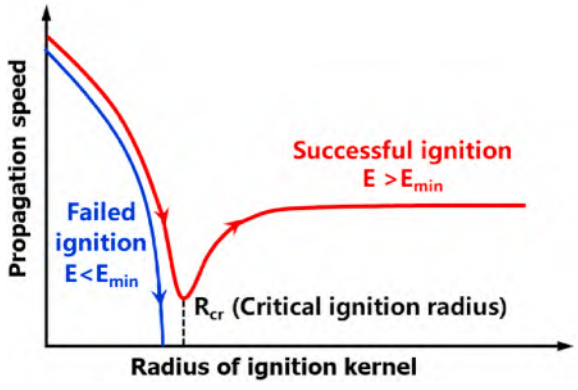

Fig. 6. Schematic for the change of ignition kernel propagation speed with its radius for successful and failed ignition.

helps focus on the propagation speed of the flame kernel beyond the critical ignition radius. The ignition kernel onset is associated with complex interaction between fluid dynamics and physiochemical processes, leading to intricate variation of flame kernel speed in a very restricted domain close to $r = 0$. While success or failure of ignition can be judged by the flame propagation speed at radial coordinates near the critical radius. For successful ignition, the flame kernel can pass through the critical radius, and the propagation speed of the flame kernel turns to increase and eventually approaches the planar adiabatic flame speed [164,181]. For failed ignition, the growth of the flame kernel ceases before arriving at the critical radius, and eventually flame extinguishment occurs.

In addition to ignition energy, there is another key parameter characterizing the ignition criterion—ignition power. The ignition power can be understood as the rate at which this energy is delivered to the combustible mixture. In analogy to minimum ignition energy, there exists a minimum ignition power below the ignition kernel can never pass through the critical size, no matter how long the ignition source lasts, or equivalently, how much the ignition energy is deposited into the combustible mixture [109,144,182]. Both the ignition energy and ignition power are intrinsic parameters that can influence the ignition outcome.

The critical ignition radius and MIE are essential concepts of spark ignition and provide fundamental knowledge for evaluating the ignitability of a combustible mixture. In the following section, a thorough review will be presented with emphasis on the theoretical development concerning the key issues of forced-ignition of premixed flames.

3. Premixed flame ignition theory

The prerequisite for chemical reaction is the mixing of reactants at the molecular level. Therefore, ignition in premixed reactants is the onset process for a variety of fundamental combustible modes, including premixed and non-premixed flames, spray combustion, and detonation. In a quiescent mixture, ignition involves the generation of a flame kernel and its subsequent evolution. The flame kernel can either develop into a self-sustained propagating flame or quench, which are referred to as successful and failed ignition, respectively. In this section, the progress in the theory for premixed flame ignition in a quiescent mixture is reviewed. Fig. 7 shows various controlling physical and chemical processes considered in different ignition theories. In Fig. 7, the governing equations for temperature and mass fraction of the deficient reactant are in the coordinate moving with the propagation front, whose propagation speed is U [144]. Therefore, the convection term (the second term on the left hand side of the governing equations) represents the consideration of flame propagation [144]. As shown in Fig. 7, the thermal ignition theory considers the balance between heat loss due to thermal conduction and heat generation due to chemical reactions. Since the chemical reaction occurring in flames is associated with both heat release and reactant consumption, the flame ball theory further considers the transport of both heat and reactant. Based on the stability of the flame ball, the critical radius for premixed ignition can be determined. The quasi-steady ignition theory describes the transition from an ignition kernel to a self-sustained, propagating spherical flame. Therefore, the convection term corresponding to flame propagation is considered in the quasi-steady ignition theory, as shown in Fig. 7. The quasi-steady ignition theory neglects the unsteady transition of the ignition kernel. The transition ignition theory further considers the unsteady term in the governing equations, as shown in Fig. 7.

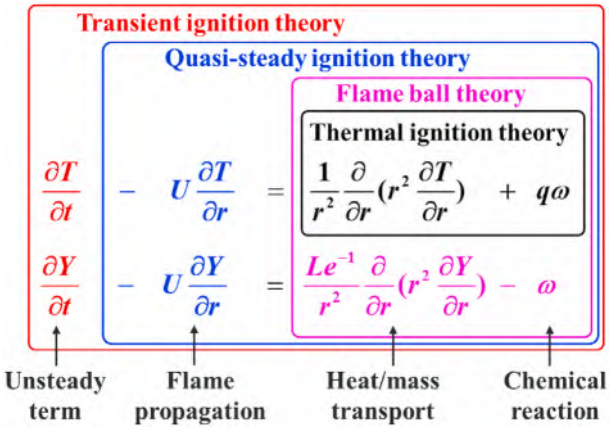

Fig. 7. Different ignition theories considering various controlling physical/chemical processes. The non-dimensional governing equations for temperature and mass fraction of the deficient reactant are shown (the tilde is omitted).

The large activation energy asymptotic (AEA) analysis has historically played a significant role in the theoretical development of premixed flame ignition. In early decades, limited kinetic and numerical tools made AEA a reasonable approach to gaining a fundamental understanding of complex combustion systems. As advanced chemical kinetics and computational fluid dynamics develop, the limitations of AEA have become more evident. The primary issue with AEA is the assumption of large activation energy, which forms the basis for the entire AEA framework in analyzing flame ignition, extinction, and flame propagation speed. Specifically, the explosion of hydrogen, influenced by the presence of radicals, typically does not exhibit large activation energies [183]. For autoignition, the real-world activation energy is controlled by chain branching reactions, such as $H + O_2 \rightarrow OH + O$ [14]. Despite these limitations, AEA has contributed valuable insights into the qualitative understanding of ignition phenomena [184,185]. The AEA has the ability to highlight key parameters and dominant processes in flame ignition, which guide focused efforts on critical aspects of combustion phenomena. Moreover, AEA remains a powerful tool for heuristic interpretation of premixed flame ignition. The analytical nature of AEA makes it an excellent framework for conceptual understanding of critical combustion processes. Even as the computational methods advance, the foundational knowledge provided by AEA continues to be relevant, helping to train new generations of combustion researchers.

The following sections give a chronological review on ignition theories, which are essentially based on the AEA theoretical framework. The theory on the onset of chemical reactions, which is characterized by thermal runaway or explosion, is reviewed in section 3.1; the thermal ignition theory is presented in section 3.2; the flame ball theory is reviewed in section 3.3; the formation of ignition kernel subject to external heating is discussed in section 3.4; the quasi-steady ignition theory is described in section 3.5; and the transient ignition theory, which provides a more comprehensive description to the process of premixed flame ignition, is discussed in section 3.6.

3.1. Thermal runaway in a homogeneous system

The overall exothermicity from chemical reactions can induce thermal runaway/explosion in a combustible mixture. Thermal runaway, also known as autoignition, represents the onset of premixed flame ignition. In classical thermal ignition theory, the chemical reaction is simplified by a one-step Arrhenius type model, and the combustible mixture is assumed to be adiabatic prior to autoignition [14]. Accordingly, the temperature of the homogeneous mixture satisfies

$$c_p\frac{dT}{dt} = -q_c\frac{dY_F}{dt} = q_cY_FBe^{-T_a/T} \tag{1}$$

where c_p is the heat capacity, and Y_F is the mass fraction of the deficient reactant, respectively. The parameters for chemical reaction are the activation temperature T_a, the collision frequency factor B and the heat release per unit mass of reactant q_c.

In general, the consumption of reactant before thermal runaway

onset tends to be insubstantial, i.e., $Y_F \approx Y_F^o$ where Y_F^o is the initial mass fraction of the deficient reactant [186,187]. Consequently, the auto-ignition process is primarily characterized by temperature variation. Usually the activation temperature T_a is much higher than the adiabatic flame temperature T_{ad}, i.e., $T_a \gg T_{ad}$, where $T_{ad} = T_0 + q_c/(\rho_0 c_p)$ derived from energy conservation. The relation $T_a \gg T_{ad}$ implies that a slight increment in temperature substantially facilitates the chemical reaction [7,161]. In general, the temperature can be expanded in an asymptotic series, and the thermal ignition process can be described by the temporal variation of temperature perturbation. Accordingly, the AEA provides a convenient approach to investigating the dynamic behavior of premixed flames [14,185]. The large activation energy asymptotic analysis requires the specification of a small parameter. In general, this parameter can be specified as $1/Ze$, where the Zel'dovich number, defined as $Ze = T_a(T_{ad} - T_0)/T_{ad}^2$, is considerably greater than unity for typical combustion systems, i.e., $Ze \gg 1$.

For simplicity and clarity, the mathematical formulation of asymptotic analysis should be conducted in nondimensional form. The temperature can be non-dimensionalized as $\widetilde{T} = \rho_0 c_p T/Q_c$ with ρ_0 being the density of the unburned mixture and q_c the specific heat release due to chemical reaction. The non-dimensional temperature is introduced in the form of an asymptotic series by regarding $1/Ze$ as the expansion parameter, i.e.,

$$\widetilde{T} = \widetilde{T}_0 + \frac{\widetilde{\theta}}{Ze} + O\left(\frac{1}{Ze^2}\right) \tag{2}$$

where $\widetilde{T}_0$ is the mixture's temperature at initial state and $\widetilde{\theta}$ describes the nondimensional temperature perturbation. Substituting Eq. (2) into Eq. (1) and retaining the first order terms of $1/Ze$, one obtains [14]

$$\frac{d\widetilde{\theta}}{d\widetilde{t}} = e^{\widetilde{\theta}} \tag{3}$$

where the non-dimensional time is defined as $\widetilde{t} = tBY_{F,0}e^{-T_a/T_0}Ze$. Subject to the initial condition of $\widetilde{\theta}(0) = 0$, the analytical solution for Eq. (3) is

$$\widetilde{\theta} = -\ln(1 - \widetilde{t}) \tag{4}$$

As $\widetilde{t} \to 1$, $|\widetilde{\theta}|$ approaches infinity as the linearized model break down, indicating the occurrence of thermal runaway. Accordingly, the ignition delay time for the adiabatic thermal runaway in dimensional form can be written as

$$t_{\text{ignition},0} = \frac{1}{ZeBY_{F,0}e^{-T_a/T_0}} \tag{5}$$

Considering volumetric heat loss in a homogeneous system, the temperature satisfies [14].

$$c_p\frac{dT}{dt} = q_cBY_Fe^{-T_a/T} - h(T - T_0) \tag{6}$$

where h is the heat transfer coefficient. Substituting Eq. (2) into Eq. (6) and retaining first order terms of $1/Ze$ yield the following equation for the temperature perturbation:

$$\frac{d\widetilde{\theta}}{d\widetilde{t}} = e^{\widetilde{\theta}} - \widetilde{h}\widetilde{\theta} \tag{7}$$

where $\widetilde{h} = h/(\rho c_v BY_{F,0}e^{-T_a/T_0}Ze)$ is the non-dimensional heat transfer coefficient. The presence of heat loss retards the accumulation of thermal energy and thereby extends the delay time for thermal runaway t_{ignition}. Integrating Eq. (7) yields

$$\frac{t_{\text{ignition}}}{t_{\text{ignition},0}} = \int_0^{\infty}\frac{d\widetilde{\theta}}{e^{\widetilde{\theta}} - \widetilde{h}\widetilde{\theta}} \tag{8}$$

The integral in Eq. (8) approaches infinity for $\widetilde{h} \geq e$, implying that thermal runaway can never occur for sufficiently severe heat loss. Consequently, the critical condition for thermal runaway is $\widetilde{h} = e$.

In general, ignition is associated with convective and conductive transport processes, which can be considered as effective heat loss for inhomogeneous combustion system. The energy conservation equation, in terms of non-dimensional temperature $\widetilde{T}$, has the following form [14]

$$\frac{\partial\widetilde{T}}{\partial t} + \nabla\cdot(\vec{v}\widetilde{T} - \alpha\nabla\widetilde{T}) = Bc_Fe^{-\tilde{T}_a/\tilde{T}} \tag{9}$$

where $\alpha = \lambda/(\rho c_p)$ is the thermal diffusivity of the mixture. The inclusion of convective and conductive transport in equation (9) suggests that the flow system exhibits inhomogeneities from a macroscopic perspective, due to the presence of temperature, mass fraction, and velocity gradients. However, when these gradients are not particularly strong, the local flow states within the reactive fluid element can be approximately regarded as homogeneous, and the gradients of temperature and mass fraction play a role in loss mechanisms. The chemical heat release within the reactive fluid element is balanced by convective and conductive heat loss in the chemically frozen fluid element nearby [14,185]. Usually, the lateral diffusion tangent to the reaction zone tends to be negligible. Consequently, the reaction zone can be treated as quasi-planar, and the conductive heat transfer is primarily in the normal direction, denoted by $\vec{n}$ [14]. In addition, as approaching the critical state for thermal runaway, the ignition delay time tends to be substantially longer than that for heat conduction and mass diffusion within the reaction zone. The separation of spatial and temporal scales suggests that the evolution of temperature in the reaction zone is determined by the competition between chemical heat release and heat conduction. The temperature variation in the reaction zone must be investigated in a zoom-in perspective by means of stretched coordinate, which is defined as $\widetilde{\chi} = nZe|\partial\widetilde{T}/\partial n|_0$. The factor $|\partial\widetilde{T}/\partial n|_0$ represents the magnitude of the temperature gradient outside the reaction zone, which is affected by the convective heat transfer. Applying the asymptotic analysis to Eq. (9), the temperature perturbation satisfies

$$\frac{d^2\widetilde{\theta}}{d\widetilde{\chi}^2} = -\frac{\Delta}{2}e^{\widetilde{\theta}} \tag{10}$$

where $\Delta = 2Bc_{F,0}Y_{O,0}e^{-T_a/T_0}/\left(\alpha|\partial\widetilde{T}/\partial n|_0^2Ze\right)$ is the modified Damköhler number [186]. Integrating Eq. (10) subject to the boundary conditions at $\widetilde{\chi} = 0$ and $\widetilde{\chi} \to \infty$, which are determined by matching with the temperature profile outside the reaction zone, one obtains [186]

$$\widetilde{\theta} = \ln\left(\frac{1}{\Delta}\left\{1 - \left[\frac{(1+\sqrt{1-\Delta})/(1-\sqrt{1-\Delta}) - e^{\mp\widetilde{\chi}}}{(1+\sqrt{1-\Delta})/(1-\sqrt{1-\Delta}) + e^{\mp\widetilde{\chi}}}\right]^2\right\}\right) \tag{11}$$

There is no solution for $\widetilde{\theta}$ when $\Delta \geq 1$, implying the occurrence of thermal runaway. Therefore, the critical ignition condition is $\Delta = 1$, which can be alternatively expressed in terms of temperature gradient [186]

$$\left|\frac{\partial\widetilde{T}}{\partial n}\right|_0 = \sqrt{\frac{2Bc_{F,0}e^{-T_a/T_0}}{\alpha Ze}} \tag{12}$$

Here $|\partial\widetilde{T}/\partial n|_0$ represents the temperature inhomogeneity experienced by the reaction zone. It can be determined by solving the temperature equation describing the heat transfer process in the outer region, which is controlled by both heat conduction and convection and is meanwhile affected by boundary conditions. Therefore, the value of $|\partial\widetilde{T}/\partial n|_0$ changes among various flow conditions.

The reaction rate strongly depends on the local temperature and pressure and so does the ignition delay time. When the temperature or pressure changes due to compression/expansion or heat transfer, the

time for thermal runaway also changes. In order to predict the occurrence of autoignition in a mixture whose temperature or pressure changes with time, Livengood and Wu [188] proposed an integration method. In the so-called Livengood-Wu (L-W) integral, the inverse of ignition delay time represents the reactivity and thermal runaway or autoignition occurs when the value of the L-W integral reaches unity [188]:

$$1 = \int_0^{t_{\text{ignition}}} \frac{1}{t_{\text{ch}}} dt' \tag{13}$$

where t_{ch} refers to the delay time of autoignition in a homogeneous system with an initial temperature identical to the central temperature of the hot spot at the current instant. The Livengood-Wu (L-W) integral records the progress of the transition from a chemically frozen state (corresponding to a large t_{ignition}) to the onset of vigorous chemical reactions (corresponding to small t_{ignition}), during which the accumulation of reactivity due to either temperature growth or radical production is appropriately taken into account [189,190]. The L-W integral has been popularly used to predict autoignition in ICEs with varying thermodynamic conditions [191]. Initially, the L-W integral was proposed for fuels with single-stage autoignition. Recently, the L-W integral has been extended for fuels with two-stage autoignition induced by low- and high-temperature chemistry [192,193]. Zhao et al. [194,195] have developed the staged L-W integral which is able to evaluate and predict the two-stage autoignition behavior for different fuels.

The L-W integral was initially proposed to predict the occurrence of homogeneous autoignition without heat and mass transport. However, during forced ignition, the mixture is not homogeneous, and the heat transport may greatly affect the local temperature of the ignition kernel/hot spot. Recently, Chen et al. [58] have proposed a method using the L-W integral to predict the critical ignition temperature of hot spot-induced ignition in a flammable mixture. In this method, first the transient temperature at the hot spot center is obtained by solving the 1D unsteady heat conduction equation. Then the ignition delay time at different central temperatures is obtained from a 0D calculation considering detailed chemistry. Finally, the critical ignition temperature is determined based on whether the L-W integral can reach unity. This method can significantly reduce the computational cost by two to three orders compared to transient simulation, taking into account detailed chemistry and transport [58]. The proposed method was tested for different mixtures, including methane/air, hydrogen/air, n-heptane/air, and dimethyl ether/air. Fig. 8 compares the critical ignition temperature predicted based on the L-W integral, $T_{H,\min,L-W}$, and that from detailed simulations, $T_{H,\min,\text{detailed}}$, for these mixtures. It is seen that good agreement is achieved for critical ignition temperatures below 2000 K. Though the method based on the L-W integral slightly over-predicts the critical ignition temperature, it is able to quickly give a conservative prediction of the critical ignition temperature, which is important for safety considerations.

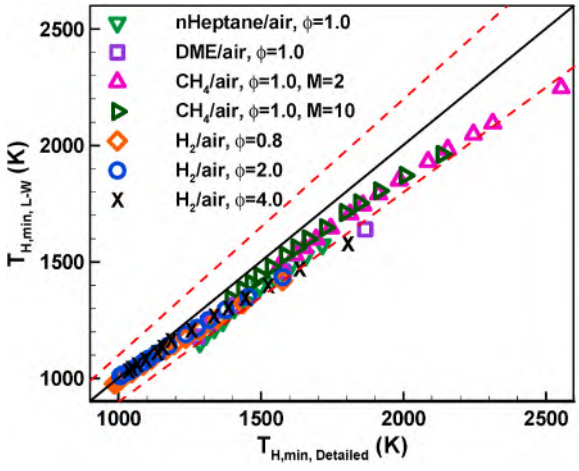

Fig. 8. Comparison of critical ignition temperature from prediction based on the L-W integral, $T_{H,\min,L-W}$, with those from detailed simulations, $T_{H,\min,\text{detailed}}$. The dashed lines denote the border of 10 % deviation of $T_{H,\min,L-W}$ from $T_{H,\min,\text{detailed}}$. Reprinted from Ref. [58] with permission from Elsevier.

It is noted that successful ignition refers to the generation of a self-sustained propagating flame, which is not assured by the occurrence of thermal runaway in real combustion problems. Therefore, additional ignition energy must be supplied to support the creation of a flame front subsequent to thermal runaway and to drive the flame front to a certain distance, i.e., the critical ignition radius R_{cr}, beyond which the flame propagation can be self-sustained [51,144]. This shall be discussed in the following sub-sections.

3.2. Thermal ignition theory

The homogeneity of the system consisting of a combustible mixture no longer remains as the appearance of flame, which can be regarded as an interface separating the unburned reactant and the burned product. Based on comprehensive experiments on spark ignition of various hydrocarbon fuels, Lewis and von Elbe [114] proposed the classical thermal ignition theory, which deals with the thermal balance between heat addition from chemical reactions and heat loss by conduction within the flame structure. Specifically, the minimum size of the spark kernel is determined by the requirement that the heat generation from chemical reactions within the kernel are in balance with the conductive heat transfer from the kernel surface. Accordingly, this minimum size of the spark kernel is regarded as the critical ignition radius, below which the conductive heat loss exceeds the chemical heat release and thereby the ignition kernel quenches.

As shown in Fig. 7, the thermal ignition theory considers the balance between conductive heat transfer and chemical heat release. The non-dimensional governing equation is

$$\frac{1}{\tilde{r}^2}\frac{d}{d\tilde{r}}\left(\tilde{r}^2\frac{d\tilde{T}}{d\tilde{r}}\right) + \tilde{\omega} = 0 \tag{14}$$

where $\tilde{r}$, $\tilde{T}$ and $\tilde{\omega}$ represent the nondimensional radial coordinate, temperature, and reaction rate.

Unless otherwise specified, the time, length, velocity, temperature, and mass fraction are non-dimensionalized as follows:

$$\tilde{t} = \frac{t}{\frac{d_L^0}{S_L^0}}, \tilde{r} = \frac{r}{d_L^0}, \tilde{U} = \frac{U}{S_L^0}, \tilde{T} = \frac{T}{T_{ad} - T_u}, \tilde{Y}_F = \frac{Y_F}{Y_{F,u}}, \tag{15}$$

where d_L^0 is the thickness of adiabatic planar premixed flame, and it is defined as $d_L^0 = \alpha/S_L^0$, with α being the thermal diffusivity of the unburned mixture and S_L^0 the laminar flame speed. The adiabatic flame temperature is $T_{ad} = T_u - q_c/(\rho_u c_p)$ with q_c being the heat release due to chemical reactions. In terms of α and S_L^0, the nondimensional reaction rate in Eq. (14) is $\tilde{\omega} = \alpha\omega/(S_L^0)^2$ [14]. Integrating Eq. (14) over the spherical domain of the ignition kernel whose radius is $\tilde{R}_{cr}$ yields

$$\frac{4}{3}\pi\tilde{R}_{cr}^3\tilde{\omega} \sim -4\pi\tilde{r}^2\frac{d\tilde{T}}{d\tilde{r}}\Big|_{\tilde{r}=\tilde{R}_{cr}} \tag{16}$$

The volume integration on the left-hand side is a simplification meant to provide an overall rate of energy release. Rigorously, the reaction rate within an ignition kernel is indeed not constant, varying spatially and temporally as the ignition proceeds. This approximation assumes an equivalent uniform distribution of average reaction intensity across the flame kernel. Despite the fact that such an approach may not capture local variations in reaction rate, it allows for the derivation of

useful insights into ignition kernel growth and evolution and facilitates a macroscopic view of the ignition process.

Equation (16) represents the requirement that the heat release rate from chemical reactions within the ignition kernel is equal to the rate of heat conduction loss from the kernel to the surrounding mixture. We assume there is no chemical reaction outside the ignition kernel, i.e., $\widetilde{r} > \widetilde{R}_{cr}$. Therefore, the temperature in the domain $\widetilde{r} > \widetilde{R}_{cr}$ satisfies

$$\frac{1}{\widetilde{r}^2}\frac{d}{d\widetilde{r}}\left(\widetilde{r}^2\frac{d\widetilde{T}}{d\widetilde{r}}\right) = 0 \tag{17}$$

The boundary conditions are

$$\widetilde{T}(\widetilde{r} = \widetilde{R}_{cr}) = \widetilde{T}_{ad}, \widetilde{T}(\widetilde{r}\to\infty) = \widetilde{T}_u \tag{18}$$

where $\widetilde{T}_u$ is the temperature of the unburned mixture, and $\widetilde{T}_{ad}$ is the temperature of the ignition kernel, which is usually approximated by the adiabatic flame temperature [14,114]. Solving Eq. (17) with boundary conditions (18) yields

$$\widetilde{T}(\widetilde{r}) = \widetilde{T}_u + (\widetilde{T}_{ad} - \widetilde{T}_u)\frac{\widetilde{R}_{cr}}{\widetilde{r}} \tag{19}$$

Substituting the temperature profile (19) into equation (16), one obtains

$$\frac{4}{3}\pi\widetilde{\omega}\widetilde{R}_{cr}^3 = 4\pi\widetilde{R}_{cr}(\widetilde{T}_{ad} - \widetilde{T}_u) \tag{20}$$

The nondimensional reaction rate and the difference in nondimensional temperature are correlated by $\widetilde{\omega} \sim \widetilde{T}_{ad} - \widetilde{T}_u$ [14]. The rationale for this correlation can be understood as follows: A stronger reaction and higher rate of heat release are directly related to a greater potential temperature increment, reflecting the system's capacity to convert chemical energy into thermal energy. The nondimensional reaction rate, denoted by $\widetilde{\omega}$, is defined in terms of the thermal diffusivity of the unburnt mixture α and the square of the laminar flame speed S_L^0, i.e., $\widetilde{\omega} = \alpha\omega/(S_L^0)^2$. This nondimensionalization process is designed to normalize the reaction rate by relevant physical quantities, facilitating a generalized analysis independent of specific units or scales. The nondimensional reaction rate $\widetilde{\omega}$ allows effective comparison of reaction rates across different systems and conditions.

Therefore, Eq. (20) suggests that $\widetilde{R}_{cr} \sim 1$, i.e., the critical ignition radius is comparable with the thickness of the standard premixed flame. In dimensional form, it has

$$R_{cr} \sim d_L^0 = \frac{\alpha}{S_L^0} \tag{21}$$

This is consistent with Zel'dovich's proposition [196] that the minimum radius of the ignition kernel leading to successful initiation of spherical flame is related to the thickness of laminar premixed flame. Equation (21) interprets the scaling relation of the critical ignition radius with the premixed flame thickness since only thermal transport is considered in thermal ignition theory. Regarding mass diffusion, the differential diffusion effect plays a decisive role in determining the ratio factor between R_{cr} and d_L^0, which is a function of Lewis number [144].

The MIE was proposed to be the energy required to heat a sphere in the critical ignition radius to the adiabatic flame temperature [114,196]:

$$E_{\min} \sim \frac{4}{3}\pi R_{cr}^3\rho c_p(T_{ad} - T_u) \tag{22}$$

In experiments, it is difficult to determine the critical ignition radius. According to Lewis and Elbe [114], the critical ignition radius is correlated with the quenching distance $d_{\text{spark,optimal}}$, which for spark ignition refers to the optimal electrode separation corresponding to the MIE. It is consistent with the experimental observations that the MIE is proportional to the cube of quenching distance, i.e., $E_{\min} \sim d_{\text{spark,optimal}}^3$. Williams [197] suggested that the quenching distance is proportional to the flame thickness, through which the thermo-chemical properties of the reactant mixture were suitably taken into account.

The critical ignition radius and MIE given by the thermal ignition theory, i.e., Eq. (21) and (22) above, well explain the effects of mixture composition (equivalence ratio, dilution) and thermal states (initial temperature and pressure) on ignition [114]. For example, the thermal ignition theory explains why it is difficult to achieve successful ignition at low pressure, which is related to high-altitude relight in jet engines. At lower pressure, the flame thickness becomes larger, as does the critical ignition radius. Consequently, according to Eq. (21), a larger MIE is required at lower pressure [114,198]. In addition, there are alternative factors beyond increased flame thickness. The lower ambient temperatures at high altitudes, along with reduced oxygen levels, can make it tremendously difficult to initiate combustion.

The thermal ignition theory also explains why it is difficult to achieve successful ignition in ultra-lean mixtures used in advanced SIEs [16–19]. The flame thickness of an ultra-lean mixture is much larger than that of a stoichiometric mixture, and so is the critical ignition radius. Therefore, Eq. (21) indicates that a much higher MIE is required for an ultra-lean mixture than for a stoichiometric mixture.

However, the thermal ignition theory only phenomenologically interprets premixed flame ignition since the processes involving reactant consumption by chemical reaction and reactant supply by mass diffusion were not considered. As shown in Fig. 7, the thermal ignition theory considers only the governing equation for temperature, without including the equations for the mass fraction of the deficient reactant. More accurate theory on premixed flame ignition must incorporate the description for the variation of reactant and thus reveal the effects of differential diffusion of heat and mass, characterized by Lewis number, during the ignition process [161,199]. Moreover, the ignition kernel has a large curvature and stretch rate, which greatly affect the propagation speed of the ignition kernel when the Lewis number is apparently different from unity. Therefore, the thermal ignition theory has been extended to consider both heat and mass diffusion (i.e., flame ball theory) and flame kernel propagation (quasi-steady ignition theory and transient ignition theory), which shall be discussed in the following sub-sections.

3.3. *Ignition theory considering both heat and mass diffusion (flame ball theory)*

Zel'dovich [200] derived a solution for stationary spherical flames or flame balls in the unbounded domain of static combustible mixtures. The flame front has zero moving speed relative to the unburned mixture, and there is no convective transport of heat and mass. The flame ball is sustained by mass diffusion and heat conduction, and thereby the Lewis number is a key parameter that determines the flame temperature and radius of the flame ball. A schematic diagram of a flame ball is shown in Fig. 9. Inside the flame ball, the burned products have a uniform flame temperature of T_f when radiative heat loss is neglected. Outside the

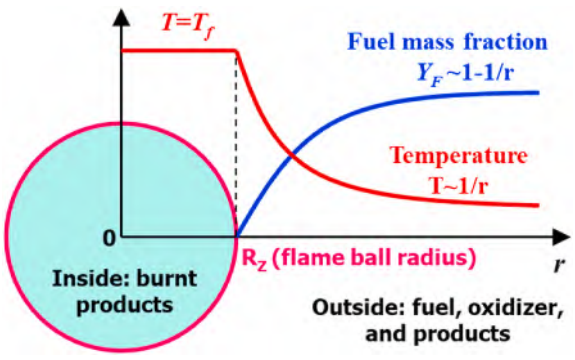

Fig. 9. Schematic diagram of a flame ball.

flame ball, there is no chemical reaction, and the temperature and fuel mass fraction are both proportional to the inverse of the radial coordinate [200]. Zel'dovich [200] showed that the normalized flame temperature is equal to the inverse of the Lewis number, i.e., $(T_f - T_u)/(T_{ad} - T_u) = 1/Le$. Moreover, the flame ball radius, R_Z, monotonically increases with the Lewis number.

The flame ball theory by Zel'dovich [200] is based on the AEA framework and the thin-flame assumption, which provide valuable insights into flame dynamics with acceptable mathematical tractability. More importantly, it has interpreted the unique conditions of flame balls and the dependence of flame ball radius on the thermodynamic and physicochemical properties of the combustible mixture. However, it should be acknowledged that the simplifications inherent in AEA and thin-flame models may overlook essential physiochemical mechanisms that are vital for accurately describing flame ball characteristics. For instance, the AEA theoretical approach may not be able to reveal the role of radicals in lowering activation energy and influencing flame stability at low temperatures [11].

3.3.1. Structure of flame ball

When the instabilities on the flame front are not taken into account, the flame ball is treated as one-dimensional due to its spherical symmetry, i.e., the geometric characteristic is interpreted by the radius from the origin, and the polar and azimuthal angles become degenerate. A theoretical interpretation of the flame ball can be obtained based on the thermal-diffusive model [109,151,201], in which the thermodynamic and transport properties of the reactant, i.e., density ρ, heat capacity at constant pressure c_p, thermal conductivity λ and mass diffusivity D are assumed to be constants. The reference length for the flame ball can be selected as the flame thickness, d_L^0, of the adiabatic planar flame, which propagates at the standard laminar flame speed S_L^0. The propagation of standard laminar speed is determined by the competition between molecular transport (mass diffusion and thermal conduction) and the chemical reaction. The value of S_L^0 can be obtained in terms of transport properties and key parameters describing the rate for a first-order one-step Arrhenius type chemical reaction [14], i.e.,

$$S_L^0 = \frac{\widetilde{T}_{ad}^2}{\widetilde{T}_a}\sqrt{2\alpha LeBe^{-\widetilde{T}_a/\widetilde{T}_{ad}}} \tag{23}$$

According to the definition of non-dimensional quantities defined in Eq. (15), the non-dimensional governing equations for energy and mass fraction of the deficient reactant F are

$$\frac{\partial \widetilde{T}}{\partial \widetilde{t}} = \frac{1}{\widetilde{r}^2}\frac{\partial}{\partial \widetilde{r}}\left(\widetilde{r}^2\frac{\partial \widetilde{T}}{\partial \widetilde{r}}\right) + \frac{Ze^2\widetilde{c}_F}{2Le}\exp\left[-Ar\left(\frac{\widetilde{T}_{ad}}{\widetilde{T}} - 1\right)\right] \tag{24}$$

$$\frac{\partial \widetilde{Y}_F}{\partial \widetilde{t}} = \frac{1}{Le}\frac{1}{\widetilde{r}^2}\frac{\partial}{\partial \widetilde{r}}\left(\widetilde{r}^2\frac{\partial \widetilde{Y}_F}{\partial \widetilde{r}}\right) - \frac{Ze^2Y_F}{2Le}\exp\left[-Ar\left(\frac{\widetilde{T}_{ad}}{\widetilde{T}} - 1\right)\right] \tag{25}$$

where the non-dimensional time and radial coordinate are defined as $\widetilde{t} = t/t_L^0$ and $\widetilde{r} = r/d_L^0$. The activation temperature is incorporated into the Zel'dovich number Ze and Arrhenius number Ar, which are defined as $Ze = T_a(T_{ad} - T_u)/T_{ad}^2$ and $Ar = T_a/T_{ad}$, respectively. For a steady-state flame ball, the time-dependent terms in Eqs. (24) and (25) can be removed, and the resulting ordinary differential equations are subjected to the following boundary conditions:

$$\widetilde{r} = 0 : d\widetilde{T}/d\widetilde{r} = 0, d\widetilde{c}_F/d\widetilde{r} = 0 \tag{26}$$

$$r \to \infty : \widetilde{T} = \widetilde{T}_u, \widetilde{c}_F = 1 \tag{27}$$

In the limit of large activation energy, the inverse of Zel'dovich number can be identified as the small parameter, i.e., $\epsilon = 1/Ze \ll 1$, based on which the flame structure can be solved by asymptotic analysis. The vigorous reaction is concentrated in a restricted region that is substantially thinner than the flame thickness. Therefore, in leading order approximation, the reaction zone can be considered an interface of zero thickness, and accordingly, the jump conditions across the reaction zone are determined as

$$\left(\frac{d\widetilde{T}}{d\widetilde{r}} + \frac{1}{Le}\frac{d\widetilde{c}_F}{d\widetilde{r}}\right)_{\widetilde{r}=\widetilde{R}_{Z-}}^{\widetilde{r}=\widetilde{R}_{Z+}} = 0 \tag{28}$$

$$\left(\frac{d\widetilde{T}}{d\widetilde{r}}\right)_{\widetilde{r}=\widetilde{R}_{Z-}} - \left(\frac{d\widetilde{T}}{d\widetilde{r}}\right)_{\widetilde{r}=\widetilde{R}_{Z+}} = \frac{\widetilde{T}_f^2}{\widetilde{T}_{ad}^2}\exp\left[-\frac{Ar}{2}\left(\frac{\widetilde{T}_{ad}}{\widetilde{T}_f} - 1\right)\right] \tag{29}$$

where $\widetilde{T}_f = T_f/(T_{ad} - T_u)$ is the non-dimensional temperature of the adiabatic flame ball, and $\widetilde{R}_Z = R_Z/d_L^0$ is the flame ball radius (see Fig. 9). The subscripts "+" and "−" respectively, refer to the unburned and burned regions separated by the flame front. Removing the unsteady and chemical reactions in Eqs. (24) and (25), the steady profiles of temperature and reactant mass fraction in the unburned and burned regimes can be obtained as follows:

$$\widetilde{T}(\widetilde{r}) = \begin{cases} \widetilde{T}_f \text{ for } \widetilde{r} < \widetilde{R}_Z \\ \widetilde{T}_f + \dfrac{\widetilde{R}_Z}{\widetilde{r}}\left(\widetilde{T}_f - \widetilde{T}_u\right) \text{ for } \widetilde{r} > \widetilde{R}_Z \end{cases} \tag{30}$$

$$\widetilde{Y}_F(\widetilde{r}) = \begin{cases} 0 \text{ for } \widetilde{r} < \widetilde{R}_Z \\ 1 - \dfrac{\widetilde{R}_Z}{\widetilde{r}} \text{ for } \widetilde{r} > \widetilde{R}_Z \end{cases} \tag{31}$$

Substituting the above expressions into the matching conditions (28) and (29), one obtains the following expressions for the flame temperature and flame ball radius, which can be determined as

$$\widetilde{T}_f = \widetilde{T}_u + \frac{1}{Le} \tag{32}$$

$$\widetilde{R}_Z = \frac{\widetilde{T}_{ad}^2}{Le\widetilde{T}_f^2}\exp\left[\frac{Ar}{2}\left(\frac{\widetilde{T}_{ad}}{\widetilde{T}_f} - 1\right)\right] \tag{33}$$

Note that the adiabatic flame temperature of a planar premixed flame is $\widetilde{T}_{ad} = 1 + \widetilde{T}_u$, which is independent of Lewis number. However, Eq. (32) indicates that the flame ball temperature depends on Lewis number of the deficient reactant. For $Le < 1$, we have $\widetilde{T}_f > \widetilde{T}_{ad}$, and the flame ball temperature is much higher than the adiabatic flame temperature when the Lewis number is much less unity. This makes the existence of flame ball in mixtures far below their lean flammability limits.

The expansion ratio is defined as $\sigma = T_u/T_{ad}$, which can be considered the density ratio across an adiabatic planar premixed flame. Substituting Eq. (32) into Eq. (33) yields a nonlinear equation for flame ball radius

$$\widetilde{R}_Z = \frac{Le}{(Le\sigma + 1 - \sigma)^2}\exp\left[\frac{Ar(Le-1)(1-\sigma)}{2(\sigma Le + 1 - \sigma)}\right] \tag{34}$$

Fig. 10 plots the change of normalized flame ball temperature and flame ball radius with Lewis number as predicted by Eq. (32) and (34). It is observed that the flame ball radius increases exponentially with Lewis number, and it is equal to the thickness of an adiabatic planar premixed flame for $Le = 1$. For $Le < 1$, the flame ball radius is smaller than the flame thickness, i.e., $R_Z < d_L^o$, and the flame ball temperature is higher than the adiabatic flame temperature of a planar flame, i.e., $T_f > T_{ad}$. This indicates that mixtures with low Lewis numbers, e.g., fuel-lean hydrogen/air, can be ignited relatively more easily [162,202] and flame balls can observed outside the flammability limit (see. In the opposite situation with $Le > 1$, we have $R_Z > d_L^o$, and $T_f < T_{ad}$). Consequently, it is relatively more difficult to ignite mixtures with large Lewis

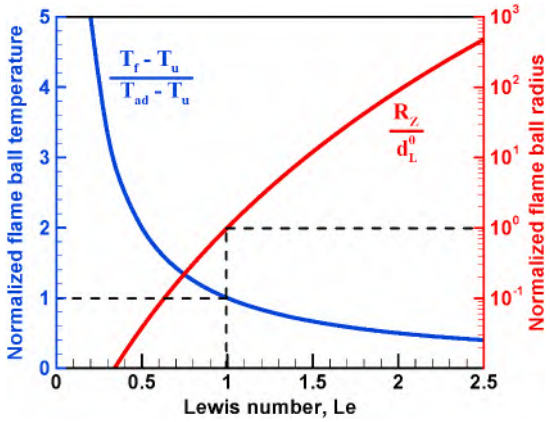

Fig. 10. Change of normalized flame ball temperature and flame ball radius with Lewis number for $\sigma = 0.2$ and $= 12.5$.

number, e.g., fuel-lean n-heptane/air [12,157].

3.3.2. Stability of flame ball

In actual situations, flame ball is subject to various perturbations. Accordingly, the stability of the flame front plays an essential role in affecting the eventual evolution of the flame ball [7,203]. Adopting large activation energy asymptotic analysis, Deshaies and Joulin [199] and Buckmaster and Weeratunga [204] analyzed the structure of flame ball and found that adiabatic flame balls without radiative heat loss are inherently unstable: a small perturbation causes the flame to propagate either inwardly and eventually collapses and extinguishes, or outwardly and possibly develops into a propagating flame.

In linear stability analysis, the amplitude of perturbation is assumed to be infinitesimal and can be decomposed into Fourier normal modes. Accordingly, the perturbed temperature, mass fraction of the deficient reactant, and flame radius can be written in the following form

$$\begin{bmatrix} \widetilde{T}(\widetilde{r},\widetilde{t}) \\ \widetilde{Y}_F(\widetilde{r},\widetilde{t}) \\ \widetilde{R}_Z(\widetilde{t}) \end{bmatrix} = \begin{bmatrix} \widetilde{T}_m(\widetilde{r}) \\ \widetilde{Y}_{F,m}(\widetilde{r}) \\ \widetilde{R}_{Z,m} \end{bmatrix} + \widetilde{R}_{Z,p} e^{\widetilde{\Omega}\widetilde{t}} \begin{bmatrix} \widetilde{T}_p(\widetilde{r}) \\ \widetilde{Y}_{F,p}(\widetilde{r}) \\ 1 \end{bmatrix} \tag{35}$$

where the subscript "m" refers to the unperturbed state of the flame ball, and "p" indicates the perturbation imposed on the relevant quantities. The perturbations in temperature and reactant mass fraction result from the perturbation of flame ball radius, $\widetilde{R}_{Z,p}$, which is thus regarded as a small parameter, i.e., $\widetilde{R}_{Z,p}/\widetilde{R}_Z \ll 1$. The frequency $\widetilde{\Omega}$ could be a complex quantity. The imaginary part of ω describes the periodic variation of the perturbed component, and the real part interprets the temporal variation of the magnitude of the perturbed quantity, i.e., the stability of the perturbed quantities over time. The perturbed temperature and reactant molar fraction grow (decay) exponentially providing that $\mathrm{Re}(\widetilde{\Omega}) > 0$ (0.

The perturbed components $\widetilde{T}_p$ and $\widetilde{c}_{Fp}$ should be obtained by substituting Eq. (35) into Eq. (24) and (25) without the chemical reaction terms and using the boundary conditions (26) and (27) and the continuity condition across the reaction zone, i.e.,

For $0 < \widetilde{r} < \widetilde{R}_Z$:

$$\widetilde{T}_p = \frac{(1-\sqrt{Le})}{2\widetilde{r}Le}\left[e^{-(\widetilde{R}_Z+\widetilde{r})\sqrt{\widetilde{\Omega}}} - e^{-(\widetilde{R}_Z-\widetilde{r})\sqrt{\widetilde{\Omega}}}\right] \tag{36}$$

$$\widetilde{c}_{Fp} = 0 \tag{37}$$

For $\widetilde{R}_Z < \widetilde{r} < \infty$:

$$\widetilde{T}_p = \frac{(1-\sqrt{Le})e^{-2\sqrt{\widetilde{\Omega}}\widetilde{R}_Z} + 1 + \sqrt{Le}}{2\widetilde{r}Le} e^{-(\widetilde{r}-\widetilde{R}_Z)\sqrt{\widetilde{\Omega}}} \tag{38}$$

$$\widetilde{c}_{Fp} = -\frac{1}{\widetilde{r}} e^{-(\widetilde{r}-\widetilde{R}_Z)\sqrt{Le\widetilde{\Omega}}} \tag{39}$$

The perturbed temperature and reactant molar fraction must satisfy the matching conditions (28) and (29). Accordingly, the dispersion relation in terms of the complex frequency can be obtained

$$\left(1-e^{-2\sqrt{\widetilde{\Omega}}\widetilde{R}_Z}\right)\left[F_{Le}+\sqrt{Le}\left(\sqrt{\widetilde{\Omega}}\widetilde{R}_Z-1\right)\right]+\left(1+e^{-2\sqrt{\widetilde{\Omega}}\widetilde{R}_Z}\right)\left(\sqrt{\widetilde{\Omega}}\widetilde{R}_Z-1\right)=0 \tag{40}$$

in which the factor F_{Le} is defined as

$$F_{Le} = \frac{\sqrt{Le}-1}{Le}\left[\frac{ZeLe^2}{(\sigma Le+1-\sigma)^2} + 4Le + \frac{4}{\widetilde{T}_{ad}}\right] \tag{41}$$

It can be verified that the real positive solution of $\sqrt{\widetilde{\Omega}}$ always exists for Eq. (40). The left-hand side of Eq. (40) is equal to -2 at $\sqrt{\widetilde{\Omega}}\widetilde{R}_Z = 0$ and grows unbounded as $\sqrt{\widetilde{\Omega}}\widetilde{R}_Z$ becomes large. This implies that the dispersion relation must have a positive root $\widetilde{\Omega}$, i.e., the real part of the frequency $\widetilde{\Omega}$ is definitely positive and the flame ball is unstable.

The analysis of Deshaies and Joulin [199] showed that an adiabatic flame ball is unstable, explaining why the flame ball predicted by Zel'dovich's theory in 1940s has not been observed in experiments for about half a century. However, Ronney et al. [205] discovered accidently stable flame balls in micro-gravity drop-tower experiments in lean hydrogen/air mixtures $Le \approx 0.3$. Stable flame balls were also observed later in aircraft microgravity experiments for other mixtures with low Lewis numbers by Ronney et al. [206]. To explain the contradiction between the theoretical analysis of Deshaies and Joulin [199] and the experimental observations of Ronney et al. [4], Buckmaster et al. [7,203] took into the volumetric radiative heat loss in their analysis of the flame ball. They derived the following relationship between the normalized flame ball radius $\widetilde{R}_Z$ and the normalized heat loss $\widetilde{L}$:

$$\widetilde{L} = \widetilde{R}_Z^{-2} \ln(\widetilde{R}_Z) \tag{42}$$

Fig. 11 shows the results predicted by the above relationship. It is observed that there are two flame ball radii when the heat loss intensity is below some critical value. The 'large' flame ball (solid black line in Fig. 11) is stabilized by volumetric heat loss. When the flame ball radius increases/decreases due to perturbation, the ratio of total radiative heat loss to total heat release increases/decreases, and thereby the flame ball becomes weaker/stronger and shrinks/expands. The radiative role plays a profound impact upon the energy balance within the flame ball, while

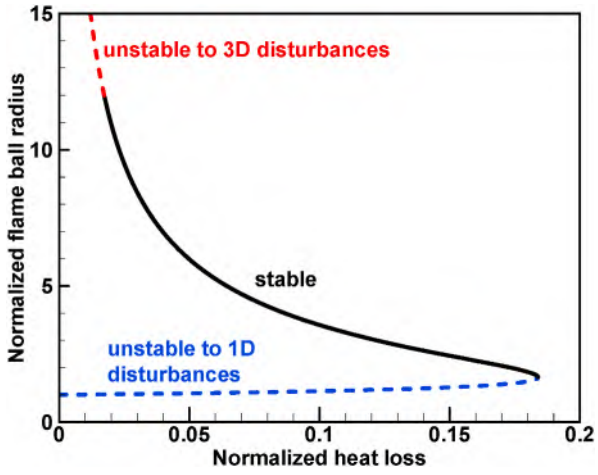

Fig. 11. Change of normalized flame ball radius with the normalized heat loss. The regimes of stability are shown. Figure refurbished from Ref. [7] with permission from Elsevier.

it should not be regarded as the single mechanism stabilizing the flame ball. In theoretical analysis, the stabilization of flame balls can be achieved without explicitly modeling radiative heat loss. There exist alternative stabilization mechanisms, relevant to higher order diffusive processes, detailed chemical kinetics, and the interplay between heat generation and convective cooling within the flow field [101,207]. The analysis by Lee and Buckmaster [208] showed that stable flame balls can only exist in mixtures with Lewis numbers below a critical value, which is consistent with the micro-gravity experiments on flame balls by Ronney and coworkers [4,209].

The stability analysis of the flame ball provides a fundamental understanding of the critical conditions for premixed flame ignition. According to the above analysis, the critical ignition radius represents the threshold intensity of stretch at which the heat release from reaction and overall heat loss are almost in balance, rendering the propagation speed of the flame front exceedingly slow [156,210]. Comparing with the planar laminar flame thickness d_L^0, a more suitable choice of the critical radius for premixed flame ignition should be the flame ball radius. The dispersion relation (40) tells the spontaneous behavior of the spherical flame close to the flame ball radius, i.e., shrinking and finally quenching for $R < R_Z$ and developing to ever-expanding spherical flame otherwise. In addition, the presence of an ignition source may quantitatively alter the characteristics of the flame ball, which then exhibits its impacts on the outcome of premixed flame ignition. The general feature forced-ignition process shall be reviewed in the next subsection.

3.3.3. Critical ignition radius based on flame ball with central heating

The instability of adiabatic flame ball demonstrates that the flame front subject to positive disturbance can propagate unboundedly. The unstable equilibrium flame ball radius was therefore considered to be a critical size in controlling flame initiation, and the MIE was proposed to be proportional to the cube of the flame ball radius instead of the flame thickness [161,196,211]. Since the flame ball radius strongly depends on the Lewis number [196], the MIE for mixtures with different Lewis numbers is totally different. This was confirmed by numerical simulation using a one-step chemistry [163].

In forced-ignition of premixed flame, the addition of thermal energy to the mixture is achieved through external heating, which, for simplicity, is usually considered a point source of constant power, denoted by Q_m [161,211,212]. The presence of external heating introduces excess enthalpy to the reaction zone due to thermal conduction, which reduces the flame ball radius [12,144]. However, according to the theoretical formulation presented by Joulin and coworkers [161,199], the existence and stability of flame balls are significantly affected by the external central heating. In addition to the conventional flame ball solution, there is another flame ball solution caused by the heating source.

The heating power of an external source could be made non-dimensional, denoted by $\widetilde{Q}_m$, i.e.,

$$\widetilde{Q}_m = \frac{Q_m}{4\pi\alpha\delta_L^0 Q_c} \tag{43}$$

In general, the origin of external heating is placed at the center of flame ball, and accordingly, the boundary conditions for temperature profile at $\widetilde{r} = 0$ would be revised to [161,211,212]

$$\widetilde{r} = 0, \widetilde{r}^2\frac{d\widetilde{T}}{d\widetilde{r}} = -\widetilde{Q}_m \tag{44}$$

Because of large activation energy, the chemical reaction rate is exceedingly sensitive to temperature. It is expected that an order of $O(1/Ze)$ intensity of external heating could lead to a considerable reduction in flame ball radius. Providing that $\widetilde{Q}_m Ze/\widetilde{R}_Z \sim O(1)$, the matching conditions (28) and (29) remain valid. The flame temperature is revised to

$$\widetilde{T}_f = \widetilde{T}_u + \frac{1}{Le} + \frac{\widetilde{Q}_m}{\widetilde{R}_Z} \tag{45}$$

Substituting $\widetilde{T}_f$ given by Eq. (45) into Eq. (33), the flame ball radius can be determined,

$$\frac{\widetilde{R}_Z}{Le}e^{Ar/2}\left(Le\sigma+1-\sigma+Le\widetilde{Q}_m\frac{1-\sigma}{\widetilde{R}_Z}\right)^2 = \exp\left[\frac{ArLe}{2(Le\sigma+1-\sigma+Le\widetilde{Q}_m(1-\sigma)/\widetilde{R}_Z)}\right] \tag{46}$$

which becomes identical to Eq. (34) for $\widetilde{Q}_m = 0$.

As shown in Fig. 12, at relatively low heating power Eq. (46) yields a pair of solutions for flame ball radius. According to Deshaies and Joulin [199] the smaller flame ball solution is stable. This indicates that for sufficiently low heating power, a flame ball can be stabilized by constant supply of ignition energy. This demonstrates that, in addition to ignition energy, the heating power of the ignition source also plays a decisive role in determining the ignition outcome. Consequently, the concept of minimum (critical) heating power must be introduced [12,109]. Fig. 12 shows that the pair of solutions merge at the critical heating power, denoted by $\widetilde{Q}_{m,cr}$, beyond which no stationary flame ball exists. For $\widetilde{Q}_m > \widetilde{Q}_{m,cr}$, the flame front originated from external heating exhibits a continually propagating spherical flame. Consequently, $\widetilde{Q}_{m,cr}$ is defined as the critical heating power for forced ignition, and the corresponding flame ball radius can thus be defined as the critical ignition radius, denoted by $\widetilde{R}_{Z,cr}$ [161].

The formation and propagation of the highly-stretched ignition kernel are important for premixed flame ignition. However, they are not considered in the flame ball theory. Consequently, the critical ignition conditions might be over-predicted by analysis based on the flame ball [12]. In the following subsections, ignition kernel formation and propagation will be discussed.

3.4. Ignition kernel formation in quiescent mixture by external heating

The formation of the ignition kernel plays a crucial role in determining the ignition process and thereby, has been widely examined in previous studies. Herweg and Maly [213] proposed a one-dimensional, time-dependent numerical model describing the flame kernel development in spark ignition engines based on a strained flamelet model. This model can predict the effects of various operation conditions on the phenomena of misfire or flame quenching. Hernández-Pérez et al. [214] conducted simulations on the creation of steady, stable and close reacting fronts in ultra-lean hydrogen-methane-air mixtures. Their

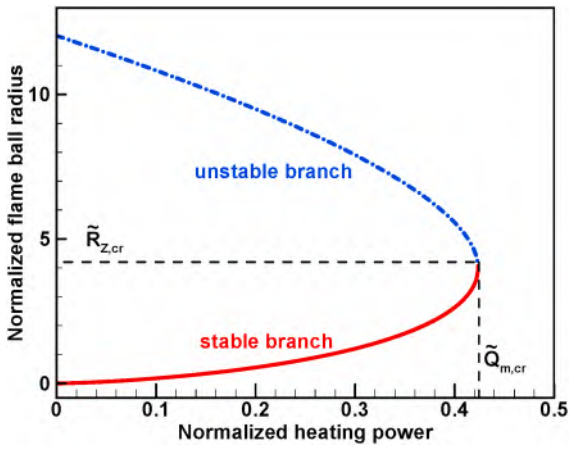

Fig. 12. Change of normalized flame ball radius with normalized heating power predicted by Eq. (46) for $Le = 1.5$, $Ar = 12.5$ and $\sigma = 0.2$. Reprinted from Ref. [161] with permission from Elsevier.

simulation results showed that, under normal gravity, the heat loss of ball-like flame by thermal radiation tends to be negligible in comparison with those due to thermal conduction and convection. Premixed flame ignition in a quiescent mixture consists of two phases: ignition kernel formation and subsequent transition to self-sustained expanding spherical flame. In this subsection, we shall briefly introduce the theoretical understandings on the ignition kernel formation. The second phase of ignition kernel propagation will be thoroughly reviewed in the next subsection.

Yu et al. [51] conducted a theoretical analysis on the evolution of ignition kernel induced by external heating within a finite domain and for a finite duration. The ignition kernel formation consists of three stages: (1) onset of thermal runaway during pure heating of a combustible mixture, (2) generation of reaction front due to depletion of reactant at the heating center, and (3) propagation of the reaction front to the edge of the heating domain. A schematic for the characteristic time scales involved in the ignition kernel formation is shown in Fig. 13.

For combustible premixtures subject to igniting sources, the local temperature increases over time. This eventually leads to thermal runaway, which is characterized by a certain delay time, denoted by $t_{\text{explosion}}$, as illustrated in Fig. 13. Following thermal runaway, the reactant continues to be consumed locally, and in specific, the mass fraction of reactant becomes vanishing at time $t_{\text{consumption}}$. It implies the formation of reaction front, which propagates outward. Since thermal runaway and establishment of reaction front are sequential processes, the characteristic time for reaction formation is $t_{\text{front}} = t_{\text{explosion}} + t_{\text{consumption}}$. The formation of ignition kernel can be understood as the passage of the reaction front beyond the ignition source domain. In the presence of continuous supply of ignition energy, the reactant premixture is of high temperature within this domain, and therefore, the propagation of reaction is assisted by autoignition. The time needed for the reaction front to reach the edge of the ignition domain is denoted by $t_{\text{propagation}}$. Consequently, the total time for the formation of the ignition kernel, represented by t_{kernel} can be calculated as $t_{\text{kernel}} = t_{\text{explosion}} + t_{\text{consumption}} + t_{\text{propagation}}$ [51].

For each stage involved in the ignition kernel formation, there is a critical heating power as depicted in Fig. 14 [51]. The first critical heating power density $Q_{cr,\text{runaway}}$ defines the lowest rate of ignition energy input below which the thermal runaway can never be observed in the combustible in spite of everlasting external source. In situations with $Q_m < Q_{cr,\text{runaway}}$, the ignition energy deposition is completely balanced with conductive heat loss, resulting in zero accumulation of thermal energy. The second and third critical heating power densities $Q_{cr,\text{front}}$ and $Q_{cr,\text{kernel}}$ respectively characterize the occurrence of reaction front and the subsequent propagation to the edge of heating domain. Those two critical heating power densities are defined subject to the condition that external heating source is removed at the instant of thermal runaway. In situations with $Q_{cr,\text{runaway}} < Q_m < Q_{cr,\text{front}}$, the initiated chemical

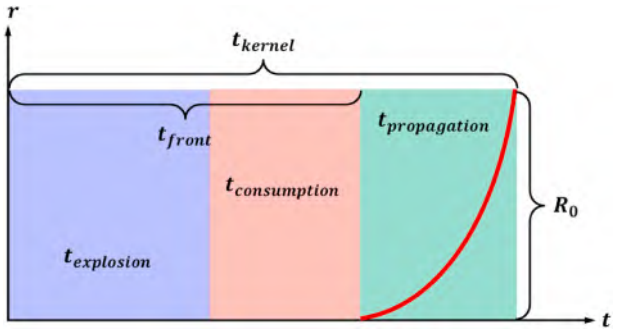

Fig. 13. The schematic for the characteristic time scales involved in the ignition kernel formation. The red solid line represents the propagation of reaction front from the center to the edge of ignition kernel. Reprinted from Ref. [51] with permission from Elsevier.

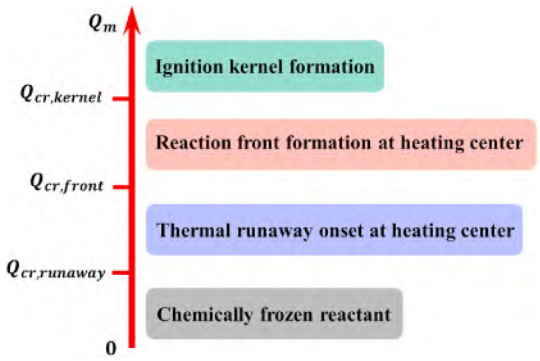

Fig. 14. The schematic for different critical heating power densities. The central heating is removed at the onset of thermal runaway, i.e., $t_0 = t_{\text{explosion}}$. Reprinted from Ref. [51] with permission from Elsevier.

reaction by thermal runaway would be rapidly terminated before establishing the reaction front, which can be understood that the chemical heat release is slower than conductive heat loss. At further higher heating power densities satisfying $Q_{cr,\text{front}} < Q_m < Q_{cr,\text{kernel}}$, the propagation speed of the reaction front is so slow that the considerable temperature drop in the absence of external heating leads to flame quench and thus forbids the ignition kernel formation. For sufficiently high heating power density, i.e., $Q_m > Q_{cr,\text{kernel}}$, the intensive ignition energy deposition can effectively increase the temperature within the heating domain and thereby ensures the successful ignition kernel formation. The schematic of three critical heating power densities corresponding to individual degree of ignition kernel formation is shown in Fig. 14.

The detailed analysis of each stage (including its characteristic time scale and critical heating power density) during ignition kernel formation can be found in Ref. [51]. Only the main results are presented here. Considering the process of ignition kernel formation due to external heating of finite domain and duration, it is not convenient to use the nondimensional time and radius previously defined in terms of standard flame thickness d_L^0 and the characteristic time scale d_L^0/S_L^0 based on laminar flame speed. For instance, the finite domain of the ignition source provides a suitable candidate for the characteristic length scale during ignition kernel formation. This necessitates a redefinition of nondimensionalization to accurately reflect the specific conditions and scales relevant to the external heating of a finite domain and the subsequent flame kernel evolution. However, to avoid extra mathematical complexity, we shall transform the mathematical formulation into a partially non-dimensional form. Specifically, the temperature and mass fraction of the deficient reactant F are converted into their non-dimensional expression given by Eq. (15), while the radial coordinate and time remain in their dimensional form. The governing equations describing the ignition kernel formation are presented in the following form

$$\frac{\partial \widetilde{T}}{\partial t} = \frac{1}{r^2}\frac{\partial}{\partial r}\left(r^2\alpha\frac{\partial \widetilde{T}}{\partial r}\right) + \frac{\Phi(r,t)}{Q_c c_{F0}} + \omega \tag{47}$$

$$\frac{\partial \widetilde{Y}_F}{\partial t} = \frac{1}{r^2}\frac{\partial}{\partial r}\left(r^2 D\frac{\partial \widetilde{Y}_F}{\partial r}\right) - \omega \tag{48}$$

where Φ represents the rate of thermal energy deposition by spark discharge within a spherical domain of radius R_0 and lasting for a finite duration t_0 at constant power density Q_m. The energy deposition can be expressed in terms of the Heaviside function $H(x)$, i.e.,

$$\Phi(r,t) = Q_m[H(r) - H(r - R_0)][H(t) - H(t - t_0)] \tag{49}$$

The reaction rate for one-step chemistry in Arrhenius form is:

$$\omega = B\widetilde{Y}_F e^{-\widetilde{T}_a/\widetilde{T}} \tag{50}$$

The initial and boundary conditions are:

$$\begin{cases} t = 0 : \widetilde{T} = \widetilde{T}_u, \ \widetilde{c}_F = 1 \\ r = 0 : \partial\widetilde{T}/\partial r = 0, \partial\widetilde{Y}_F/\partial r = 0 \\ r \to \infty : \widetilde{T} = \widetilde{T}_u, \widetilde{Y}_F = 1 \end{cases} \tag{51}$$

Before autoignition onset, heat release from chemical reactions tends to be insignificant. Accordingly, the chemical reaction terms on the right-hand side of Eq. (47) and (48) can be neglected. The solution for $\widetilde{c}_F$ subject to the initial and boundary conditions is trivial, i.e., $\widetilde{c}_F = 1$ in the whole space. With help of Green's function, the transient evolution of temperature distribution can be determined analytically [51]. This indicates that the highest temperature can be found at the center of heating domain. Consequently, autoignition first takes place at the heating center. Analytical solutions indicate that the central temperature $\widetilde{T}_{\text{center}}$ grows almost linearly with time, the slop of which is proportional to the heating power density. At the end of the heating duration, the central temperature appears to be saturated, whose magnitude depends upon both the power density and duration of the external heating source. Due to the presence of an external heating source, the central temperature continuously increases. Therefore, the historical effect must be taken into account when evaluating the delay time of thermal runaway, which can be determined by the Livengood-Wu integral [189,190], i.e.,

$$1 = \int_0^{t_{\text{explosion}}} \frac{1}{t_{\text{ch}}} dt \tag{52}$$

where t_{ch} represents the characteristic time for the chemical reaction and is the ignition delay time for a homogeneous system with an initial temperature equal to the given central temperature. According to Eq. (5), t_{ch} is given in the following form:

$$t_{\text{ch}} = \frac{e^{T_a/T_{\text{center}}}}{ZeBY_{F,0}} \tag{53}$$

The second stage of ignition kernel formation is characterized by the appearance of reaction front at the center of the heating domain. According to Vázquez-Espí and Liñán [151,152], chemical reactions mainly occur in the Frank-Kamenetskii region (abbreviated for FK region hereinafter) of radius r_{FK}, within which the temperature drop is of order $O(1/Ze)$. Subsequent to thermal runaway, the heat release and reactant consumption by chemical reaction must be taken into account, which makes the analytical solutions for Eq. (47) and (48) become unavailable. In terms of temperature at the center $\widetilde{T}_{\text{center}}$ and the edge of the FK region $\widetilde{T}_{FK}$, an approximate temperature profile within the FK region could be constituted as [51]

$$\widetilde{T} = \widetilde{T}_{\text{center}} - (\widetilde{T}_{\text{center}} - \widetilde{T}_{FK})\frac{r^2}{r_{FK}^2} \tag{54}$$

which is the simplest mathematical form of temperature profile that satisfies the symmetry condition at the center, i.e., $(d\widetilde{T}/dr)_{r=0} = 0$, and $\widetilde{T} = \widetilde{T}_{FK}$ at the edge of the FK region. A similar reactant mass fraction profile could also be introduced as

$$\widetilde{Y}_F = \widetilde{Y}_{F,\text{center}} + 3\left(1 - \widetilde{Y}_{F,\text{center}}\right)\frac{r^2}{r_{FK}^2} - 2\left(1 - \widetilde{Y}_{F,\text{center}}\right)\frac{r^3}{r_{FK}^3} \tag{55}$$

With the help of constituted profiles (54) and (55), the integration of Eq. (47) and (48) over the heating domain gives a pair of ordinary differential equations describing the transient variation of temperature and reactant concentration at the heating center, i.e.,

$$\frac{d\widetilde{T}_{\text{center}}}{dt} = -\alpha\frac{15(\widetilde{T}_{\text{center}} - \widetilde{T}_{FK})}{r_{FK}^2} + \frac{5}{2}\frac{Q_m}{Q_c Y_{F,0}} + \frac{5}{2}Be^{-\widetilde{T}_a/\widetilde{T}_{\text{center}}}F\left(\widetilde{T}_{\text{center}}, \widetilde{Y}_{F,\text{center}}\right) \tag{56}$$

$$\frac{d\widetilde{Y}_{F,\text{center}}}{dt} = -5Be^{-\widetilde{T}_a/\widetilde{T}_{\text{center}}}F\left(\widetilde{T}_{\text{center}}, \widetilde{Y}_{F,\text{center}}\right) \tag{57}$$

where the function $F\left(\widetilde{T}_{\text{center}}, \widetilde{Y}_{F,\text{center}}\right)$ is defined in the following form [51]

$$\begin{aligned} F(\widetilde{T}, \widetilde{Y}_F) = &-\frac{3\widetilde{T}^2 e^{-\widetilde{T}_a(\widetilde{T}-\widetilde{T}_{FK})/\widetilde{T}^2}}{2\widetilde{T}_a(\widetilde{T}-\widetilde{T}_{FK})} + \frac{3\widetilde{Y}_F\sqrt{\pi}\widetilde{T}^3}{4\widetilde{T}_a^{3/2}(\widetilde{T}-\widetilde{T}_{FK})^{3/2}}\text{erf}\left[\frac{\sqrt{\widetilde{T}_a(\widetilde{T}-\widetilde{T}_{FK})}}{\widetilde{T}}\right] \\ &-\frac{3(1-\widetilde{Y}_F)\widetilde{T}^4 e^{-\widetilde{T}_a(\widetilde{T}-\widetilde{T}_{FK})/\widetilde{T}^2}}{4\widetilde{T}_a^{\,2}(\widetilde{T}-\widetilde{T}_{FK})^2} + \frac{27\sqrt{\pi}(1-\widetilde{Y}_F)\widetilde{T}^5}{8\widetilde{T}_a^{\,5/2}(\widetilde{T}-\widetilde{T}_{FK})^{5/2}}\text{erf}\left[\frac{\sqrt{\widetilde{T}_a(\widetilde{T}-\widetilde{T}_{FK})}}{\widetilde{T}}\right] \\ &-\frac{6(1-\widetilde{Y}_F)T^6}{\widetilde{T}_a^{\,3}(\widetilde{T}-\widetilde{T}_{FK})^3}\left[1 - e^{-\widetilde{T}_a(\widetilde{T}-\widetilde{T}_{FK})/\widetilde{T}^2}\right] \end{aligned} \tag{58}$$

The occurrence of reactant front is characterized by the depletion of reactant concentration at the heating center, which is infinitely long because of the long tail exponential decay of $\widetilde{Y}_{F,\text{center}}$. For practical consideration, we set a threshold value of $\widetilde{Y}_{F,\text{center}} = 0.1$ to represent the end of reactant consumption. Consequently, the characteristic time for the reactant consumption can be extrapolated with the help of numerical solutions of Eq. (56) and (57) according to the relation

$$\widetilde{Y}_{F,\text{center}}\left(t_{\text{consumption}}\right) = 0.1 \tag{59}$$

The total time lapse for the reaction front formation t_{front} is therefore defined as

$$t_{\text{front}} = t_{\text{explosion}} + t_{\text{consumption}}. \tag{60}$$

The established reaction front propagates outwardly. Due to external heating, the temperature of the reactant mixture inside the heating domain is close to that of autoignition, which substantially facilitates the propagation of the reaction front. According to the gradient theory by Zel'dovich [93], the propagation of the reaction can be regarded as the spatial onset of reaction fronts at a suitable temporal sequence, and therefore the moving speed of the reaction front u_{front} is correlated to the gradient of the ignition delay time, which exhibits the following form

$$u_{\text{front}} = \left(\frac{\partial t_{\text{front}}}{\partial r}\right)^{-1} \tag{61}$$

The formation of the ignition kernel is characterized by the arrival of the reaction front at the edge of the heating domain. The characteristic time scale for this propagation process $t_{\text{propagation}}$ can be evaluated in the form of

$$t_{\text{propagation}} = \int_0^{R_0} \frac{1}{u_{\text{front}}} dr \tag{62}$$

So far, the characteristic time scales for individual stages have been obtained, the total time lapse of ignition kernel formation, denoted by t_{kernel}, is the summation, i.e.,

$$t_{\text{kernel}} = t_{\text{explosion}} + t_{\text{consumption}} + t_{\text{propagation}} \tag{63}$$

The time scales characterizing individual stages of ignition kernel formation depend upon the properties of the igniting source, e.g., the heating power, the size of the heating domain, and the duration of the ignition energy supply. To present those relations compactly and concisely, we shall introduce the non-dimensional time and non-dimensional heating power in the following form

$$\widehat{t} = t\alpha/R_0^2, \widehat{Q} = QR_0^2/\lambda T_u \quad (64)$$

where λ is the thermal conductivity of the mixture and T_u the ambient temperature.

The variation of characteristic time scales with the power density of an external heating source is shown in Figs. 15 and 16. The numerical results, denoted by the hollow symbols, are obtained using in-house code A-SURF [37], which examines the transient ignition process in a methane-air mixture subject to a uniform heating within a finite duration of $t_0 = 0.2$ ms and a finite spherical domain in the radius of $R_0 = 0.2$ mm.

In summary, this section highlights the significance of ignition kernel formation as a critical and frequently underexplored aspect of flame ignition. Three stages of ignition kernel formation induced by external heating within a finite domain and duration are analyzed. The characteristic time scales of these stages are evaluated, which provides an in-depth understanding of the ignition kernel formation process. The theoretical analysis identifies the critical thresholds of external heating power density, interprets the underlying mechanism of reaction front establishment at the external heating center, and assesses the central role of thermal runaway, which makes a primary contribution to the total time lapse of ignition kernel formation.

Subsequent to ignition kernel formation, the outcome of forced ignition depends on the dynamic evolution of the flame kernel driven by the ignition energy deposition from an external source. To interpret the radius as well as the expanding speed of the spherical ignition kernel, the mass and energy balance at the flame front must be considered simultaneously. In the following sub-section, we shall first consider a simplified quasi-steady ignition theory, in which the unsteady variation of both temperature and reactant mass fraction is not taken into account. A more general transient ignition theory considering unsteady effects will be reviewed in section 3.6.

The existing works on the theoretical models of ignition, including those summarized in this review, often simplify the combustion process by excluding convection terms to focus on the dominant chemical and thermal mechanisms in ignition and flame propagation. Such simplification helps isolate key processes and reduce the mathematical complexity of the of the underlying ignition process. Combustion invariably leads to thermal expansion and the generation of non-uniform velocity fields due to the conversion of reactants to products. Ignoring convection can indeed result in qualitatively different outcomes in theoretical models compared to observations from the real-life ignition process. Specifically, convection plays a crucial role in distributing heat and species within the flame kernel, affecting its shape and development [167]. While a thorough discussion on the effects of combustion induced convection is beyond the scope of this review.

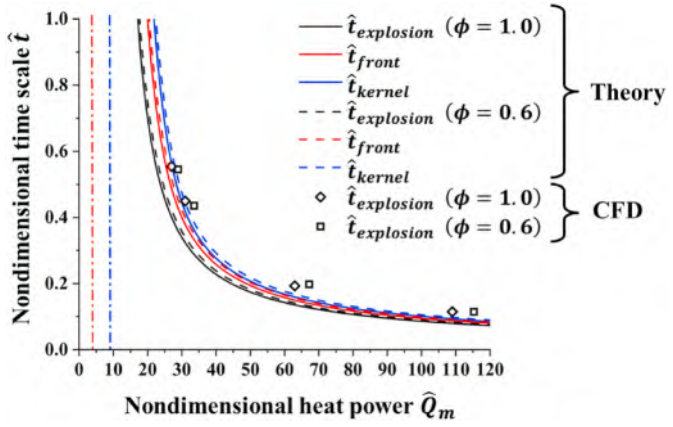

Fig. 15. Change of different characteristic time scales with heating power density. The solids $\varphi = 1.0$ and dashed $\varphi = 0.6$ lines represent results predicted by theory and the symbols correspond to results from simulation. Reprinted from Ref. [51] with permission from Elsevier.

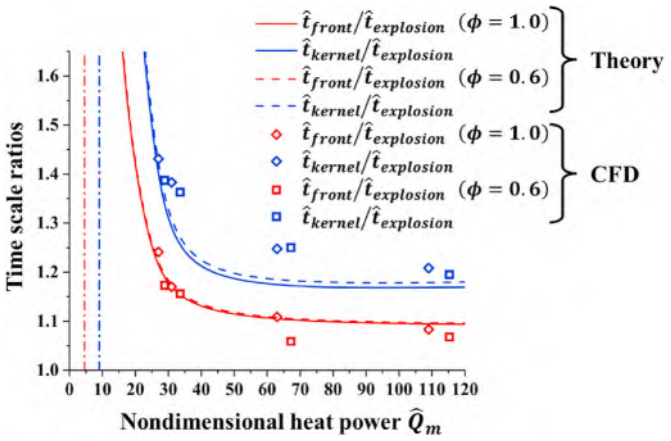

Fig. 16. Change of time scale ratios with heating power density. The theoretically predicted $\hat{t}_{\text{front}}/\hat{t}_{\text{explosion}}$ and $\hat{t}_{\text{kernel}}/\hat{t}_{\text{explosion}}$ are represented by red and blue lines (solid lines for $\varphi = 1.0$ and dashed lines for $\varphi = 0.6$), respectively. The corresponding ratios obtained via numerical simulation are represented by hollow symbols of diamond and square shapes, respectively. Reprinted from Ref. [51] with permission from Elsevier.

3.5. Ignition theory considering flame kernel propagation (quasi-steady ignition theory)

Premixed flame ignition involves the onset of a chemical reaction due to autoignition, the creation of ignition kernel resulting from the consumption of reactant, and the expansion of the ignition kernel to critical size beyond which the spherical flame propagates in self-sustained manner [51,144]. In the previous four subsections, the propagation of the ignition kernel was not considered. Since the ignition kernel is highly stretched/curved, its propagation speed is strongly affected by the flame stretch when the effective Lewis number is apparently different from unity. In fact, the formation of ignition kernel is the necessary rather than sufficient condition for successful flame initiation. Therefore, ignition kernel propagation plays a crucial role in the overall process of premixed flame initiation. The relevant problems are reviewed in this subsection.

Based on large activation energy asymptotic analysis, Joulin and coworkers [211,212,215,216] made analytical attempts to interpret the dynamic evolution of the ignition kernel subject to a time-dependent point source of energy. The temperature and mass fraction were asymptotically constituted in separate domains that are close to the flame ball front and at remote distances, respectively. Utilizing the matching conditions across the reaction front, an integro-differential equation was derived, describing the trajectory of the flame kernel radius driven by central heating. Nevertheless, for combustible mixture with $Le > 1$, the critical ignition radius is substantially smaller than the radius of flame ball [12] due to the dynamic propagation of the ignition kernel front, which was not appropriately considered in the theoretical model of Joulin and coworkers [212,216]. He and Law [8,217] proposed a theoretical formulation that interprets the dynamics of flame kernel propagation subject to external heat addition. They demonstrated that the onset of the flame kernel cannot guarantee premixed flame ignition, which is controlled by the critical ignition radius that strongly depends on the Lewis number. Accordingly, the external ignition source should drive the flame kernel to a radius beyond the critical ignition radius to successfully initiate a self-sustained flame. Through a series of theoretical and numerical investigations, Chen et al. [12,144] proposed a revised criterion to determine the critical ignition radius, with emphasis on the effects of differential diffusion and heat loss. A critical Lewis was introduced, beyond which the critical ignition radius is smaller than the

flame ball radius but greater than the flame thickness. In addition, the cubic scaling law between the MIE and the critical ignition radius was verified. Rich results could be obtained based on quasi-steady ignition theory. In the following sub-sections, recent work on quasi-steady ignition theory is reviewed.

3.5.1. Quasi-steady ignition theory considering one-step chemistry

The ignition kernel propagation induced by central heating in a quiescent mixture was analyzed by He [8] and Chen and Ju [144] using the thermal-diffusion model, in which the density was assumed to be constant and thereby the thermal expansion was neglected. As shown in Fig. 17, the flame front, $R_f = R_f(t)$, is characterized by the flame temperature of T_f and the propagation speed of $U = dR_f/dt$. The apparent sudden rise in temperature as $r \to 0$ is due to concentrated ignition energy deposition in a restricted area.

To describe the dynamic evolution of the ignition kernel, we fix the observing coordinate at the flame front, which proceeds in the course of time, i.e., $R_f = R_f(t)$. Accordingly, a new coordinate with the subscript s is defined as [144]

$$r_s = r - R_f(t), t_s = t \tag{65}$$

The flame front separates the burned and unburned regions, and the propagation of the ignition kernel leads to a moving boundary in solving the temperature and reactant molar fraction distributions on both sides of the flame front. In leading order approximation of large activation asymptotical analysis, the flame front can be modeled as an interface of zero thickness, across which the deficient reactant is completely depleted, i.e., $Y_F|_{r=R_{f+}} = Y_F|_{r=R_{f-}} = 0$. Consequently, the chemical reaction tends to be negligible in both burned and unburned regions. The quasi-steady theory assumes that the characteristic time of flame kernel evolution, $t_{\text{evolution}} = R_f/U$ is sufficiently longer than the unsteady evolution of temperature and reactant molar fraction during the propagation of the flame front, according to which, Eq. (24) and (25) can be further simplified by removing the time-dependent term. This quasi-steady assumption has been widely adopted in the development of premixed flame ignition theories and validated by transient simulations [144,157,218,219]. Consequently, in terms of the nondimensional quantities, defined in Eq. (15), the temperature and reactant molar fraction in the burned and unburned regions satisfy the following ordinary differential equations in the coordinated attached to the propagating flame front [144], which exhibit the following form

$$-\widetilde{U}\frac{d\widetilde{T}}{d\widetilde{r}_s} = \frac{1}{(\widetilde{r}_s + \widetilde{R}_f)^2}\frac{d}{d\widetilde{r}_s}\left[(\widetilde{r}_s + \widetilde{R}_f)^2\frac{d\widetilde{T}}{d\widetilde{r}_s}\right] \tag{66}$$

$$-\widetilde{U}\frac{d\widetilde{Y}_F}{d\widetilde{r}_s} = \frac{1}{Le}\frac{1}{(\widetilde{r}_s + \widetilde{R}_f)^2}\frac{d}{d\widetilde{r}_s}\left[(\widetilde{r}_s + \widetilde{R}_f)^2\frac{d\widetilde{Y}_F}{d\widetilde{r}_s}\right] \tag{67}$$

The boundary conditions are:

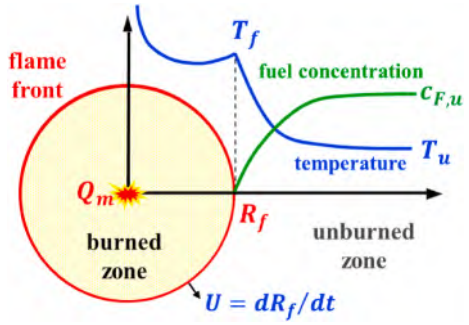

Fig. 17. Schematic of the model of ignition kernel propagation.

$$\widetilde{r}_s = -\widetilde{R}_f : \left(\widetilde{r}_s + \widetilde{R}_f\right)^2\frac{d\widetilde{T}}{d\widetilde{r}_s} = -\widetilde{Q}_m,\ \frac{d\widetilde{Y}_F}{d\widetilde{r}_s} = 0 \tag{68}$$

$$\widetilde{r}_s = 0 : \widetilde{T} = \widetilde{T}_f, \widetilde{Y}_F = 0 \tag{69}$$

$$\widetilde{r}_s \to \infty : \widetilde{T} = \widetilde{T}_u, \widetilde{Y}_F = 1 \tag{70}$$

The analytical solutions subject to boundary conditions can be obtained in the burned and unburned regions [144]. In the burned region with $\widetilde{r}_s \le 0$, we have:

$$\widetilde{T}(\widetilde{r}_s) = \widetilde{T}_f - \widetilde{Q}_m\left[\widetilde{U}\left(\Gamma\left[-1, \widetilde{R}_f\widetilde{U}\right] - \Gamma\left[-1, \left(\widetilde{R}_f + \widetilde{r}_s\right)\widetilde{U}\right]\right)\right] \tag{71}$$

$$\widetilde{Y}_F(\widetilde{r}_s) = 0 \tag{72}$$

In the unburned region with $\widetilde{r}_s \ge 0$, we have:

$$\widetilde{T}(\widetilde{r}_s) = \widetilde{T}_u + \left(\widetilde{T}_f - \widetilde{T}_u\right)\frac{\Gamma\left[-1, \left(\widetilde{R}_f + \widetilde{r}_s\right)\widetilde{U}\right]}{\Gamma\left(-1, \widetilde{R}_f\widetilde{U}\right)} \tag{73}$$

$$\widetilde{Y}_F(\widetilde{r}_s) = 1 - \frac{\Gamma\left[-1, Le\left(\widetilde{R}_f + \widetilde{r}_s\right)\widetilde{U}\right]}{\Gamma\left(-1, Le\widetilde{R}_f\widetilde{U}\right)} \tag{74}$$

where Γ is the incomplete gamma function defined in the general form

$$\Gamma(a, x) \equiv \int_x^\infty t^{a-1}e^{-t}dt \tag{75}$$

In the particular situation of $\widetilde{U} = 0$, the temperature and reactant molar fractions are identically reduced to the solutions of the flame ball, which are discussed in section 3.3. Substituting the preceding solutions for $\widetilde{T}$ and $\widetilde{Y}_F$ into the matching conditions (28) and (29), we obtain the following algebraic equations [144]:

$$\widetilde{T}_f = \widetilde{T}_u + \Gamma\left(-1, \widetilde{R}_f\widetilde{U}\right)\left\{\widetilde{Q}_m\widetilde{U} + \frac{\exp\left[(1-Le)\widetilde{R}_f\widetilde{U}\right]}{Le^2\Gamma\left(-1, Le\widetilde{R}_f\widetilde{U}\right)}\right\} \tag{76}$$

$$\frac{\exp\left(-\widetilde{R}_f\widetilde{U}\right)\left\{\widetilde{T}_f - \widetilde{T}_u - \widetilde{Q}_m\widetilde{U}\Gamma\left(-1, \widetilde{R}_f\widetilde{U}\right)\right\}}{\widetilde{R}_f^2\widetilde{U}\Gamma\left(-1, \widetilde{R}_f\widetilde{U}\right)} = \frac{\widetilde{T}_f^2}{\widetilde{T}_{ad}^2}\exp\left[-\frac{Ar}{2}\left(\frac{\widetilde{T}_{ad}}{\widetilde{T}_f} - 1\right)\right] \tag{77}$$

The above algebraic equations implicitly describe the change in flame temperature $\widetilde{T}_f$ and flame propagation speed $\widetilde{U}$ with flame radius $\widetilde{R}_f$. Therefore, with the help of these two equations, the dynamic evolution of the ignition kernel subject to central heating from an external source can be interpreted by investigating the trajectory in the phase space constituted by $\widetilde{U}$ and $\widetilde{R}_f$.

In the presence of heat loss due to various mechanisms, such as radiation and immersed particles, an additional term related to the nondimensional temperature should appear on the right side of the energy equation (66). Such analysis was conducted by Chen and Ju [144] who interpreted the dynamic propagation of flame kernels subject to volumetric radiative heat loss and various effects of heat loss enriching the ignition characteristics. Because of the heat transfer properties that control the energy balance across the flame front, the analytical solution for $\widetilde{T}$ is in much more complicated mathematical form, which is not presented in this review. The readers are referred to Ref. [144] for details on how radiation affects the ignition and propagation of a premixed spherical flame. Note that outwardly propagating spherical flames are popularly used to measure the laminar flame speed, which is one of the most important parameters of a flammable mixture [157,220–223].

In quasi-steady ignition theory, the key assumption of constant density simplifies the analysis by eliminating the need to account for the complexities introduced by thermal expansion and the variable density

effect. This assumption allows for a more tractable analytical or semi-analytical treatment of ignition phenomena, with focus on the chemical kinetics and heat transfer mechanisms central to ignition. Relaxing the constant density assumption can significantly complicate the analysis because it introduces nonlinearities associated with both fluid flow and changes in material properties [224]. The adoption of constant density assumption conceals significant physical processes that can affect the dynamics and stability of the flame kernel, such as buoyancy-driven flow and variation of flow velocity due to density changes [225]. However, this realism comes at the cost of increased mathematical complexity and the loss of concise and beautiful formulas interpreting the fundamental mechanisms dominating the ignition process.

Fig. 18 plots the normalized flame propagation speed with flame radius for different Lewis numbers. There is no central ignition power and no radiative heat loss. For each Lewis number, the intersection between the solution curve and the horizontal axis with $\widetilde{U}=0$ corresponds to radius of adiabatic flame ball. For very large flame radius, unity normalized flame propagation speed is approached and thereby the solution for an adiabatic, planar, premixed flame is recovered. The solution curve connecting the flame ball solution and planar flame solution depicts the expanding spherical flame between them. Therefore, the present theory can describe the flame transition from the flame ball to an outwardly propagating spherical flame and thereby be used to study flame kernel propagation. Fig. 18 shows that each mixture with a certain Lewis number has a critical flame radius, $\widetilde{R}_{cr}$, above which the spherical flame can propagate outwardly along the solution curve in a self-sustained manner [12]. There is no quasi-steady solution below the critical flame radius. Therefore, to achieve successful ignition, the ignition source must be strong enough to drive the flame kernel to a radius beyond $\widetilde{R}_{cr}$. It is seen that the critical radius increases significantly with the Lewis number. This is because the positive stretch rate of the outwardly propagating spherical flame kernel makes the flame weaker at larger Lewis number.

As discussed in Section 3.3, the flame ball radius ($\widetilde{R}_Z$, corresponding to $\widetilde{U}=0$ in Fig. 18) has been popularly considered to be a critical length scale for ignition. However, Fig. 18 shows that $\widetilde{R}_Z$ is the same as $\widetilde{R}_{cr}$ only for $Le=0.5$, 0.7 and 1.0 (more exactly we have $\widetilde{R}_Z=\widetilde{R}_{cr}$ for $Le<1.36$). For large Lewis numbers, the propagation spherical flame can exist even when its radius is less than $\widetilde{R}_Z$, and thereby the critical flame radius controlling spherical flame initiation is not the stationary flame ball radius.

For non-vanishing external heating, Fig. 19 shows that there are two branches in the $\widetilde{U}-\widetilde{R}_f$ phase diagram. For sufficiently low heating powers, these two branches are separated from each other, yielding a pair of intersecting points on the $\widetilde{R}_f$ axis corresponding to zero propagation speed, which are identified as the inner and outer flame ball radius, $\widetilde{R}_Z^-$ and $\widetilde{R}_Z^+$ respectively. In general, the distance between $\widetilde{R}_Z^-$ and $\widetilde{R}_Z^+$ on the $\widetilde{R}_f$ axis differs from the minimum distance between those two branches in the $\widetilde{U}-\widetilde{R}_f$ phase diagram. The maximum possible flame radius on the inner branch of $\widetilde{U}-\widetilde{R}_f$ phase diagram is defined as the lower critical flame radius, denoted by $\widetilde{R}_{cr}^-$, and similarly the minimum possible flame radius on the upper branch is regarded as the upper critical flame radius, denoted by $\widetilde{R}_{cr}^-$. As the external heating power increases, the inner branch of $\widetilde{U}-\widetilde{R}_f$ diagram swells outwardly, while the outer branch retreats inwardly. Consequently, there exists a critical ignition power, beyond which both branches of phase diagrams merge with each other at an intermediate phase point. Fig. 19 shows that the critical ignition power is between 0.96 and 0.97 for $Le=2$.

The above results indicate that the critical ignition condition is determined by the critical flame radius. Fig. 20 shows the change of upper and lower critical flame radii and flame ball radii with the ignition power. The vertical dashed lines denote the minimum/critical ignition

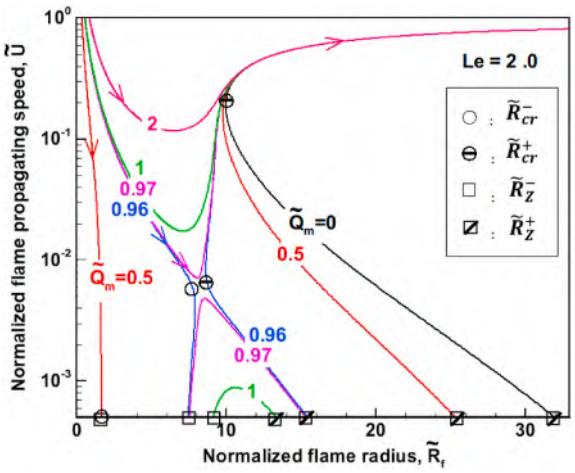

Fig. 19. Change of the normalized flame propagation speed with flame radius for different central ignition powers but fixed Lewis number of $Le=2$. Reprinted from Ref. [12] with permission from Elsevier.

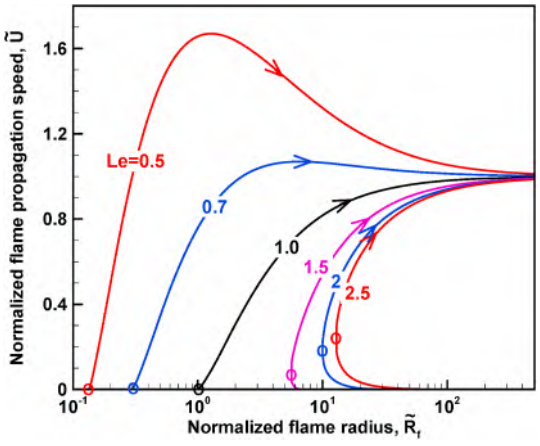

Fig. 18. Change of normalized flame propagation speed with flame radius for different Lewis numbers. The central ignition power is zero. The critical flame radius for each case is denoted by a circle at the corresponding minimum flame radius. Reprinted from Ref. [12] with permission from Elsevier.

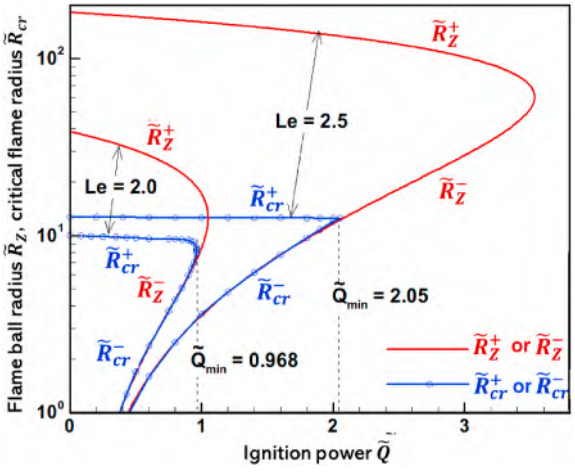

Fig. 20. Change of the upper and lower critical flame radii (in blue color) and flame ball radii (in red color) with the central ignition power for $Le=2$ and $Le=2.5$. Reprinted from Ref. [12] with permission from Elsevier.

power for successful ignition under the requirement of $\widetilde{R}_{cr}^{+} = \widetilde{R}_{cr}^{-}$. It is also observed that the minimum ignition power based on the flame ball radius, i.e., $\widetilde{R}_{Z}^{+} = \widetilde{R}_{Z}^{-}$, is higher than that based on critical flame radius, i.e., $\widetilde{R}_{cr}^{+} = \widetilde{R}_{cr}^{-}$. Therefore, for mixtures with large Lewis numbers, the minimum ignition power is overpredicted based on the flame ball radius. Moreover, Fig. 20 indicates that $\widetilde{R}_{cr}^{+}$ remains almost constant as the ignition power increases. Therefore, the critical flame radius at zero ignition power can be considered to be the critical length of premixed flame ignition.

The critical ignition radius and MIE strongly depend on the Lewis number of the reactant mixture. In the theoretical and numerical study by Chen et al. [12], it was demonstrated that there exists a critical Lewis number slightly beyond unity, Le^{*}, below which the inner and outer flame ball radii are identical with the inner and outer critical flame radii, i.e., $\widetilde{R}_{z}^{-} = \widetilde{R}_{c}^{-}$ and $\widetilde{R}_{z}^{+} = \widetilde{R}_{c}^{+}$, and the propagation speed of the flame kernel monotonically grows as its radius departs from $\widetilde{R}_{z}^{+}$ (see the lines for $Le \leq 1$ in Fig. 18). However, for reactant mixtures with $Le > Le^{*}$, it was found that the outer branch tends to be C-shaped, i.e., the outer critical flame radius tends to be smaller than the outer flame ball radius, i.e., $\widetilde{R}_{c}^{+} < \widetilde{R}_{z}^{+}$ (see the lines for $Le \geq 1.5$ in Fig. 18). Fig. 21 compares the critical flame radius and the flame ball radius (both normalized by the flame thickness) for a broad range of Lewis numbers. Three different regimes in terms of the Lewis number were identified [12]. In regimes I ($Le < 1$) and II ($1 < Le < Le^{*} = 1.36$), the critical flame radius is respectively smaller and larger than the flame thickness. Nevertheless, in regimes I and II, the critical flame radius is the same as the flame ball radius, indicating that the flame ball can be used to determine the critical ignition condition. However, in regime III with $Le > Le^{*}$, the critical flame radius is smaller than the flame ball radius but larger than the flame thickness. Consequently, the MIE is substantially over- or under-predicted based on the flame ball radius and flame thickness for mixtures with large Lewis number. This suggests that the flame ball radius or flame thickness cannot be a suitable candidate to define the critical ignition length scale for mixtures with a large Lewis number.

In addition to MIE, the minimum ignition power $\widetilde{Q}_{\min}$, referring to the lower threshold of ignition energy deposition rate necessary to generate a self-sustaining spherical flame, also plays a decisive role in affecting the outcome of forced ignition. Specifically, if the ignition energy input rate is lower than the minimum ignition power, the ignition kernel cannot expand to the critical ignition radius, no matter how much ignition energy is deposited. Thus, the magnitude of the critical ignition radius gives a quantitative interpretation of the difficulty of the ignition process. Ignition theory based on quasi-steady state assumptions demonstrates that the minimum ignition power of the igniting source tends to be proportional to the cube of the critical ignition radius, i.e., $\widetilde{Q}_{\min} \sim \widetilde{R}_{cr}^{3}$, as shown in Fig. 22. Similar results were also obtained by numerical simulation [12], which verifies the scaling relation. It was demonstrated that for mixtures with large Lewis numbers (i.e., thermal diffusivity being substantially higher than mass diffusivity, e.g., lean hydrogen/air or rich n-heptane/air mixture), a stronger igniting source must be adopted to ensure the creation of self-sustained flame kernel and subsequently the successful initiation of premixed flame.

In the quasi-steady ignition theory, a series of assumptions were adopted for simplicity in theoretical formulation and mathematical convenience in obtaining analytical solutions, e.g., one-step irreversible reaction model, absence of Soret diffusion and reactant mixture in a single phase. Remedying those simplifications helps improve the theoretical predictions. Adopting large activation energy asymptotic analysis, Li et al. [219] conducted a theoretical investigation, examining the impact of reaction reversibility on the characteristics of spherical flame propagation. The reversibility is characterized by the ratio of pre-exponential factors of the backward and forward reactions, denoted by Γ. It was found that reaction reversibility plays a similar role as heat loss. The reaction reversibility reduces the spherical flame propagation speed while increasing the absolute value of the Markstein length. For the ignition process, the reaction reversibility increases both the minimum ignition power and the critical ignition radius [219]. Fig. 23 plots the variation of minimum ignition power and critical ignition radius, which are normalized by the corresponding values evaluated in the absence of reaction reversibility, i.e., $\Gamma = 0$. It is seen that both the minimum ignition power and the critical ignition radius grow monotonically with the reversibility parameter Γ, i.e., ignition becomes increasingly difficult as reversible reactions occur. This is consistent with the recognition that reversibility can be regarded as a heat loss mechanism during the ignition process. Moreover, Fig. 23 indicates that the influence of reaction reversibility becomes weaker at a larger Lewis number.

Han and Chen [218] conducted a theoretical analysis to assess the influence of Soret diffusion on the ignition of a spherical flame. They derived a general correlation between the flame propagation speed and flame radius, considering Soret diffusion and external energy deposition. Based on this correlation, the effects of Soret diffusion on spherical flame propagation speed, Markstein length, and critical ignition conditions were assessed. The absolute value of Markstein length was found to increase linearly with the magnitude of Soret diffusion coefficient. This indicates that the highly stretched flame kernel becomes more sensitive to stretch rate after including Soret diffusion. For light/heavy fuels, Soret diffusion increases/decreases the flame propagation speed by modifying the local equivalence ratio. Consequently, the Soret diffusion

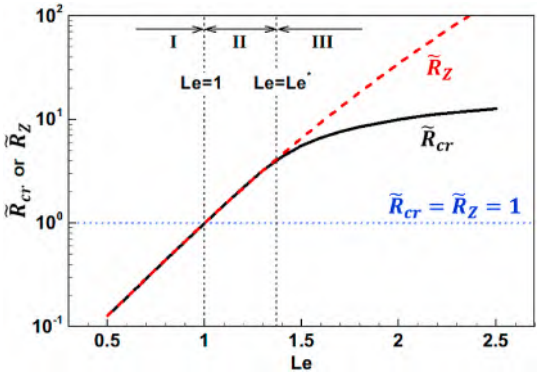

Fig. 21. Change of the critical flame radius (solid black line) and the flame ball radius (dashed red line) with the Lewis number. Reprinted from Ref. [12] with permission from Elsevier.

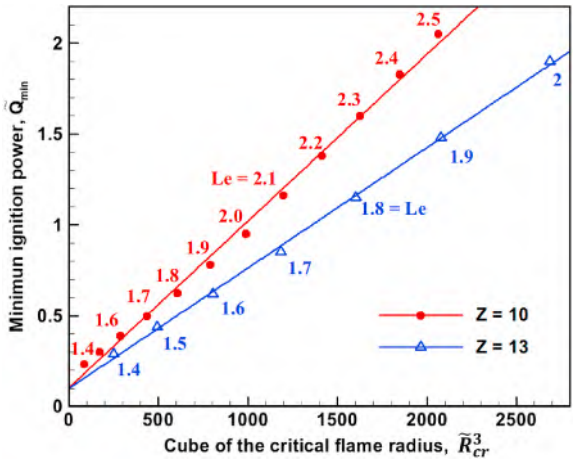

Fig. 22. Change of the minimum ignition power with the cube of the critical flame radius for different Lewis numbers and Zel'dovich numbers. Reprinted from Ref. [12] with permission from Elsevier.

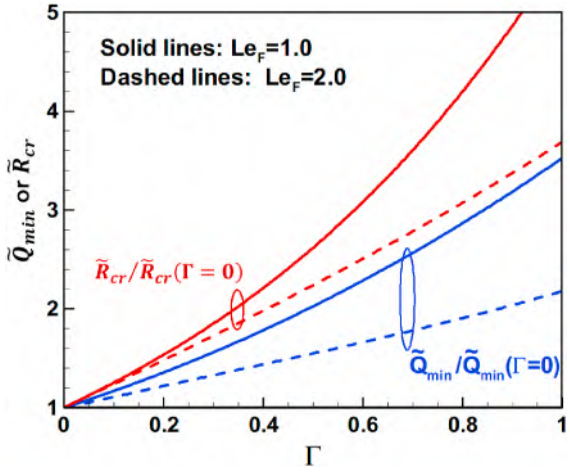

Fig. 23. Change of the minimum ignition power and critical ignition radius with reaction reversibility. Reprinted from Ref. [219] with permission from Springer.

affects the minimum ignition power and makes flame initiation easier (more difficult) for light (heavy) fuel. Numerical simulations considering detailed chemistry and transport properties by Liang et al. [226] demonstrated that the Soret diffusion tends to vary the concentration of light species and radicals, e.g., H_2 and H, and thus alters the local reactivity of the combustible mixture. Depending on the molecular weight of the fuels, the Soret diffusion asymmetrically affects the ignition process. The influence of Soret diffusion on ignition predicted by simulation in Ref. [226] is consistent with theoretical prediction in Ref. [218].

As mentioned before, the propagating spherical flame method has been popularly used to measure the laminar flame speed S_L^0 [157,221]. In this method, the flame evolution of the flame radius, $R_f = R_f(t)$, is recorded by a high-speed schlieren or shadow photograph. For relatively small flame radii, the burned gas inside the expanding flame is nearly static, and thereby the flame speed relative to the burned gas is $S_b = dR_f/dt$. Since the propagating spherical flame is positively stretched, extrapolation to zero stretch rate needs to be conducted to obtain the unstretched flame speed with respect to burned gas, S_b^0 and the Markstein length, L_b. Different linear or nonlinear models based on stretch, $K = 2S_b/R_f$, or curvature, $\kappa = 2/R_f$, can be derived from the quasi-steady ignition theory described above [223]. Several typical models are listed in Table 3. It was shown that the laminar flame speed

Table 3
Different models used in the extrapolation of unstretched flame speed S_b^0 [223].

Model	Expression	Notes	Ref.
LS	$S_b = S_b^0 - L_bK$	**L**inear model based on **S**tretch	[228]
LC	$S_b = S_b^0(1 - L_b\kappa)$	**L**inear model based on **C**urvature	[229]
NQ	$\left(\frac{S_b}{S_b^0}\right)^2 \ln\left(\frac{S_b}{S_b^0}\right)^2 = -\frac{2L_bK}{S_b^0}$	**N**onlinear **Q**uasi-steady model	[230]
N3P	$\frac{S_b}{S_b^0} = 1 - L_b\kappa + \frac{C}{R_f^2}$	**N**onlinear model with **3** **P**arameters	[231]
NQH	$\left(\frac{S_b}{S_b^0}\right)^2 \ln\left(\frac{S_b}{S_b^0}\right)^2 = -\frac{2L_bK}{S_b^0} + \frac{C}{R_f^2}$	**NQ** model with a **H**igh-order term	[223]
NE	$\frac{S_b}{S_b^0}\left[1 + L_b\kappa + (L_b\kappa)^2 + \frac{2}{3}(L_b\kappa)^3\right] = 1$	**N**onlinear model in **E**xpansion form	[232]
FTE	$\left(\frac{S_b}{S_b^0} + d_L^0\kappa\right)\ln\left(\frac{S_b}{S_b^0} + d_L^0\kappa\right) = -\left(L_b - d_L^0\right)\kappa$	**F**inite flame **T**hickness **E**xpression	[233]

measured from the propagating spherical flame method strongly depends on the extrapolation model and different models were recommended for mixtures with different Lewis numbers [220,223,227]. Different extrapolation models may account for various physical phenomena differently, such as heat loss, flame curvature, or preferential diffusion effects, which are especially relevant in mixtures with varying Lewis numbers. At different Lewis numbers, the dynamic behaviors of the ignition kernel show considerable influence on spherical flame propagation and thus exhibit impacts on the measurement of premixed flame speed.

3.5.2. *Quasi-steady ignition theory considering radical and chain-branching reaction*

In theoretical studies on ignition and flame dynamics, the one-step global reaction model is widely adopted for its inherent simplicity. It has been recognized that qualitatively correct results can be obtained using a one-step reaction. Nevertheless, the direct conversion of fuel into products and heat via a one-step global reaction neglects the pivotal role of intermediate species and radicals that participate in the ignition and combustion processes of practical hydrocarbon fuels in engines [234]. Therefore, ignition and flame propagation are affected not only by the properties of fuel, but also by those of the radicals involved in the chain reactions. To acquire in-depth understandings of flame initiation and propagation, the multi-step reaction model involving the generation, transformation, and termination of various radicals should be taken into account. A simple generalization of the one-step reaction model is the Zel'dovich-Liñán model [184,196], which consists of a chain branching reaction, $F + Z \rightarrow 2Z$, and a chain-breaking/recombination reaction, $Z + Z \rightarrow 2P$, where F, Z, and P represent fuel, radical, and product, respectively. The Zel'dovich-Liñán model was simplified by Dold and coworkers [235,236] so that the analytical solutions for flame balls and premixed flames could be obtained. The simplified version of the Zel'dovich-Liñán model is

$$F + Z \rightarrow 2Z, k_B = A_B \exp\left(-\tilde{T}_{a,B}/\tilde{T}\right) \tag{78}$$

$$Z + M \rightarrow P + M, k_R = A_R \tag{79}$$

where M denotes any type of molecule in the system. The chain branching reaction is thermally sensitive, and the reaction rate coefficient is of the Arrhenius type characterized by the normalized activation temperature $\tilde{T}_{a,B}$. The chain-breaking/recombination reaction is supposed to be chemically activated, whose rate coefficient is independent of temperature. For simplicity, it can be understood that the occurrence of the chemically activated reaction is associated with molecular collision, and therefore, its rate coefficient can be considered equal to the frequency factor, i.e., $k_R = A_R$. The rate of the recombination reaction in the simplified version of the Zel'dovich-Liñán model depends linearly on the radical concentration, while nonlinear dependence happens in the original Zel'dovich-Liñán model. Nevertheless, this two-step model does not capture the complete kinetic behavior of the complex combustion reactions. It serves to bridge the gap between simplistic one-step models and the detailed chemical kinetics mechanisms. The assumption of a quasi-steady state of radical Z introduces additional simplification to the two-step reaction model and thus leads to its degeneration to a one-step reaction model under specific mathematical arrangements.

When the simplified Zel'dovich-Liñán model given in Eq. (78) and (79) is considered in theoretical analysis [237], the ignition caused by radical deposition and the effects of radical transport on ignition and flame propagation can be examined. Fig. 24 shows the schematic of the model of ignition kernel propagation determined by chain-branching and recombination reaction considered by Zhang and Chen [237]. In the ignition theory considering one-step chemistry (see the model in Fig. 17), ignition can be caused only by heat deposition. In practical ignition processes, both heat and radicals are generated by the spark, and the radicals can support flame kernel propagation. Recent studies on

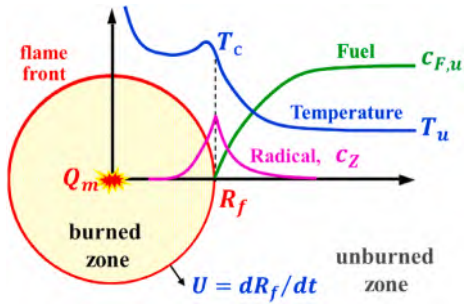

Fig. 24. Schematic of the model of ignition kernel propagation considering radical and chain-branching reaction.

plasma-assisted combustion [105,106] showed that the chemical effect of radicals generated by non-equilibrium plasma can be stronger than the thermal effect on ignition and flame stabilization. In the ignition theory, considering the simplified Zel'dovich-Liñán model, the process of chemical ignition due to the accumulation of radicals can be interpreted in addition to thermal ignition [238].

The thermal sensitivity of the chain branching reaction in Eq. (78) implies that a slight increment in temperature results in substantial enhancements in radical production. The ignition process involving the simplified Zel'dovich-Liñán mechanism can also be solved analytically by means of large activation energy asymptotics, in which the Zel'dovich number and Arrhenius number are defined in terms of the activation temperature of the chain branching reaction and satisfy $Ze_B = \widetilde{T}_{a,B}/\widetilde{T}_{ad}^2 \gg 1$ and $Ar_B = \widetilde{T}_{a,B}/\widetilde{T}_{ad} \gg 1$. Moreover, there exists an infinitesimal region similar to the concept of reaction zone in which the rate of the chain-branching reaction, denoted by ω_B, significantly exceeds that of the recombination reaction, denoted by ω_R, i.e., $\omega_B \sim Ze_B^2 \omega_R$ based on asymptotic analysis [235,236].

In the leading-order approximation, the chain-branching reaction tends to be frozen on both sides of the radical generation zone. Accordingly, the governing equations in quasi-steady theory can be written in the following form

$$-\widetilde{U}\frac{d\widetilde{Y}_F}{d\widetilde{r}_s} = \frac{1}{Le_F}\frac{1}{\left(\widetilde{r}_s+\widetilde{R}_f\right)^2}\frac{d}{d\widetilde{r}_s}\left[\left(\widetilde{r}_s+\widetilde{R}_f\right)^2\frac{d\widetilde{Y}_F}{d\widetilde{r}_s}\right] \tag{80}$$

$$-\widetilde{U}\frac{d\widetilde{Y}_Z}{d\widetilde{r}_s} = \frac{1}{Le_Z}\frac{1}{\left(\widetilde{r}_s+\widetilde{R}_f\right)^2}\frac{d}{d\widetilde{r}_s}\left[\left(\widetilde{r}_s+\widetilde{R}_f\right)^2\frac{d\widetilde{Y}_Z}{d\widetilde{r}_s}\right] - \widetilde{Y}_Z \tag{81}$$

$$-\widetilde{U}\frac{d\widetilde{T}}{d\widetilde{r}_s} = \frac{1}{\left(\widetilde{r}_s+\widetilde{R}_f\right)^2}\frac{d}{d\widetilde{r}_s}\left[\left(\widetilde{r}_s+\widetilde{R}_f\right)^2\frac{d\widetilde{T}}{d\widetilde{r}_s}\right] + \widetilde{Y}_Z \tag{82}$$

where Le_F and Le_Z are the Lewis numbers of the fuel and radical, respectively. The above equations are similar to the governing equations, (66) and (67) for one-step chemistry. The main difference is that the transport and reaction of radicals are included. Besides, the definitions of reference length and time scales involve the propagation speed of an adiabatic planar flame, S_L^0, which, according to Eq. (23), depends on the chemical reaction rate. For the two-step reaction model given by Eq. (78) and (79), the laminar flame speed is derived based on the rate of recombination reaction (through which heat is released). Accordingly, the relevant quantities are non-dimensionalized in a revised manner, for which the details can be found in Ref. [237].

As mentioned before, the ignition processes caused by both heat and radical deposition can be studied when the simplified Zel'dovich-Linan mechanism is considered. The addition of radicals (e.g., due to plasma) can be introduced in analogy to thermal energy deposition at the center of the ignition kernel, which can be characterized by the non-dimensional chemical ignition power $\widetilde{Q}_c$ [238]. Accordingly, the boundary conditions shall be supplemented in the following form:

At the center of ignition kernel with $\widetilde{r}_s = -\widetilde{R}_f$,

$$\frac{d\widetilde{Y}_F}{d\widetilde{r}_s} = 0, \left(\widetilde{r}_s+\widetilde{R}_f\right)^2\frac{d\widetilde{Y}_Z}{d\widetilde{r}_s} = -Le_Z\widetilde{Q}_c, \left(\widetilde{r}_s+\widetilde{R}_f\right)^2\frac{d\widetilde{T}}{d\widetilde{r}_s} = -\widetilde{Q}_m \tag{83}$$

At the far field from the ignition kernel with $\widetilde{r}_s \to \infty$:

$$\widetilde{Y}_F = 1, \widetilde{Y}_Z = 0, \widetilde{T} = \widetilde{T}_u \tag{84}$$

As show in Fig. 24, $\widetilde{R}_f$ refers to the flame front position where the radical is generated by the chain-branching reaction. The following conditions should hold across or at the flame front [237]

$$\left(\frac{d\widetilde{T}}{d\widetilde{r}_s}\right)_{\widetilde{r}_s=0+} - \left(\frac{d\widetilde{T}}{d\widetilde{r}_s}\right)_{\widetilde{r}_s=0-} = 0 \tag{85}$$

$$\left(\frac{1}{Le_F}\frac{d\widetilde{Y}_F}{d\widetilde{r}_s}+\frac{1}{Le_Z}\frac{d\widetilde{Y}_Z}{d\widetilde{r}_s}\right)_{\widetilde{r}_s=0+} - \left(\frac{1}{Le_F}\frac{d\widetilde{Y}_F}{d\widetilde{r}_s}+\frac{1}{Le_Z}\frac{d\widetilde{Y}_Z}{d\widetilde{r}_s}\right)_{\widetilde{r}_s=0-} = 0 \tag{86}$$

$$\widetilde{T}(\widetilde{r}_s = 0+) = \widetilde{T}(\widetilde{r}_s = 0-) = \widetilde{T}_{\text{crossover}} \tag{87}$$

$$\widetilde{Y}_F(\widetilde{r}_s = 0+) = \widetilde{Y}_F(\widetilde{r}_s = 0-) = 0 \tag{88}$$

$$\widetilde{Y}_Z(\widetilde{r}_s = 0+) = \widetilde{Y}_Z(\widetilde{r}_s = 0-) \tag{89}$$

where $\widetilde{T}_{\text{crossover}}$ is the crossover temperature beyond which the chain branching reaction is fully initiated so that the condition $\omega_B \sim Ze_B^2\omega_R$ is satisfied [235,236]. The governing equations involving Zel'dovich-Liñán mechanism include additional conservation for radicals, which must be associated with one more matching condition at the reaction zone. It is noted that the temperature gradient is continuous at $\widetilde{r} = \widetilde{R}_f$, which can be attributed to the fact that the heat release rate tends to be insubstantial compared with the radical production within the radial generation zone with crossover temperature.

Subject to the boundary conditions at the origin and the far field, equations (80) – (82) yield partial solutions of $\widetilde{T}$, $\widetilde{Y}_F$ and $\widetilde{Y}_Z$ on each side of the radical generation zone. Then the flame radius $\widetilde{R}_f$, flame propagation speed $\widetilde{U}$, and radical concentration $\widetilde{Y}_{Z,f}$ at the flame front can be determined via the matching conditions (85) – (89). Consequently, a correlation depicting the change in flame propagation speed with flame radius can be obtained, which was shown in Refs. [237,238]. The correlation was shown to be able to describe flame balls, propagating spherical flames, and planar flames with thermally sensitive intermediate kinetics given in Eq. (78) and (79) [237]. Therefore, it was used to study the flame kernel growth and the transition among different flame regimes at different Lewis numbers, Le_F and Le_Z, and different ignition/or ignition powers $\widetilde{Q}_m$ and $\widetilde{Q}_c$ [237,238].

Fig. 25 shows the $\widetilde{U} - \widetilde{R}_f$ phase diagram for different ignition powers. When there is only thermal heating at zero chemical ignition power, Fig. 25(a) shows similar results as those shown in Fig. 19 obtained from ignition theory considering a one-step chemistry model. However, the $\widetilde{U} - \widetilde{R}_f$ curves have different shapes when only chemical ignition power is considered. At relatively low ignition powers, both Fig. 25(a) and (b) show that the $\widetilde{U} - \widetilde{R}_f$ curves exhibit to be C-shaped, which indicates that there is no flame ball solution. As ignition power increases, an inner branch of the bell-shaped $\widetilde{U} - \widetilde{R}_f$ curve appears in Fig. 25(b), which expands with the magnitude of ignition power. For $\widetilde{Q}_c = 1.0$, the bell-shaped inner branch approaches towards the origin corresponding to $\widetilde{U} = 0$ and $\widetilde{R}_f = 0$. Nevertheless, a spherical flame cannot be established at this ignition power, because the flame undergoes extinction with a finite propagation speed around $\widetilde{R}_f \approx 2.7$ along the bell-shaped $\widetilde{U} - \widetilde{R}_f$ curve in Fig. 25(b). This phenomenon can be understood as follows: Less radical (because of large flame radius) and less fuel (due to relatively

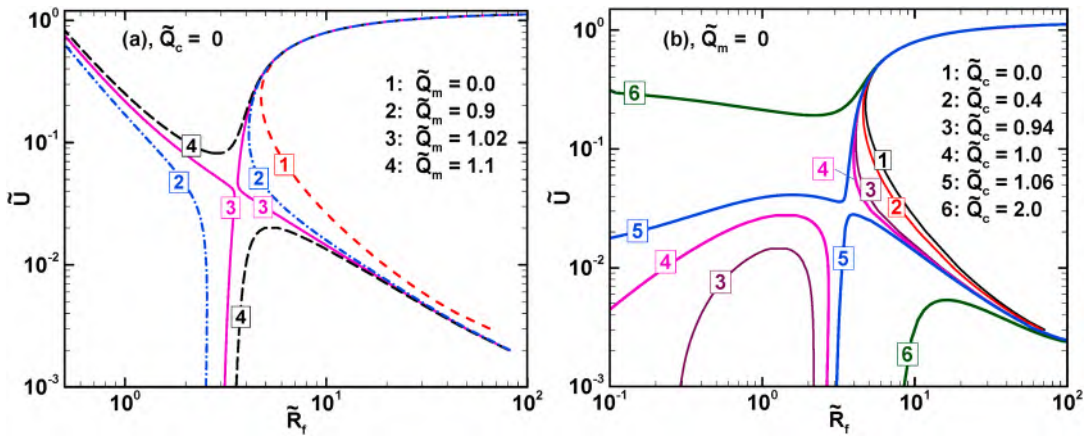

Fig. 25. Flame propagation speed as a function of flame radius for $Le_F = 2.5$ and $e_Z = 1$: (a) different thermal ignition powers but zero chemical ignition power; (b) different chemical ignition powers but zero thermal ignition power. Reproduced from Refs. [237,238] with permission from Elsevier.

large fuel Lewis number) can be provided to the reaction zone from the center and thereby the flame front can hardly propagate outwardly in a self-sustained manner. Further increasing the ignition power to $Q_c = 1.06$, the C-shaped outer branch merges with the bell-shaped inner branch, resulting in an upper branch of $\tilde{U} - \tilde{R}_f$ curve, through which a spherical flame can propagate outwards and thereby the successful initiation of a premixed flame is thus achieved.

The minimum thermal ignition power and the minimum chemical ignition power can both be evaluated based on the bifurcation of $\tilde{U} - \tilde{R}_f$ curves, as shown in Fig. 25. The minimum thermal ignition power and minimum chemical ignition power were found to increase with the fuel Lewis number and to decrease with the radical Lewis number [237,238]. The increase in the minimum ignition power with fuel Lewis number is mainly due to the coupling between the positive stretch rate and the preferential diffusion between heat and fuel. A similar trend is predicted by ignition theory considering one-step chemistry, as shown in Fig. 22. The decrease in minimum ignition power with a radical Lewis number is mainly due to the fact that radicals with a large Lewis number are less inclined to diffuse away from the ignition kernel, and consequently, the radical accumulation induces an explosive chain branching reaction and thereby facilitates the ignition process. It is noted that fuel and radicals diffuse in opposite directions. Therefore, Le_F and Le_Z have different impacts on ignition kernel propagation and critical ignition conditions.

Both heat deposition and radical addition can lead to ignition. The comparison between $\tilde{Q}_{m,\min}$ and $\tilde{Q}_{c,\min}$ for pure thermal ignition (i.e., $\tilde{Q}_c = 0$) and pure thermal chemical (i.e., $\tilde{Q}_m = 0$), respectively, is shown in Fig. 26. For most situations, the critical ignition powers satisfy $\tilde{Q}_{c,\min} > \tilde{Q}_{m,\min}$, i.e., thermal ignition due to heat deposition is more efficient than chemical ignition resulting from radical addition. In a particular situation with a large fuel Lewis number and a small radical Lewis number (see the shadow region in Fig. 26), i.e., the transport of fuel molecules to the flame front is less effective than the diffusion of radicals from the external source, chemical ignition occurs more readily than thermal ignition and thereby $\tilde{Q}_{c,\min} < \tilde{Q}_{m,\min}$. Therefore, under certain conditions, the radicals produced by plasma help promote premixed flame ignition. This was demonstrated in simulations considering detailed chemistry and transport by Wang et al. [239].

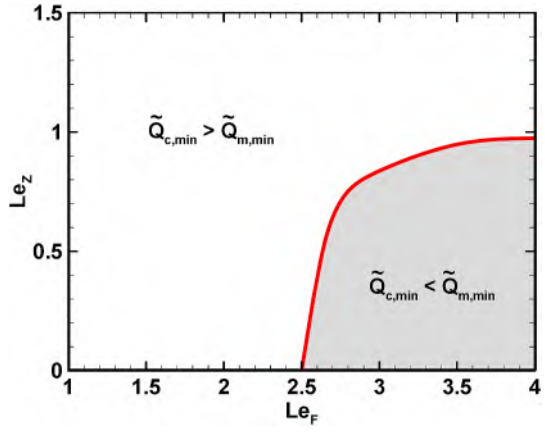

Fig. 26. The comparison between the minimum chemical and thermal ignition powers. Reproduced from Ref. [238] with permission from Elsevier.

In the simplified Zel'dovich-Liñán model given in Eqs. (78) and (79), the chain-branching reaction was usually assumed to be thermally neutral, and thereby the combination reaction releasesd all the heat. However, in the practical combustion process, the chain-branching reaction is usually endothermic [236] and the endothermicity of the chain-branching reaction might affect premixed flame ignition and propagation. Li et al. [240] conducted theoretical analysis on spherical flame initiation and propagation, considering an endothermic chain-branching reaction and an exothermic recombination reaction. Following the similar analysis procedure in Ref. [237], Li et al. [240] derived an implicit correlation depicting the change of the flame propagation speed with flame radius, based on which the effects of the endothermicity of the chain-branching reaction on ignition kernel propagation and critical ignition conditions were assessed. It was found that the endothermicity of the chain-branching reaction can inhibit the radical accumulation at the flame front and thereby suppresses the flame intensity. The Markstein length increases monotonically with endothermicity, indicating that the effects of endothermicity tend to become stronger on the propagation of stretched flames with large fuel Lewis numbers. In addition, the endothermicity of the chain-branching reaction also affects the transition among various flame regimes, including ignition kernel, flame ball, propagating spherical flame, and planar flame. The critical ignition radius was found to increase with endothermicity. Therefore, endothermicity inhibits the ignition process, though it does not change the adiabatic flame temperature [240].

3.5.3. *Quasi-steady ignition theory considering droplet or solid particle*

In practical combustion devices, such as internal combustion engines, gas turbines, and rocket engines, usually liquid fuels are supplied. The operation process requires that liquid fuels are vaporized before taking part in the ignition and subsequent combustion processes [241,242]. Therefore, the initiation of premixed flame in multi-phase systems plays a crucial role in affecting the overall performance of different types of engines.

For liquid fuels injected into a gaseous oxidizer, the fuel spray is

generated by atomization, which produces a large number of droplets of exceedingly small size. A schematic of a premixed spherical spray flame consisting of droplet evaporation is shown in Fig. 27. The flame structure is shown to consist of four zones: the outer pre-vaporization zone with negligible droplet evaporation, the pre-flame zone, where finite-rate vaporization occurs, the thin reaction zone which is assumed to be infinitely thin at large-activation energy, and the post-flame zone. The front of the onset of vaporization is located at the radius of R_v and the flame front is at R_f. The droplet vaporization provides gaseous fuel, and meanwhile, absorbs thermal energy from the surroundings. Such two-fold impacts result in additional complexity in the ignition process.

Based on large activation energy asymptotics, Han and Chen [29] proposed a simplified theoretical model interpreting the ignition and propagation of premixed spherical spray flames. This model incorporates various key parameters, e.g., initial droplet load, finite vaporization rate, Lewis number, and ignition power, into analytical correlations describing the change of flame propagation speed with flame radius. A theoretical interpretation of the dynamic characteristics of spray flame initiation was obtained in the limit of infinitesimal droplets, i.e., the droplets are embedded in the gaseous environment with zero dimension and thus can instantaneously adjust to the velocity of the surrounding gas [29]. In such situations, the spray system is considered a continuum composed of fuel droplets, fuel vapor, and gaseous oxidizer. The simplified spray models in the AEA theoretical framework aim to reduce the complexity of spray combustion to a manageable analytical form. However, it should be understood that the vaporization rate is inherently transient, and moreover, the accumulation rate of fuel vapor depends upon the droplet size [243]. The transiency of droplet vaporization induces an induction period in addition to the quasi-steady vaporization period predicted by the d^2-law [244]. Droplet vaporization can lower the temperature of the combustible mixture, affect reaction rates, and thus exhibit substantial impacts on chemical kinetics. Those effects, due to mathematical complexity, were not taken into account in theoretical models based on AEA.

The initiation of spray combustion also involves the creation and expansion of the ignition kernel. The high temperature at the flame front substantially facilitates the vaporization of droplets nearby, which results in a pre-flame zone enveloping the ignition kernel, as shown in Fig. 28. The fuel-rich and fuel-lean cases are determined by the global equivalence ratio based on the total fuel concentration, including both fuel vapor and droplets. However, the reaction rate is mainly

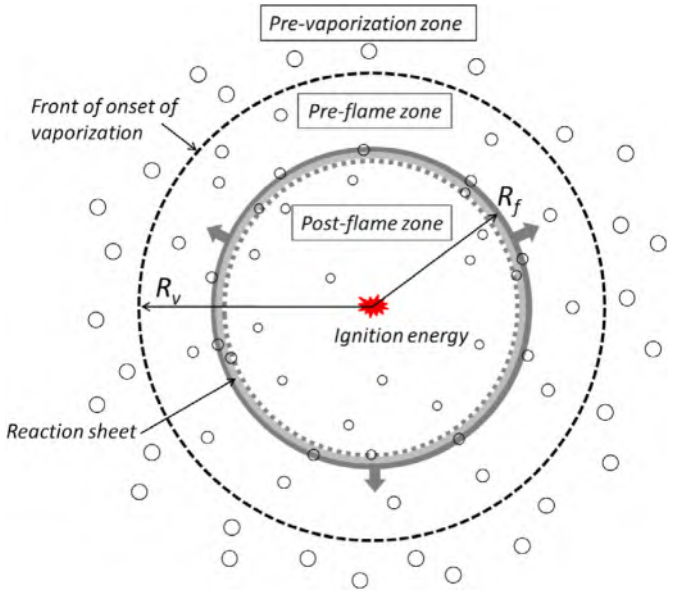

Fig. 27. Configuration for premixed spherical spray flame with finite-rate droplet evaporation. Reprinted from Ref. [29] with permission from Elsevier.

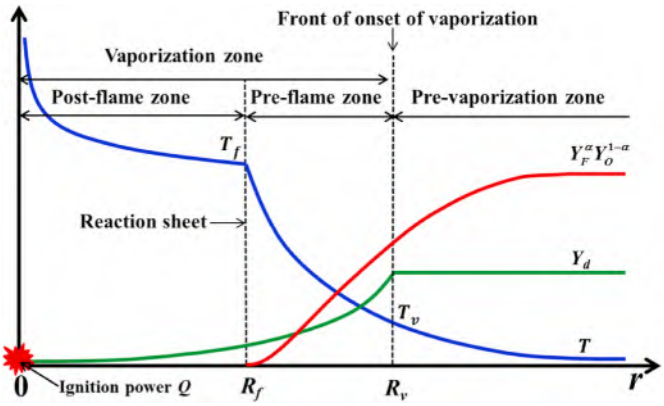

Fig. 28. Schematic of different zones and temperature and mass fraction distributions in a premixed spherical spray flame for fuel-rich $\alpha = 0$ and fuel-lean $\alpha = 1$ cases. Reprinted from Ref. [29] with permission from Elsevier.

determined by the effective equivalence ratio, which is based on only the fuel vapor concentration. For a fuel-rich case with a local effective equivalence ratio at the flame front above unity, oxygen is completely consumed in the pre-flame zone. Therefore, the fuel droplets may traverse through the flame front and continue vaporization inside the post-flame zone. For the fuel-lean case, the absence of fuel within the post-flame zone implies that, in addition to vaporization in the pre-flame zone, the remaining fuel droplets are completed by burning as they cross the flame front.

The presence of the vaporization-dominant pre-flame zone does not affect the characteristics of the chemical reaction. Accordingly, the flame front can also be solved by means of large activation energy asymptotics. In quasi-steady theory, the temperature and molar fraction of fuel vapor on either side of the flame front satisfy the following equations in nondimensional form [29]:

$$-\widetilde{U}\frac{d\widetilde{T}}{d\widetilde{r}_s} = \frac{1}{(\widetilde{r}_s+\widetilde{R}_f)^2}\frac{d}{d\widetilde{r}_s}\left[(\widetilde{r}_s+\widetilde{R}_f)^2\frac{d\widetilde{T}}{d\widetilde{r}_s}\right] - \widetilde{q}_v\widetilde{\omega}_v + H(1-\varphi)\varpi \tag{90}$$

$$-\widetilde{U}\frac{d\widetilde{Y}_{F,V}}{d\widetilde{r}_s} = \frac{1}{Le_F}\frac{1}{(\widetilde{r}_s+\widetilde{R}_f)^2}\frac{d}{d\widetilde{r}_s}\left[(\widetilde{r}_s+\widetilde{R}_f)^2\frac{d\widetilde{Y}_{F,V}}{d\widetilde{r}_s}\right] + \widetilde{\omega}_v + H(1-\varphi)\varpi \tag{91}$$

$$-\widetilde{U}\frac{d\widetilde{Y}_{F,D}}{d\widetilde{r}_s} = -\widetilde{\omega}_v \tag{92}$$

where $\widetilde{Y}_{FV}$ and $\widetilde{Y}_{FD}$ are molar fractions of fuel vapor and fuel droplet, respectively, and φ the global equivalence ratio, $\widetilde{\omega}_v \sim Da\widetilde{Y}_F H(\widetilde{T}-\widetilde{T}_v)$ the non-dimensional vaporization rate, Da the vaporization Damköhler number (defined as the ratio between the characteristic time of flame and that of evaporation), $\widetilde{T}_v$ the non-dimensional reference temperature close to the boiling point of fuel droplet, $\widetilde{q}_v = q_v/q_c$ the non-dimensional latent heat of vaporization of fuel droplet, $\varpi = \widetilde{\omega}_v H(-\widetilde{r}_s)$ the non-dimensional burning rate of droplet, and H the Heaviside step function. The closure of the present mathematical formulation requires the determination of those quantities, which becomes available with knowledge of the theoretical model for droplet vaporization.

The boundary conditions at the far field, i.e., $\widetilde{r}_s \to \infty$, should be revised to $\widetilde{Y}_{F,V} = 1-\delta_D$ and $\widetilde{c}_{F,D} = \delta_D$, where δ_D refers to the initial droplet load. The presence of a pre-flame zone further introduces detailed structure in the unburned domain since droplet vaporization tends to be negligible outside the pre-flame zone. According to the definition of finite vaporization rate $\widetilde{\omega}_v$, the vaporization front, denoted by $\widetilde{r}_v$, could be determined as the radial coordinate where the local temperature is equal to the reference vaporization temperature $\widetilde{T}_v$,

$$\widetilde{T}(\widetilde{r}=\widetilde{R}_v)=\widetilde{T}_v \tag{93}$$

and moreover, the molar fractions of both fuel vapor and fuel droplets remain smooth across the vaporization front, i.e.,

$$\widetilde{Y}_{F,V}|_{\widetilde{R}_{v+}}=\widetilde{Y}_{F,V}|_{\widetilde{R}_{v-}},\ \widetilde{Y}_{F,D}|_{\widetilde{R}_{v+}}=\widetilde{Y}_{F,D}|_{\widetilde{R}_{v-}} \tag{94}$$

$$\frac{d\widetilde{Y}_{F,V}}{d\widetilde{r}_s}|_{\widetilde{R}_{v+}}=\frac{d\widetilde{Y}_{F,V}}{d\widetilde{r}_s}|_{\widetilde{R}_{v-}},\frac{d\widetilde{Y}_{F,D}}{d\widetilde{r}_s}|_{\widetilde{R}_{v+}}=\frac{d\widetilde{Y}_{F,D}}{d\widetilde{r}_s}|_{\widetilde{R}_{v-}} \tag{95}$$

The temperature and fuel vapor and droplet distributions in the unburned region could be solved separately on either side of the vaporization front, which are then joined by the matching conditions (93) – (95). Droplet vaporization may affect the solutions in the burned region, depending on the equivalence ratio.

In the leading-order approximation, the droplet vaporization has no impact on the reaction zone structure, so the matching conditions (28) and (29) remain valid. Following a similar approach, substituting the solutions of temperature and fuel vapor on the burned and unburned sides into those matching conditions, one can determine the propagation speed $\widetilde{U}$ and flame temperature $\widetilde{T}_f$ for given flame radius $\widetilde{R}_f$ according to the following algebraic system [29]:

For the fuel-rich case ($\alpha=0$):

$$\underbrace{\frac{\widetilde{T}_f\widetilde{R}_f^{-2}e^{-\widetilde{U}\widetilde{R}_f}}{I_1(0,U)}}_{\text{heat absorbed by gaseous fuel}}-\underbrace{\widetilde{Q}\widetilde{R}_f^{-2}e^{-\widetilde{U}\widetilde{R}_f}}_{\text{heat provided by ignition energy}}+\underbrace{\widetilde{q}_v Da\delta_D\widetilde{R}_f^{-2}e^{-\widetilde{U}\widetilde{R}_f}\left[E(\widetilde{U},-\widetilde{R}_f,\eta_v)-\frac{I_2(0,\widetilde{U})}{I_1(0,\widetilde{U})}\right]}_{\text{heat absorbed for droplet evaporation}}=\underbrace{\frac{Le_O^{-1}\widetilde{R}_f^{-2}e^{-\widetilde{U}\widetilde{R}_f}}{I_1(0,\widetilde{U}Le_O)}}_{\text{heat supplied by oxygen}}=\underbrace{\left[\sigma+(1-\sigma)\widetilde{T}_f\right]^2\exp\left[\frac{Ze(\widetilde{T}_f-1)}{2\sigma+2(1-\sigma)\widetilde{T}_f}\right]}_{\text{heat produced by reaction}} \tag{96}$$

For the fuel-lean case ($\alpha=1$):

$$\begin{aligned}&\underbrace{\frac{\widetilde{T}_f\widetilde{R}_f^{-2}e^{-\widetilde{U}\widetilde{R}_f}}{I_1(0,U)}}_{\text{heat absorbed by gaseous fuel}}-\underbrace{\widetilde{Q}\widetilde{R}_f^{-2}e^{-\widetilde{U}\widetilde{R}_f}}_{\text{heat provided by ignition energy}}+\underbrace{\widetilde{q}_v Da\delta_D\widetilde{R}_f^{-2}e^{-\widetilde{U}\widetilde{R}_f}E(\widetilde{U},-\widetilde{R}_f,0)}_{\text{heat supplied by droplet burning}}+\underbrace{q_v Da\delta_D\widetilde{R}_f^{-2}e^{-\widetilde{U}Le_F\widetilde{R}_f}\left[E(U,-\widetilde{R}_f,\eta_v)-\frac{I_2(0,\widetilde{U})}{I_1(0,\widetilde{U})}\right]}_{\text{heat absorbed for droplet evaporation}}\\&=\underbrace{\frac{(1-\delta)Le_F^{-1}\widetilde{R}_f^{-2}e^{-\widetilde{U}Le_F\widetilde{R}_f}}{I_1(0,\widetilde{U}Le_F)}}_{\text{heat supplied by initial fuel vapor}}+\underbrace{Da\delta\widetilde{R}_f^{-2}e^{-\widetilde{U}Le_F\widetilde{R}_f}\left[E(\widetilde{U}Le_F,0,\eta_v)-\frac{I_2(0,\widetilde{U}Le_F)}{I_1(0,\widetilde{U}Le_F)}\right]}_{\text{heat supplied by fuel vapor from droplet evaporation}}=\underbrace{\left[\sigma+(1-\sigma)\widetilde{T}_f\right]^2\exp\left[\frac{Ze(\widetilde{T}_f-1)}{2\sigma+2(1-\sigma)\widetilde{T}_f}\right]}_{\text{heat produced by reaction}}\end{aligned} \tag{97}$$

where

$$E(x,\kappa_1,\kappa_2)=\int_{\kappa_1}^{\kappa_2}\left\{\left(\xi+\widetilde{R}_f\right)^2\exp\left[x\left(\xi+\widetilde{R}_f\right)+Da\left(\xi-\widetilde{R}_v+\widetilde{R}_f\right)/\widetilde{U}\right]\right\}d\xi$$

$$I_1(x,\kappa)=e^{-\kappa\widetilde{R}_f}\int_x^{\infty}\left(\xi+\widetilde{R}_f\right)^{-2}e^{-\kappa\xi}d\xi$$

$$I_2(x,\kappa)=e^{-\kappa\widetilde{R}_f}\int_x^{\widetilde{R}_v-\widetilde{R}_f}\left(\xi+\widetilde{R}_f\right)^{-2}e^{-\kappa\xi}\cdot E\left(\kappa,\xi,\widetilde{R}_v-\widetilde{R}_f\right)d\xi$$

In the limit of zero droplet load, i.e., $\delta_D=0$, Eq. (97) can be reduced to Eq. (76) and (77) describing ignition and flame propagation in purely gaseous mixtures as described in Section 3.5.1. By numerically solving Eq. (96) or (97), we can we can obtain the change in flame propagation speed $\widetilde{U}$ with flame radius $\widetilde{R}_f$ at any specified values for central ignition power $\widetilde{Q}_m$, initial droplet load δ_D, vaporization Damköhler number Da, and Lewis number for fuel Le_F or oxidizer Le_O. Consequently, the effects of initial droplet load and vaporization Damköhler number (which is proportional to the evaporation rate) on the ignition of a spherical spray flame can be examined [29].

Fig. 29 shows the change of spherical flame propagation speed with flame radius at different ignition powers for the fuel-lean case. For a purely gaseous mixture with $\delta_D=0$, the results are the same as those in Section 3.5.1. At relatively low ignition powers, there exist two separate branches of the $\widetilde{U}-\widetilde{R}_f$ phase diagram, which collapse into a single curve when the ignition power grows beyond the minimum ignition power, i.e., $\widetilde{Q}_m>\widetilde{Q}_{\min}$. Comparison between the results without $\delta_D=0$ and with droplet evaporation $\delta_D=0.2$ indicates that the separation of the inner and outer branches of the $\widetilde{U}-\widetilde{R}_f$ phase diagram becomes wider in situations with $\delta_D=0.2$. This demonstrates that droplet evaporation shows inhibiting effects upon the ignition process, and the critical ignition power grows with δ_D concomitantly. For larger fuel Lewis numbers, e.g., $Le_O=2.0$, the outer branch of the $\widetilde{U}-\widetilde{R}_f$ phase diagram exhibits to be C-shaped, which is consistent with the results obtained in pure gaseous combustible mixture. Therefore, droplet evaporation does not qualitatively affect the characteristics of flame kernel evolution during the forced ignition process.

The minimum ignition power depends upon the Lewis numbers of fuel (oxidizer) for fuel rich (lean) combustible mixtures. It was found that droplet evaporation has a much stronger effect on ignition in fuel-lean cases than in fuel-rich cases [29]. Fig. 30 shows that the minimum ignition power grows monotonically with Lewis number for both gaseous ($\delta_D=0$) and spray ($\delta_D>0$) flames. In a fuel-rich environment, the minimum ignition power hardly changes with the droplet load because the ignition kernel has a high flame temperature and wide vaporization zone, which ensures complete vaporization of the droplet in the pre-flame zone. However, for fuel-lean cases, the minimum ignition power increases significantly with droplet load, especially at large Lewis numbers. Note that the droplet vaporization in the fuel-lean case changes the local effective equivalence ratio in addition to absorbing the

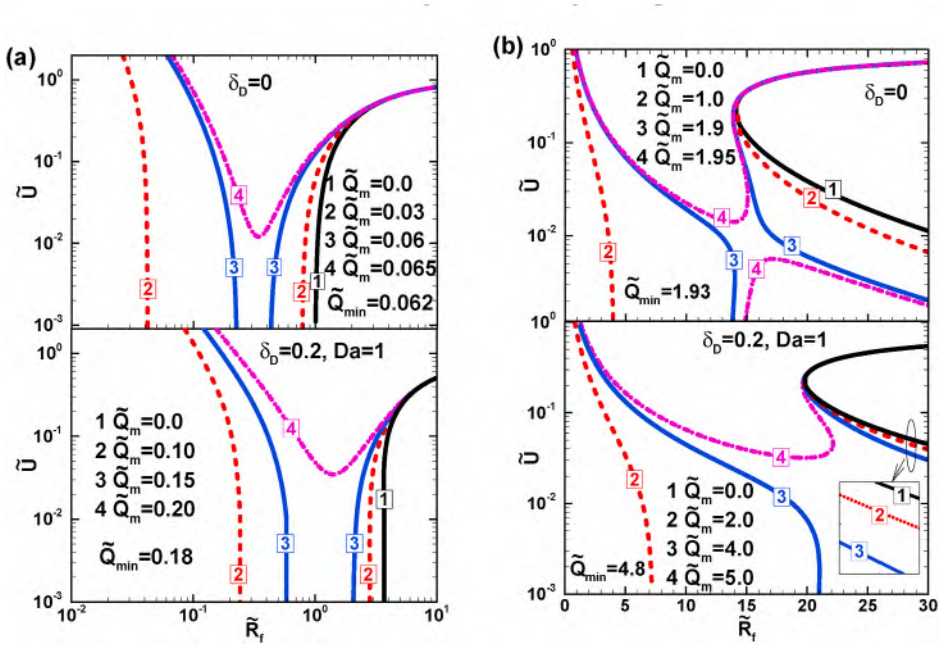

Fig. 29. Change of the normalized flame propagation speed with flame radius for different central ignition powers at (a) $Le_F = 1$ and (b) $Le_F = 2$ for fuel-lean case. Reprinted from Ref. [29] with permission from Elsevier.

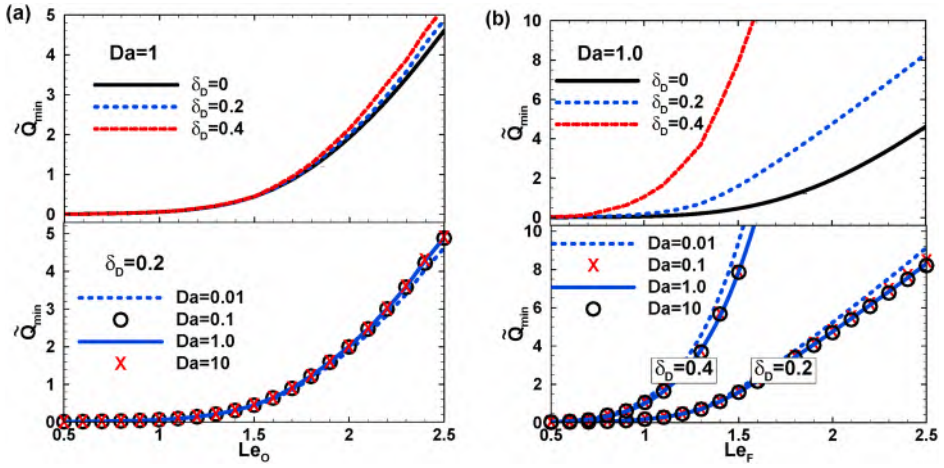

Fig. 30. Change of the minimum ignition power with the Lewis number for fuel-rich (a) and fuel-lean (b) cases. Reprinted from Ref. [29] with permission from Elsevier.

latent heat of vaporization in the pre-flame and post-flame zones. Therefore, the spray flame of lean hydrocarbon fuels with a large Lewis number is much more difficult to ignite compared to an equivalent purely gaseous flame.

The theory of Han and Chen [29] was extended by Li et al. [245] by considering the unsteady evolution of droplet distribution caused by droplet evaporation. They studied two types of flames, heterogeneous and homogeneous flames, determined by the relative position of the flame front and droplet evaporation completion front. The evaporative heat loss was found to have a different impact on the ignition of homogeneous and heterogeneous spray flames.

For a combustible mixture in a humid environment, Zhuang and Zhang [246] conducted a theoretical analysis and found that the presence of water droplets exhibits substantial impacts on the ignition and extinction characteristics of the premixed spherical flame. At relatively large heat exchange coefficients, the total evaporation heat loss from the pre-flame and post-flame zones is sufficiently intensive to induce a self-extinguishing flame. In addition, the combined effects of differential diffusion and stretch rate compete with the evaporation heat loss, which substantially changes the flammability of the mixture. Zhuang and Zhang [247] further extended their analysis by considering the continuously evolving (fully or partially dispersed) distributions of evaporating droplets. They demonstrated that the Lewis number has a great impact on the ignition and propagation of droplet-laden spherical flames.

Gaseous combustible mixtures laden with dispersed solid particles are widely encountered in engineering applications (e.g., pulverized coal combustion and sooty flames in gas turbine engines) as well as dust explosions. The existence of particles can result in new phenomena in the ignition and combustion processes through inter-phase interactions with the gaseous environment in terms of mass, momentum, and energy exchange [248]. Based on quasi-steady assumptions and large activation energy asymptotics, Li et al. [249] conducted a theoretical investigation on spherical flame initiation and propagation in a static mixture laden with chemically inert solid particles. They derived the correlation describing spherical flame propagation speed as a function of flame

radius and assessed the effects of particle properties on the ignition and propagation of spherical flames. For particle-laden flames, the MIE also increases monotonically with the Lewis number. At a larger Lewis number, the presence of particles has a stronger influence on the MIE. Since the particle thermal response time determines the heat transfer between gas and particle phases, it has a great impact on the propagation speed of the ignition kernel and, thereby, on the critical ignition conditions for particle-laden flames [249].

3.6. Transient ignition theory

In the quasi-steady theory of premixed flame initiation, external heating is applied as an ever-lasting deposition of thermal energy from a concentrated point. Due to the absence of time scales, the essential concept of MIE is unavailable in existing ignition theories based on the quasi-steady state assumption [12,29,144,219]. In addition, the initiation and development of the ignition kernel during its transition to a self-sustained spherical flame is a highly transient process [109,250]. Therefore, it requires transient ignition theory that can provide more accurate description of the dynamic evolution of the ignition kernel and a sensible evaluation of MIE.

3.6.1. Theory of thermal wave propagation

Sanchez et al. [251] conducted an analytical study on the ignition process with emphasis on the transient, one-dimensional flow induced by the localized energy source. It demonstrated that the convection resulting from thermal expansion helps the transport of heat away from the source and thus supports the propagation of thermal waves. Kurdyumov and coworkers [9,176] investigated the formation of planar, cylindrical, and spherical flame fronts due to energy sources. The hydrodynamic and thermodynamic behaviors of heat propagation were comprehensively analyzed by separating dominant mechanisms into distinct spatial regions. Based on time scale analysis, the dynamic evolution of the temperature profile was obtained, according to which the ignition characteristics were interpreted, and the MIE was evaluated. Fernandez-Tarrazo et al. [252] proposed a method to calculate the MIE for gaseous fuel/air mixtures considering detailed kinetic models. This method was tested for methanol-air mixtures considering detailed chemistry with 38 elementary reactions and reduced chemistry with 8 elementary reactions. Good agreement between the numerically predicted MIE and the available experimental results was achieved (see Fig. 1 in Ref. [252]), which supports the robustness of the computational method.

For a concentrated energy source with a finite deposition time, the ignition outcome can be predicted by integrating the unsteady heat propagation process, and the MIE can be evaluated. Existing studies have shown that the heat propagation process is characterized by a two-regime-structure, when the heating duration is comparable with the acoustic time scale [9,152,176]. A brief description is presented as follows: The time lapse of the external heating is denoted by t_0, during which a total amount of thermal energy E_0 is released, suggesting an average heating power of $\overline{q} = E_0/t_0$. The energy deposition induces a hot pocket with the length scale of r_0, in which the temperature is exceedingly high due to external heating. Under the uniform pressure condition, the high temperature environment creates remarkably low density. The front of this low-density regime exhibits to be a contact surface that acts as a piston pushing the fluid outwards. The motion of the piston creates a pressure wave that propagates at the local sound speed. The acoustic time scale could be evaluated in terms of the pressure p_0 and ρ_0 of the unperturbed gas, i.e., $t_{\text{acoustic}} \sim r_0/\sqrt{p_0/\rho_0}$.

To simplify the governing equations describing aerothermodynamic behavior of the unburnt gas subject to finite domain external heating, the following nondimensional quantities are introduced:

$$\check{r} = \frac{r}{r_0}, \check{t} = \frac{t}{t_{\text{acoustic}}}, \check{p} = \frac{p}{p_0}, \check{T} = \frac{T}{T_0}, \check{\rho} = \frac{\rho}{\rho_0} \tag{98}$$

The overhead symbol is selected to be "∨" in order to avoid misunderstanding with the nondimensional quantities defined based on the properties of laminar flame, which are denoted by the overhead symbol "∼".

Pressure waves are incessantly produced by external heating. They collapse ahead of the hot pocket to form shock waves when the heating duration is comparable with the acoustic time, i.e., $t_0 \sim t_{\text{acoustic}}$ or in nondimensional form $\check{t}_0 \sim 1$. The non-dimensional radial distance of the shock wave is denoted by $\check{r}_N$, whose time derivative gives the propagation speed, i.e., $\check{u}_N = d\check{r}_N/d\check{t}$. Behind the shock wave, the fluid element moves at the speed of $\check{v}_N$ with density $\check{\rho}_N$ and pressure $\check{p}_N$, which are determined by the following matching conditions:

$$\frac{d\check{r}_N}{d\check{t}} = \sqrt{\frac{\gamma - 1 + (\gamma+1)\check{p}_N}{2}} \tag{99}$$

$$\frac{d\check{r}_N}{d\check{t}} - \check{v}_N = \frac{\gamma + 1 + (\gamma-1)\check{p}_N}{\sqrt{2\left[\gamma - 1 + (\gamma+1)\check{p}_N\right]}} \tag{100}$$

$$\check{\rho}_N = \frac{\gamma - 1 + (\gamma+1)\check{p}_N}{\gamma + 1 + (\gamma-1)\check{p}_N} \tag{101}$$

As indicated by Vázquez-Espí and Liñán [152], the ratio between the acoustic time scale and thermal conduction time scale is a small parameter, i.e., $\varepsilon = t_{\text{acoustic}}/t_{\text{conduction}} \ll 1$. In terms of the small parameter ε, asymptotic analysis can be conducted. Close to the heating source, the temperature within the hot pocket is extraordinarily high, and thus it is convenient to define a rescaled temperature $\theta = \varepsilon\widehat{T}$ of order unity, which satisfies the following thermal energy equation

$$\frac{\partial}{\partial\check{t}}\left(\frac{\check{p}_e}{\theta}\right) + \frac{1}{\check{r}^2}\frac{\partial}{\partial\check{r}}\left[\frac{1}{\theta}\left(\frac{\check{q}}{\check{t}_d} - \frac{\check{r}^3}{\gamma}\frac{d\check{p}_e}{d\check{t}} + \check{r}^2\frac{\partial\theta}{\partial\check{r}}\right)\right] = 0 \tag{102}$$

where $\check{q} = q/\overline{q}$ is the non-dimensional heating power and $\gamma = c_p/c_v$ the heat capacity ratio. The quantity $\check{p}_e$ refers to the uniform pressure in the hot pocket and is equal to that at the edge of the thermal wave. The initial and boundary conditions for Eq. (102) are

$$\check{t} = 0, \theta = 0 \tag{103}$$

$$\check{t} > 0, \check{r} \to 0, \check{r}^2\partial\theta\Big/\partial\check{r} = -\check{q}\Big/\check{t}_0 \tag{104}$$

$$\check{t} > 0, \check{r} = \widehat{r}_e, \partial\theta/\partial\check{r} = 0 \tag{105}$$

where $\check{r}_e$ represents the edge of the hot pocket, i.e., the thermal wave front, beyond which the magnitude of θ is of order $O(\varepsilon)$ and thus tends to be negligible in the first approximation. The thermal wave behaves as a contact surface, indicating that the propagation speed of the thermal front is identical to the moving velocity of the fluid, i.e.,

$$\frac{d\check{r}_e}{d\check{t}} = \check{v}_e \tag{106}$$

In addition, the heat flux vanishes there, providing the energy balance relationship

$$\frac{\check{r}_e^3}{\gamma}\frac{d\check{p}_e}{d\check{t}} + \check{p}_e\check{v}_e = \frac{\check{q}}{\check{t}_0} \tag{107}$$

which states that the thermal energy delivered by external heating is used to increase the internal energy of the hot pocket region and, in the meantime, to displace the outer cold fluid outward.

In the regime between the hot pocket and the resulting shock wave, the Reynolds number is of order $\varepsilon^{-1} \gg 1$ and thus the fluid flow can be described by Euler equations. Integrating the Euler equations with

boundary conditions (106) and (107) at $\check{r}=\check{r}_e$ and boundary conditions (99) – (101) at $\check{r}=\check{r}_N$ determines the instantaneous locations of the thermal front and the leading shock along with the hot pocket pressure as functions of time, i.e., $\check{r}_e=\check{r}_e(t)$, $\check{r}_N=\check{r}_N(\widehat{t})$, and $\check{p}_e=\check{p}_e(\widehat{t})$. With knowledge of those informations, the structure of the thermal wave, i.e., the temperature profile in the hot pocket region, can be determined by integrating Eq. (102) subject to initial and boundary conditions (103) – (105), through which the dynamic evolution of the thermal wave can be fully determined at a given heating power $\check{q}$ and duration $\check{t}_0$. In the post-heating stage, the rate of hot pocket expansion diminishes, leading to a rapid decrease of pressure $\check{p}_e$ and a reduction in the propagation speed of the thermal wave front. Therefore, the final state of the thermal wave is determined by the characteristics of external heating.

In limit situations of $\check{t}_0\ll 1$, the thermal energy is deposited instantaneously. It generates a blast wave, whose intensity decays as it propagates outward. The pressure settles to the ambient value in the stage $1\ll\check{t}\ll\varepsilon^{-1}$, which yields the asymptotic distribution of temperature and thus determines the thermal wave structure.

In the opposite limit of $\check{t}_0\gg 1$ the propagation of the thermal wave proceeds under nearly isobaric conditions, and the thermal wave structure is dominated by pure conduction.

Corresponding to each physicochemical state of a combustible mixture, there exists a critical ignition radius that depends on various fuel parameters, such as molecular structure, equivalence ratio, and Lewis number, and must be known before evaluating the ignition outcome. Successful ignition is characterized by the passage of the thermal wave through the critical ignition radius so that a self-sustained spherical flame appears. The MIE can be determined by the requirement of equality between the final radius of the thermal front and the critical ignition radius.

3.6.2. General theory on transient ignition and spherical flame propagation

Evaluation of MIE based on thermal wave theory implies that the duration of external heating is much shorter than the conduction time scale, i.e., $t_0\ll t_{\text{conduction}}$. In the meanwhile, the reaction time scale under the critical ignition condition is comparable with the conduction time scale. This implies that the chemical reaction tends to be frozen during the thermal energy deposition from external heating, according to which the development of thermal waves is not affected by heat release from the chemical reaction. A more accurate interpretation of premixed flame ignition involves the transient development of the ignition kernel, during which a self-sustained spherical flame is supported by both external heating and heat release from chemical reactions.

Yu and Chen [109,253] conducted theoretical studies on the forced-ignition of a premixed expanding spherical flame in a quiescent mixture with emphasis on the transient evolution of the flame kernel subject to finite duration external heating. Their results indicated that the unsteady effect leads to a longer critical ignition radius and high critical ignition power, i.e., the ignition process becomes more difficult when the unsteady effect is considered. In addition, the transient ignition theory can appropriately describe the sustaining propagation of the flame kernel subsequent to switching off the external heating, and is thereby able to deal with external heating with a finite duration, enabling the prediction of MIE. The transient ignition theory [109] generalizes the quasi-steady formulation by incorporating the time-dependent terms in the governing equations, through which the transient evolution of the temperature and reactant mass fraction are taken into account.

The general theory for transient ignition and flame propagation developed by Yu and Chen [109,253] was established based on the AEA framework, adopting constant density assumption and simplified one-step reaction model. In real-life ignition problem, the variable density effect, detailed reaction kinetics model, and accurate equation of state offer a more detailed and potentially accurate representation of the ignition process. However, this high accuracy comes at the cost of a significant increase in mathematical complexity and thus the impossibility of obtaining analytical solutions for ignition problem. The simplified theoretical model based on AEA yields an analytical, albeit implicit, expression describing the flame kernel propagation, which is instrumental in elucidating the core dynamics of ignition and flame kernel development under transient conditions. Analytical expressions provide a direct means to examine the influence of key parameters on ignition outcome.

In the AEA framework of transient premixed ignition, the dynamic characteristics during the expansion of the ignition kernel consist of two parts, i.e., the unsteady motion of the flame front and the transient evolution of the temperature and reactant molar fraction profiles across the flame front. It should be noted that the sphericity of the flame front suggests that a suitable time scale describing the transient variation of temperature and reactant molar fraction profiles due to conduction and diffusion, which are related to the derivatives $\partial\widetilde{T}/\partial\widetilde{r}$ and $\partial\widetilde{Y}_F/\partial\widetilde{r}$, should be proportional to the surface area of the flame front, i.e., $\widetilde{t}_{\text{evolution}}\sim\widetilde{R}_f^2$. A suitable coordinate transform shall be defined by normalizing the spatial coordinate with the flame ball radius that varies in the course of time and scaling the time by the surface area of the flame ball, i.e. [109],

$$\sigma_s=\frac{\widetilde{r}}{\widetilde{R}_f(t)},\ t_s=\int_0^{\widetilde{t}}\frac{dt'}{\widetilde{R}_f^2(t')} \tag{108}$$

Applying the coordinate transform (108) to governing Eqs. (24) and (25), one obtains

$$\frac{\partial\widetilde{T}}{\partial t_s}-\widetilde{R}_f\sigma_s\widetilde{U}\frac{d\widetilde{T}}{d\sigma_s}=\frac{1}{\sigma_s^2}\frac{d}{d\sigma_s}\left(\sigma_s^2\frac{d\widetilde{T}}{d\sigma_s}\right)+\frac{Ze^2\widetilde{Y}_F}{2Le}\exp\left[-Ar\left(\frac{\widetilde{T}_{ad}}{\widetilde{T}}-1\right)\right] \tag{109}$$

$$\frac{\partial\widetilde{Y}_F}{\partial t_s}-\widetilde{R}_f\sigma_s\widetilde{U}\frac{d\widetilde{Y}_F}{d\sigma_s}=\frac{1}{Le}\frac{1}{\sigma_s^2}\frac{d}{d\sigma_s}\left(\sigma_s^2\frac{d\widetilde{Y}_F}{d\widetilde{r}}\right)-\frac{Ze^2\widetilde{Y}_F}{2Le}\exp\left[-Ar\left(\frac{\widetilde{T}_{ad}}{\widetilde{T}}-1\right)\right] \tag{110}$$

The initial and boundary conditions are:

$$t_s=0:\widetilde{T}=\widetilde{T}_u\text{and}\ \widetilde{Y}_F=1\ \text{for}\ \sigma_s>1 \tag{111}$$

$$\widetilde{T}=\widetilde{T}_b\ \text{and}\ \widetilde{Y}_F=0\ \text{for}\ \sigma_s<1$$

$$\sigma_s=0:\ \frac{\partial\widetilde{T}}{\partial\sigma_s}=\widetilde{Q}\ \text{and}\ \widetilde{Y}_F=0 \tag{112}$$

$$\sigma_s\to\infty:\widetilde{T}=\widetilde{T}_u\ \text{and}\ \widetilde{Y}_F=1 \tag{113}$$

The choice of initial conditions can influence the evaluation of key ignition parameters, such as minimum ignition energy and critical ignition radius. In the transient theoretical model, the initial conditions are simplified to be a point-less energy source that provides ignition energy into the combustible mixture within the given period. Such an approach helps focus on the primary influence of ignition deposition rate and amount upon the subsequent flame kernel propagation process and facilitates the derivation of analytical insights into transient ignition processes.

Adopting large activation energy asymptotic analysis, the reaction terms disappear on the sides of the ignition kernel front in the leading-order approximation. The first order derivative corresponding to flame front propagation causes mathematical difficulty in obtaining analytical solutions for temperature and reactant molar fractions. Such an issue can be fixed by introducing additional coordinate transformation separately on each side of the flame front [109].

On the unburned side, the coordinate transform is defined as

$$\xi_{uT}=\left(\int_0^{\infty}\frac{e^{-\bar{R}_f\bar{U}\left(\sigma_s^2-1\right)/2}}{\sigma_s^2}d\sigma_s\right)^{-1}\left(\int_0^{\sigma_s}\frac{e^{-\bar{R}_f\bar{U}\left(\sigma_s^2-1\right)/2}}{\sigma_s^2}\sigma_s'\right) \tag{114}$$

$$\xi_{uc}=\left(\int_0^{\infty}\frac{e^{-Le\tilde{R}_f\tilde{U}\left(\sigma_s^2-1\right)/2}}{\sigma_s^2}d\sigma_s\right)^{-1}\left(\int_0^{\sigma_s}\frac{e^{-Le\tilde{R}_f\tilde{U}\left(\sigma_s^2-1\right)/2}}{\sigma_s^2}d\sigma_s'\right) \tag{115}$$

In terms of ξ_{uT} and ξ_{uc}, the governing equations are simplified to

$$\frac{\partial\tilde{T}}{\partial t_s}=\mathscr{T}_{uT}^2\frac{\partial^2\tilde{T}}{\partial\xi_{uT}^2} \tag{116}$$

$$\frac{\partial\tilde{c}_F}{\partial t_s}=\frac{\mathscr{T}_{uc}^2}{Le}\frac{\partial^2\tilde{c}_F}{\partial\xi_{uc}^2} \tag{117}$$

where the factors $\mathscr{T}_{uT}$ and $\mathscr{T}_{uc}$ are functions of σ_s, i.e.,

$$\mathscr{T}_{uT}=\frac{e^{-\tilde{R}_f\tilde{U}\left(\sigma_s^2-1\right)/2}}{\sigma_s^2}\left(\int_0^{\infty}\frac{e^{-\tilde{R}_f\tilde{U}\left(\sigma_s^2-1\right)/2}}{\sigma_s^2}d\sigma_s\right)^{-1} \tag{118}$$

$$\mathscr{T}_{uc}=\frac{e^{-Le\tilde{R}_f\tilde{U}\left(\sigma_s^2-1\right)/2}}{\sigma_s^2}\left(\int_0^{\infty}\frac{e^{-Le\tilde{R}_f\tilde{U}\left(\sigma_s^2-1\right)/2}}{\sigma_s^2}d\sigma_s\right)^{-1} \tag{119}$$

The initial and boundary conditions are specified as.

(i) at $t_s=0:\tilde{T}=\tilde{T}_u$ and $\tilde{c}_F=1$:

(b1) at $\xi_{uT}=0:\tilde{T}=\tilde{T}_f$:

at $\xi_{uc}=0:\tilde{Y}_F=0$:

(b2) at $\xi_{uT}=1:\tilde{T}=\tilde{T}_u$:

at $\xi_{uc}=1:\tilde{Y}_F=1$:

On the burned side, the coordinate transform is

$$\xi_{bT}=\frac{\mathrm{erf}\left(\sigma_s\sqrt{\tilde{R}_f\tilde{U}/2}\right)}{\mathrm{erf}\left(\sqrt{\tilde{R}_f\tilde{U}/2}\right)} \tag{120}$$

In terms of ξ_{bT}, the thermal energy equation can be written as

$$\frac{\partial\tilde{T}}{\partial t_s}=\mathscr{T}_{bT}^2\frac{\partial^2\tilde{T}}{\partial\xi_{bT}^2} \tag{121}$$

where the factor $\mathscr{T}_{bT}$ is defined as

$$\mathscr{T}_{bT}=\frac{2\sqrt{\tilde{R}_f\tilde{U}/2}e^{-\sigma_s^2\tilde{R}_f\tilde{U}/2}}{\sqrt{\pi}\mathrm{erf}\left(\sqrt{\tilde{R}_f\tilde{U}/2}\right)} \tag{122}$$

The initial and boundary conditions are specified as.

(i') at $t_s=0:\tilde{T}=\tilde{T}_b$:

(b1') at $\xi_{bT}=0:\tilde{T}=Q(t)$:

(b2') at $\xi_{bT}=1:\tilde{T}=\tilde{R}_f\tilde{T}_f$:

The temperature and reactant molar fraction distributions on both burned and unburned sides of the ignition kernel could be obtained by analytically solving Eqs. (116), (117) and (121) subject to preceding initial and boundary conditions [109]. For one-step global reaction model, the matching conditions (28) and (29) are still valid, which involves the derivatives of $\tilde{T}$ and $\tilde{c}_F$ with respect to $\tilde{r}$. With knowledge of analytical solutions, those quantities can be written in the following explicit forms:

$$\left(\frac{\partial\tilde{T}}{\partial\tilde{r}}\right)_{\tilde{R}_{f+}}=-\frac{\widehat{\mathscr{T}}_{uT}}{\tilde{R}_f}\left\{\tilde{T}_f+T_b^0\left[\vartheta_3\left(e^{-\mathscr{T}_{uT}^2\pi^2t\Big/\tilde{R}_f^2}\right)-1\right]\right\} \tag{123}$$

$$\left(\frac{\partial\tilde{c}_F}{\partial\tilde{r}}\right)_{\tilde{R}_{f+}}=\frac{\widehat{\mathscr{T}}_{uY}}{\tilde{R}_f}\vartheta_3\left(e^{-\pi^2\mathscr{T}_{uY}^2t\Big/\tilde{R}_f^2Le}\right) \tag{124}$$

$$\left(\frac{\partial\tilde{T}}{\partial\tilde{r}}\right)_{\tilde{R}_{f-}}=\frac{\widehat{\mathscr{T}}_{bT}}{\tilde{R}_f}\left(\tilde{T}_f-T_b^0\right)-\frac{Q_m}{\tilde{R}_f^2}\widehat{\mathscr{T}}_{bT}S\left(t,U,\tilde{R}_f\right) \tag{125}$$

where $\widehat{\mathscr{T}}_{uT}=\mathscr{T}_{uT}(\sigma_s=1)$, $\widehat{\mathscr{T}}_{uY}=\mathscr{T}_{uY}(\sigma_s=1)$, and $\widehat{\mathscr{T}}_{bT}=\mathscr{T}_{bT}(\sigma_s=1)$. The Jacobi theta function ϑ_3 and ϑ_4 respectively denote the sums $\vartheta_3(x)=1+2\sum_{n=1}^{\infty}x^{n^2}$ and $\vartheta_4(x)=1+2\sum_{n=1}^{\infty}(-1)^nx^{n^2}$. The function S is defined as

$$S\left(t,U,\tilde{R}_f\right)=\begin{cases}\vartheta_4\left(e^{-\mathscr{T}_{bT}^2\pi^2\tilde{t}\Big/\tilde{R}_f^2}\right),\tilde{t}<\tilde{t}_h\\ \vartheta_4\left(e^{-\mathscr{T}_{bT}^2\pi^2\tilde{t}\Big/\tilde{R}_f^2}\right)-\vartheta_4\left(e^{-\mathscr{T}_{bT}^2\pi^2\left(\tilde{t}-\tilde{t}_h\right)\Big/\tilde{R}_f^2}\right),\tilde{t}>\tilde{t}_h\end{cases} \tag{126}$$

where $\tilde{t}_h$ represents the duration of external heating. Substituting equations (123) – (125) into the matching conditions (28) and (29), one obtains the following expression for flame temperature, i.e.,

$$\tilde{T}_f=\tilde{T}_b^0+\frac{\widehat{\mathscr{T}}_{uY}\vartheta_3\left(e^{-\pi^2\mathscr{T}_{uY}^2\tilde{t}\Big/\tilde{R}_f^2Le}\right)\Big/Le+Q_m\widehat{\mathscr{T}}_{bT}S\left(\tilde{t},\tilde{U},\tilde{R}_f\right)\Big/\tilde{R}_f-\widehat{\mathscr{T}}_{uT}\tilde{T}_b^0\vartheta_3\left(e^{-\mathscr{T}_{uT}^2\pi^2\tilde{t}\Big/\tilde{R}_f^2}\right)}{\widehat{\mathscr{T}}_{bT}+\widehat{\mathscr{T}}_{uT}-1} \tag{127}$$

and the expression interpreting the consumption of reactant mixture across the flame front, i.e.,

$$\frac{\widehat{\mathscr{T}}_{uY}}{Le\tilde{R}_f}\vartheta_3\left(e^{-\pi^2\mathscr{T}_{uY}^2\tilde{t}\Big/\tilde{R}_f^2Le}\right)=\frac{\tilde{T}_f^2}{\tilde{T}_{ad}^2}\exp\left[-\frac{Ar}{2}\left(\frac{\tilde{T}_{ad}}{\tilde{T}_f}-1\right)\right] \tag{128}$$

The solutions in Eqs. (127) and (128) yield the time-dependent temperature $\tilde{T}_f$, radius coordinate $\tilde{R}_f$, and flame propagation speed $\tilde{U}$ of the ignition kernel [109]. The phase diagrams interpreting the dynamic propagation of flame kernels in combustible mixtures subject to different heating powers are presented in Fig. 31. The geometric characteristic of the phase diagram changes drastically as the magnitude of central heating power increases. For relatively low values of $\tilde{Q}_m$, the phase diagram consists of separate branches, the inner of which bounds the expansion of the ignition kernel originating from central heating, i.e., an ever-expanding spherical flame cannot be established. In situations with relatively high heating powers, the separate diagrams merge into a single curve, which suggests that the ignition kernel induced by central heating could successfully evolve into a self-sustaining spherical flame, i.e., a successful flame initiation process is achieved.

Based on the $\tilde{U}-\tilde{R}_f$ diagram given by solutions in Eq. (127) and (128), the premixed flame initiation process consists of four stages, namely, the fast establishment of the ignition kernel, the ignition-energy-supported flame kernel propagation, the unsteady transition of the flame kernel, and quasi-steady spherical flame propagation. Time scale analysis demonstrates that the transient ignition theory is consistent with the quasi-steady theory at the particular situation of a stationary flame ball ($\tilde{U}=0$) and the limit of a planar adiabatic premixed flame $\tilde{R}_f\to\infty$ [109]. However, at intermediate radius with comparably low propagation speed, i.e., $\tilde{R}_f\tilde{U}\sim O(1)$, the transient evolution for

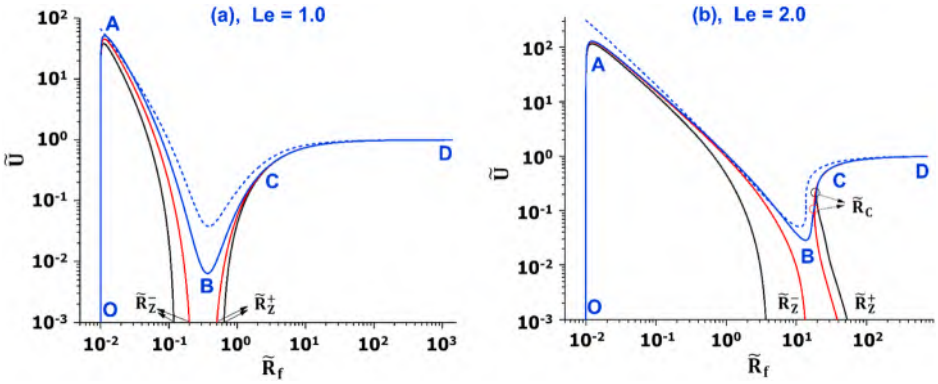

Fig. 31. Change of flame propagation speed with flame radius for different central heating powers. The solid lines are solutions from the transient formulation, while the dashed lines are results from quasi-steady theory. The heating powers are indicated by colors of the solid/dashed lines. (a) black for $\widetilde{Q}_m = 0.05$, red for $\widetilde{Q}_m = 0.06$, and blue for $\widetilde{Q}_m = 0.07$; (b) black for $\widetilde{Q}_m = 1.0$, red for $Q_m = 2.0$, and blue for $\widetilde{Q}_m = 2.5$. R_Z and $\widetilde{R}_C$ respectively denote the flame ball radius and critical radius for flame initiation. Reproduced from Ref. [109] with permission from Cambridge University Press.

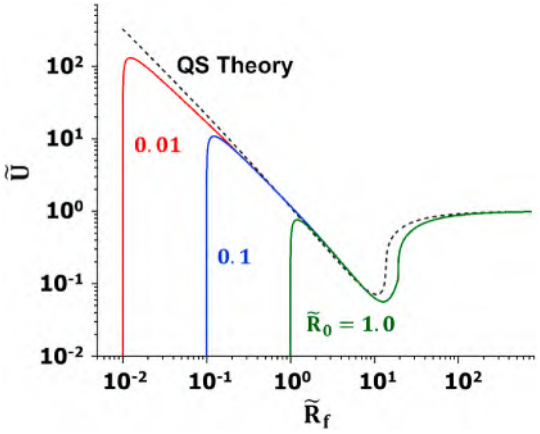

Fig. 32. Change of flame propagation speed with flame radius for different initial flame kernel radius of $\widetilde{R}_0 = 0.01$, 0.1 and 1.0. The solid lines are solutions from the transient formulation, while the dashed lines are results from quasi-steady theory. The Lewis number is 2.0 and the central heating power is $\widetilde{Q}_m = 2.5$. Reproduced from Ref. [109] with permission from Cambridge University Press.

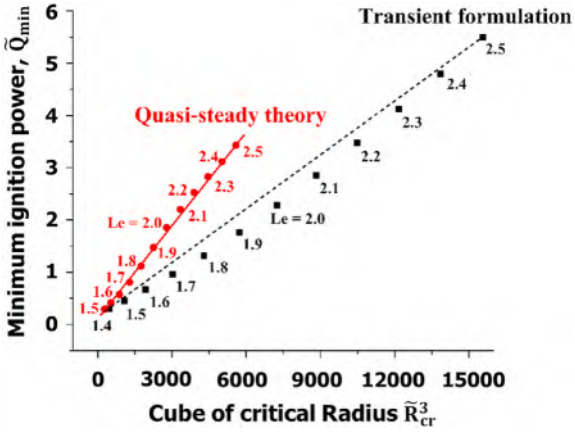

Fig. 34. Change of the minimum ignition power with the cube of critical ignition radius. The symbols represent results from quasi-steady theory or transient formulation, and the lines represent the scaling relationship of $\widetilde{Q}_{cr} \sim R_{cr}^3$. Reproduced from Ref. [109] with permission from Cambridge University Press. s

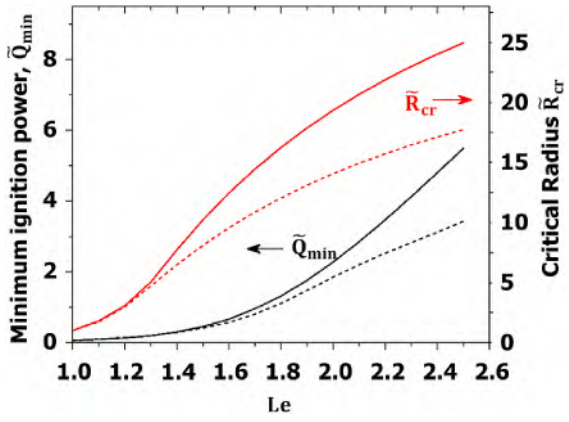

Fig. 33. Change of critical heating power and critical ignition radius with the Lewis number. The solid lines are solutions from the transient formulation, while the dashed lines are results from quasi-steady theory. Reproduced from Ref. [109] with permission from Cambridge University Press.

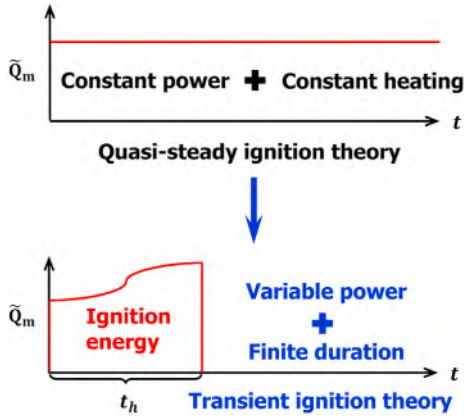

Fig. 35. The improvements of heating scheme in transient ignition theory in comparison with that in quasi-steady ignition theory.

temperature/reactant molar fraction tends to reduce the propagation speed of the expanding ignition kernel.

According to the transient formulation, the evolution of the ignition kernel requires knowledge of its initial size, denoted by $\widetilde{R}_{f0}$, which is

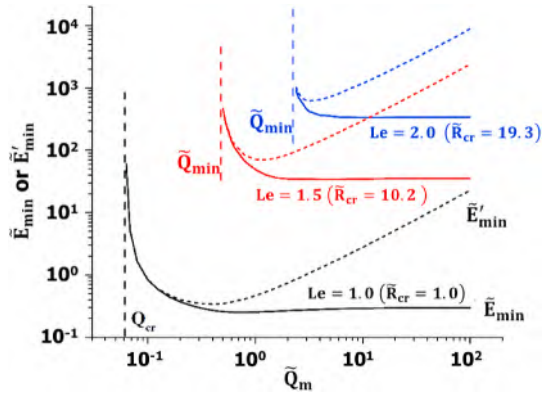

Fig. 36. Change of the MIE with heating power for different Lewis numbers. The solid lines represent $\widetilde{E}_{\min}$ determined by the transient formulation with memory effect, while the dashed lines stand for $\widetilde{E}'_{\min}$ predicted by the quasi-steady theory without considering memory effect. Reproduced from Ref. [109] with permission from Cambridge University Press.

selected to be $\widetilde{R}_{f0} = 0.01$ in the preceding results. Fig. 32 compares the phase diagram for successful ignition processes with different initial radii of the ignition kernel. It suggests that initially larger ignition kernels require a shorter distance subject to the driving effect of central heating on the critical ignition radius, which facilitates the ignition process. Beyond the critical ignition radius, Fig. 32 shows that various curves corresponding to different values of $\widetilde{R}_{f0}$ collapse, which implies that the propagation of a self-sustaining spherical flame does not inherit the history of ignition kernel evolution subject to central heating.

Besides, as shown in Fig. 33, the minimum ignition powers and critical ignition radii predicted by transient ignition theory appear to be uniformly greater than those evaluated in quasi-steady ignition theory. This is due to the fact that the local temperature gradient ahead of the flame front predicted by the transient ignition theory is larger than that predicted by the quasi-steady theory, implying stronger heat loss in the transient formulation at the same flame radius. Consequently, the critical radius determined by the transient ignition theory is larger than that determined by the quasi-stead theory. Therefore, the unsteadiness of flame kernel propagation exhibits inhibiting effects during the premixed flame ignition process.

Fig. 34 shows the change of the minimum ignition power with the cube of the critical flame radius. For the quasi-steady ignition theory, the minimum ignition power is shown to be linearly proportional to the cube of the critical radius, i.e., $\widetilde{Q}_{\min} \sim \widetilde{R}_{cr}^3$ [12]. However, the minimum ignition power predicted by the transient ignition theory formulation changes more rapidly than the cube of the critical radius, and the scaling law should be phenomenologically revised to $\widetilde{Q}_{\min} \sim \widetilde{R}_{cr}^{3+\delta}$ with $\delta > 0$ [109].

More importantly, the flexible external heating can be defined as arbitrary functions of time in the transient ignition theory, as shown in Fig. 35. Therefore, the memory effect of external heating, i.e., the flame front could sustain propagation for a while after the removal of the heating source, can also be interpreted appropriately based on the transient ignition theory, and it is found that the memory effect becomes stronger as the external heating power increases [109,253]. Since the heat release from the flame front during the transient of the ignition kernel to the ever-expanding spherical flame is taken into account, the transient ignition theory yields the lower bound for MIE, which provides helpful guidelines for fire safety issues.

Fig. 36 shows that at relatively low heating powers, the $\widetilde{E}'_{\min}$ given by the quasi-steady ignition theory, agrees well with $\widetilde{E}_{\min}$ obtained from the transient ignition theory. Both $\widetilde{E}'_{\min}$ and $\widetilde{E}_{\min}$ rise abruptly as central heating power $\widetilde{Q}_m$ approaches the critical value. The difference between $\widetilde{E}'_{\min}$ and $\widetilde{E}_{\min}$ becomes apparent as the heating power increases. When heating power becomes sufficiently high, the heating duration t_0 can be made arbitrarily short in the transient formulation, and consequently, the external heating could be modeled by a delta function, whose magnitude is the total energy deposition. Therefore, in the limit of $\widetilde{Q}_m \to \infty$, both $\widetilde{Q}_m$ and t_0 do not appear explicitly in the formulation, which implies the independence of MIE on Q_m, i.e., the existence of an asymptotic value of MIE in that limit. However, $\widetilde{E}'_{\min}$ without considering memory effect changes with the heating power following an approximate scaling law, i.e., $\widetilde{E}'_{\min} \sim \widetilde{Q}_m^{0.7}$ as indicated by the slope of the dashed lines in Fig. 36, which does not satisfy the physical plausibility. The growing discrepancy between the $\widetilde{E}_{\min}$ and $\widetilde{E}'_{\min}$ manifests the increasing importance of the memory effect in determining the MIE. It is noted that Fig. 5 in Ref. [8] also shows that the quasi-steady theory tends to overestimate the value of MIE, which is consistent with the results in Fig. 36 shown above. Nevertheless, the range of the heating power considered in Ref. [8] was restricted to the neighborhood of $\widetilde{Q}_{cr}$, which is much narrower than that concerned in the present transient formulation. Therefore, the substantial impact of the memory effect on the MIE was not observed in Ref. [8].

The above transient ignition theory helps to assess the unsteady effects on ignition kernel propagation and to determine the MIE. It was found that the memory effect of external heating helps to sustain flame front propagation even after the removal of the heating source and thereby reduces the MIE. The memory effect becomes stronger with higher ignition power. Note that the transient ignition theory is based on the assumption of one-step global chemistry. In future works, it would be interesting to take into account radical and chain-branching reactions [238] in the transient ignition theory.

3.6.3. *Transient ignition by repetitive heating pulse*

Forced-ignition by nanosecond-repetitive-pulsed-discharge (NRPD) has received great attention since it can greatly promote ignition [169,170,239,254]. Lefkowtiz and coworkers [168,255] conducted a series of experimental studies investigating forced-ignition by NRPD in flowing mixtures. They identified three distinct regimes, i.e., fully coupled, partially coupled, and decoupled between sequential pulses. Castela et al. [256] showed that appropriate vortical fluid motion could be produced by nanosecond discharges, which can bring fresh gas into the gap between the electrodes. In turbulent environments, Shy and coworkers [169] observed the synergistic effect between the frequency of NRPD and the recirculation frequency of turbulence, which can effectively transport the ignition energy to the ignition kernel front and thus promote ignition probability.

Modifying the transient formulation by incorporating multiple pulses, Yu and Chen [253] provided a theoretical analysis on the ignition of a quiescent flammable mixture by multiple discharges and assessed the influence of repetitive pulse on the ignition process. For repetitive

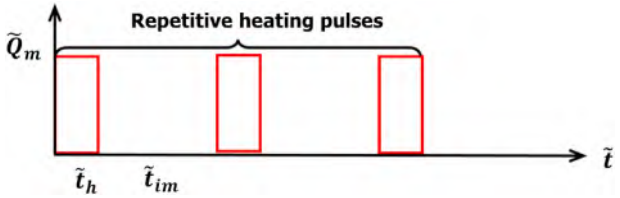

Fig. 37. Schematic of repetitive heating pulses.

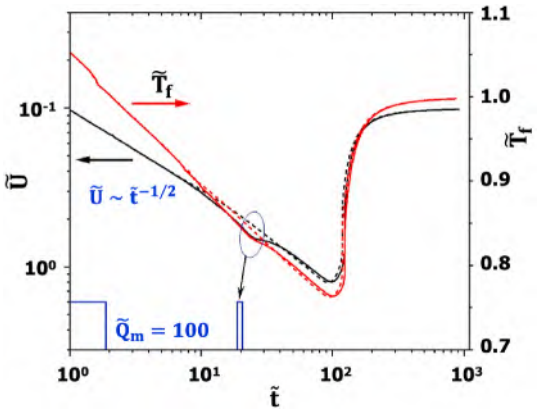

Fig. 38. Evolution of flame propagation speed (black lines) and flame temperature (red line) during the ignition kernel development into a self-sustained expanding flame. The solid and dashed lines are for double and single pulse, respectively. Each heating scheme is characterized by equal ignition energy of $\widetilde{E}_{\text{ignition}} = 380$ and heating power of $\widetilde{Q}_m = 100$. The instants corresponding to the switching-on and -off of individual pulse are indicated by the squares adjacent to the abscissa for two pulse cases. Reproduced from Ref. [253] with permission from Elsevier.

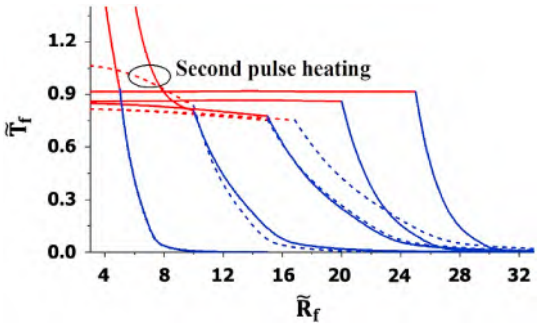

Fig. 39. Evolution of temperature profiles at selected instants (or equivalently the flame front locations) characterizing the flame kernel evolution corresponding to conditions of $\lambda_{tm} = 0$ (dashed lines) and $\lambda_{tm} = 0.93$ (solid lines). Reprinted from Ref. [253] with permission from Elsevier.

heating pulses, the heating scheme shall be expressed as the summation of Heaviside functions in the following form [253].

$$\widetilde{Q}(t) = \widetilde{Q}_m \sum_{k=1}^{2n_p} (-1)^{k+1} H(\tilde{t} - \tilde{t}_k) \tag{129}$$

where $\widetilde{Q}_m$ is the heating power of an individual pulse, and n_p the total

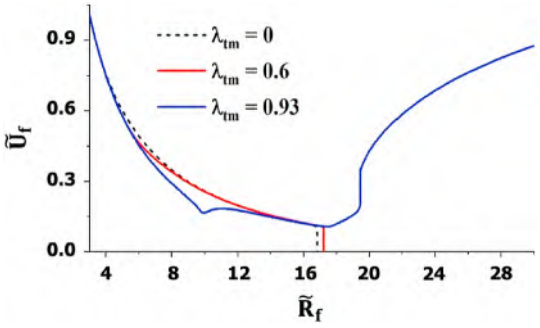

Fig. 40. The impact of two-pulse heating on ignitability, in which the same amount of ignition energy $\widetilde{E}_{ig} = 350$ is released at constant heating power $\widetilde{Q}_m = 100$ with various intermittent durations. Reprinted from Ref. [253] with permission from Elsevier.

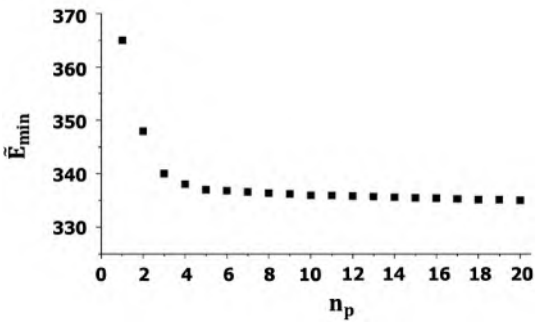

Fig. 41. Change of the minimum ignition energy with heating pulse number. Reproduced from Ref. [253] with permission from Elsevier.

number of pulses, in which the kth pulse is initiated at $\tilde{t} = \tilde{t}_{2k-1}$ and ends at $\tilde{t} = \tilde{t}_{2k+1}$, $k = 1, 2, \ldots, n_p$. Fig. 37 shows the schematic of a repetitive heating pulse, in which $\tilde{t}_h$ is the duration of the individual pulse and $\tilde{t}_m$ the intermittent period.

The transient variation of flame temperature exhibits the same form given by Eq. (127), in which the central heating related function $S(\tilde{t}, \widetilde{U}, \widetilde{R}_f)$ should be revised into the following form:

$$S_k(\tilde{t}, \widetilde{U}, \widetilde{R}_f) = \sum_{m=1}^{k} (-1)^{m+1} \vartheta_4 \left[e^{-\pi^2 \widetilde{\mathcal{F}}_{bT}^2 (\tilde{t} - \tilde{t}_m) / \widetilde{R}_f^2} \right] \tag{130}$$

which includes the key information of multistage heating parameters, e.g., pulse number, duration of individual pulse, and intermittent period between neighboring pulses.

Fig. 38 shows that the repetitive pulses can improve the ignition capability due to the flame revitalization effect, which is attributed to the memory effect of flame front propagation [253]. It can be understood as follows: Introducing the subsequent heating pule provides additional ignition energy, which is subsequently supplied to the flame front by convective/conductive transport, depending on presence of fluid motion in the ignition kernel. Since the flame front distance is still shorter than the critical ignition radius, the flame front propagation is sustained by the memory effect. The mechanism of the revitalization effect is shown in Fig. 39. When the ignition energy reinforcement provided by the subsequent heating pulse arrives at the flame front before quenching, it lowers the rate of heat loss and thus facilitates the propagation of the flame front.

Theoretical analysis indicates that replacing a single heating pulse with two pulses and arranging them with an appropriate intermittent duration can reduce the ignition energy [253]. This is demonstrated by Fig. 40. It is seen that the flame kernel extinction happens around $\widetilde{R}_f = 17$ for a single heating pulse (i.e., $\lambda_{tm} = 0$). When the intermittent factor is increased to $\lambda_{tm} = 0.93$ (i.e., two heating pulses), Fig. 40 shows that the flame front can successfully propagate across the critical radius and achieve successful ignition.

For a heating scheme with multiple pulses, it was found that the MIE, in general, reduces as the pulse number increases [253]. Fig. 41 shows that the MIE decreases monotonically with the pulse number. This indicates that the revitalization effect results in ignition energy reinforcement between sequential pulses, and accordingly enhances the ignition process. Moreover, Fig. 41 shows that the MIE gradually decays with heating pulse numbers and tends to approach an asymptotic value as $n_p \to \infty$.

The fall of minimum ignition with heating pulse number n_p as well as the insensitivity of minimum ignition energy $\widetilde{E}_{\min}$ to the heating pulse number as $n_p \to \infty$ can be interpreted as follows: The total energy of the flame kernel at the ignition instant, i.e., $\widetilde{R} = \widetilde{R}_{cr}$, consists of three parts, i.e.,

The thermal energy inside the flame kernel, $\widetilde{E}_{\text{burnt}}$,

$$\widetilde{E}_{\text{burnt}} \propto \int_0^{\widetilde{R}_{cr}} 4\pi \widetilde{T}_b \widetilde{r}^2 d\widetilde{r} \tag{131}$$

The thermal energy in the unburnt region, $\widetilde{E}_{\text{unburnt}}$,

$$\widetilde{E}_{\text{unburnt}} \propto \int_{\widetilde{R}_{cr}}^{\infty} 4\pi \widetilde{T}_u \widetilde{r}^2 d\widetilde{r} \tag{132}$$

The heat released by consuming fresh mixtures inside the flame kernel of critical radius

$$\widetilde{E}_{\text{release}} \propto \frac{4}{3}\pi \widetilde{R}_{cr}^3 \widetilde{Q}_m \tag{133}$$

Driven by the MIE, the last term becomes identical for every n_p. Since the temperature in the unburnt region is significantly lower than that in the burnt side, we may assume that the difference in $\widetilde{E}_{\text{unburnt}}$ would be immaterial in determining the MIE. Therefore, the decreasing of $\widetilde{E}_{\min}$ with n_p might be attributed to the similar behavior of $\widetilde{E}_{\text{burnt}}$.

As the number of heating pulses increases, the central heating power corresponding to individual pulses increases dramatically. In the limiting situation of $n_p \to \infty$, the heating pulse of finite duration can be regarded as instantaneous deposition of a finite amount of energy, i.e., the function $\widetilde{Q}(t)$ in the boundary condition for equation (121) shall be replaced by

$$\widetilde{Q}(t) = \sum_{k=1}^{n_p} \frac{\widetilde{E}_{\text{ignition}}}{n_p} \delta(t - \tau_k) \tag{134}$$

where τ_k refers to the instant when the ignition energy is introduced. The solution of equation (121) subject to the reduced boundary condition (134) could be written in the form

$$\widetilde{T}_b(\xi_b, t) = 2\frac{\widetilde{E}_{\text{ignition}} \cdot \mathscr{T}_{bT}^2}{n_p \widetilde{R}_f^2} \sum_{k=1}^{n_p} \sum_{n=1}^{\infty} n\pi \sin(n\pi\xi_b) e^{-\mathscr{T}_{bT}^2 n^2 \pi^2 (t-\tau_k) \Big/ \widetilde{R}_f^2} + \xi_b \left(\widetilde{T}_f - \widetilde{T}_b^0\right)\left(1 - e^{-\mathscr{T}_{bT}^2 \pi^2 t \Big/ \widetilde{R}_f^2}\right) \tag{135}$$

The temperature gradient at the flame front inside the flame kernel can be determined accordingly

$$\left(\frac{d\widetilde{T}_b}{d\widetilde{r}}\right)_{\widetilde{r}=\widetilde{R}_f^-} = \frac{\widetilde{E}_{\text{ignition}}}{n_p \widetilde{R}_f^2} \sum_{k=1}^{n_p} G_k(t;\tau_k) + \frac{1}{\widetilde{R}_f}\left(\widetilde{T}_f - \widetilde{T}_b^0\right)\left(1 - e^{-\mathscr{T}_{bT}^2 \pi^2 t \Big/ \widetilde{R}_f^2}\right) - \frac{\widetilde{T}_f}{\widetilde{R}_f} \tag{136}$$

where $G_k(t;\tau_k)$ represents the series

$$G_k(t;\tau_k) = 2\mathscr{T}_{bT}^2 \sum_{n=1}^{\infty} (-1)^n n^2 \pi^2 e^{-\mathscr{T}_{bT}^2 n^2 \pi^2 (t-\tau_k) \Big/ \widetilde{R}_f^2} \tag{137}$$

which is convergent in the range $t > \tau_k$, i.e., the release of k th heating pulse. The remaining gradients $(d\widetilde{T}_u/d\widetilde{r})_{\widetilde{r}=\widetilde{R}_f^+}$ and $(d\widetilde{c}_F/d\widetilde{r})_{\widetilde{r}=\widetilde{R}_f^+}$ are not affected by central heating, according to equations (123) and (124). Substituting equation (136) into the matching conditions for reactant mass fraction and temperature, an implicit ordinary differential equation for flame radius can be obtained, in which the heating power does not appear explicitly. Thus, we may expect that the $E_{\min}$-Q_m curve will become flat at sufficiently high heating power.

To ensure flame revitalization by subsequent heating pulses, the intermittent duration $\Delta\tau = \tau_i - \tau_{i-1}$, $i = 2, \cdots, n_p$, should not be arbitrarily long. As n_p increases, the energy added by each pulse decays following $1/n_p$, and the heating duration $\Delta\tau$ must drop accordingly. We assume that it takes a comparably long period for the flame kernel to arrive at the critical ignition state $\widetilde{R} = \widetilde{R}_{cr}$ and $\widetilde{U} = \widetilde{U}_{cr}$ at $t = t_c$ subsequent to the deposition of the last heating pulse, i.e., we can assume the relation $t \sim t_c \gg \tau_{n_p}$ when evaluating the series (137). Expanding the series $G_k(t;\tau_k)$ in terms of τ_k/t and retaining the leading order term, we have

$$G_k(t;\tau_k) \approx 2\mathscr{T}_{bT}^2 \sum_{n=1}^{\infty} (-1)^n n^2 \pi^2 e^{-\mathscr{T}_{bT}^2 n^2 \pi^2 t \Big/ \widetilde{R}_f^2} = \overline{G}(t) \tag{138}$$

which does not include the transient information for individual heating pulses explicitly. Replacing $G_k(t;\tau_k)$ by $\overline{G}(t)$ in equation (136), it reduces to

$$\left(\frac{dT_b}{dr}\right)_{R^-} = \frac{\widetilde{E}_{\text{ignition}}}{\widetilde{R}_f^2}\overline{G}(t) + \frac{1}{\widetilde{R}_f}\left(\widetilde{T}_f - \widetilde{T}_b^0\right)\left(1 - e^{-\mathscr{T}_{bT}^2 \pi^2 t \Big/ \widetilde{R}_f^2}\right) - \frac{\widetilde{T}_f}{\widetilde{R}_f} \tag{139}$$

In analogy, the resulting $\widetilde{U} - \widetilde{R}_f$ relation derived by substituting equation (139) into the matching conditions does not include the heating pulse number n_p explicitly. Consequently, it demonstrates that the minimum ignition energy tends to vary indiscernibly as n_p increases.

The preceding formulation revises the transient ignition theory reviewed in the previous section by taking into account the effects of multiple heating pulses on the evolution process of the ignition kernel. Interestingly, it was observed that the minimum ignition energy decreases as the heating pulse number increases and is asymptotic towards a lower bound value in the limit of $n_p \to \infty$. However, this revised transient ignition theory still focuses on the ignition process induced in a quiescent mixture. In practical situations, the mixture might not be static. Shy and coworkers [169,170] experimentally observed that coherence between the frequency of the heating pulse and the recirculation frequency of the turbulent flow of reactant leads to a synergistic effect on the ignition kernel development, which promotes ignition. Therefore, it would be of practical interest to conduct theoretical analysis on the forced ignition of a flowing mixture by a repetitive heating pulse in future works.

4. Summary and future research

4.1. Summary of major advances

A detailed review on the development of premixed flame ignition theory is presented in this article, with increasing intricacies of mathematical formulation. The major advances are summarized below.

4.1.1. Homogeneous explosion theory

The homogeneous explosion of a combustible mixture can be considered the most fundamental phenomenon of combustion. The fundamental mechanism can be attributed to the net accumulation of heat and radicals by consuming the reactant, leading to the self-acceleration of chemical reactions. The homogeneous explosion theory answers the question of whether chemical reactions can be initiated in a combustible mixture. However, the absence of characteristic length scale implies the nonequivalence between homogeneous explosion and premixed flame ignition.

4.1.2. Thermal ignition theory

The thermal ignition theory introduces the characteristic length scale for premixed flame ignition. The critical size of the spark kernel is determined by the thermal balance between heat release from chemical reactions and heat loss by conduction, characterized by the local temperature gradient. The minimum size of the spark kernel can be considered the critical ignition radius, beyond which the chemical heat release exceeds the conductive heat loss and leads to the successful ignition of a premixed flame. According to thermal ignition theory, the critical ignition radius is comparable to the flame thickness or

quenching distance. The MIE is the energy required to heat a sphere in the radius of flame thickness to the adiabatic flame temperature. Nevertheless, the thermal ignition theory does not take into account mass diffusion and fuel consumption, which, in association with thermal balance, also play a decisive role in premixed flame ignition.

4.1.3. Flame ball theory

A more accurate description of premixed flame ignition, including the effect of preferential diffusion of heat and mass (the Lewis number effect), is given by the flame ball theory. The flame ball theory indicates that there exists a stationary spherical flame in a static combustible mixture. The reactant consumed at the reaction front is supplied by pure diffusion. Stability analysis indicates that a small perturbation causes the flame ball to propagate either inwardly (flame extinguishment, i.e., ignition failure) or outwardly (self-sustained expanding flame, i.e., successful ignition). Therefore, the flame ball radius is considered to be the critical length controlling premixed flame ignition. The MIE is proportional to the cube of the flame ball radius instead of the flame thickness. Since the flame ball radius strongly depends on the Lewis number, the change of MIE with the Lewis number is quantified by the flame ball theory.

4.1.4. Quasi-steady ignition theory

Both the thermal ignition theory and flame ball theory do not consider flame kernel propagation, which profoundly affects the dynamic process of premixed flame ignition. The quasi-steady ignition takes into account the impact of flame stretch on flame propagation by including convective terms (see Fig. 7) and thus interprets the dynamic evolution of the ignition kernel. The quasi-steady ignition theory deals with both thermal and mass balance across the flame front of the ignition kernel, which is supported by energy supply from the external ignition source and tends to propagate outwards. It can describe the transition between the initial flame kernel, the flame ball, the outwardly propagating spherical flame, and the propagating planar flame. Therefore, compared to thermal ignition theory and flame ball theory, the quasi-steady ignition theory more rigorously interprets premixed flame ignition and critical ignition radius. According to the quasi-steady ignition theory, the critical flame radius depends strongly on the Lewis number; and for large Lewis numbers, the MIE can be substantially over-predicted based on the flame ball radius and under-predicted based on the flame thickness. The quasi-steady ignition theory has been extended to consider the effects of Soret diffusion, reaction reversibility, transport and chain branching reactions of radicals, finite droplet vaporization, and dispersed solid particles, which may have a great impact on premixed flame ignition.

4.1.5. General theory on transient ignition and spherical flame propagation

The temporal dependence is absent in the quasi-steady ignition theory. In practice, the ignition source exists for a finite duration. Consequently, a more accurate interpretation of premixed flame ignition must consider the transient evolution of the ignition kernel. The general theory on transient ignition and spherical flame propagation has been developed by further incorporating the unsteady terms in the governing equations (see Fig. 7). The general theory reveals the memory effect of flame kernel evolution, which can be interpreted that the flame kernel can sustain propagation at some distance subsequent to the removal of an external ignition source. Comparing with quasi-steady ignition theory, the transient framework can deal with finite ignition energy deposition through a single or multiple heating pulses. It has been found that repetitive heating pulses can improve ignition due to the flame revitalization effect, i.e., ignition energy reinforcement to the flame kernel via heat conduction induced by subsequent heating pulses. The MIE can be reduced by increasing the number of heating pulses, which is consistent with experimental observation. Besides, the general theory on transient ignition and spherical flame propagation provides an in-depth description of the birth of the ignition kernel subject to an external heating source of finite domain and duration. Time scale analysis indicates that the ignition kernel formation process consists of three stages: onset of thermal runaway at the heating center, occurrence of reaction fronts due to depletion of reactant concentration, and arrival of the reaction front at the edge of the heating domain. Corresponding to each stage, there exists a critical heating power of the ignition source below which the ignition kernel cannot be established, and thereby premixed flame ignition can hardly take place.

4.1.6. Applications of premixed flame ignition theory in ignition enhancement

The above advances in premixed ignition theory not only provide insights on the fundamental mechanisms of ignition but also help develop ignition enhancement techniques. It is well known that reliable relight at high altitude with relatively low pressure and temperature of inlet air is crucial in jet-engine design. According to the premixed ignition theory mentioned above, at lower pressure, the critical ignition radius is larger, and thereby larger ignition kernel should be generated to achieve successful ignition. Multi-channel nanosecond discharge has been proposed and demonstrated to be able to induce a large ignition kernel so that successful ignition can be achieved even at very low pressures [257]. Similarly, the three-channel spark ignition technique has been developed by Zhao et al. [17] to increase the ignition kernel size while maintaining the same total ignition energy. As mentioned in the Introduction section, advanced ICEs tend to operate in ultra-lean or highly diluted conditions so that high thermal efficiency can be achieved. However, the critical ignition radius is very large in ultra-lean or highly diluted conditions, according to the premixed ignition theory above. An innovative three-pole igniter [22,258] has been developed to enlarge the volume of the ignition kernel and thereby improve ignition in gasoline engines with high charge dilution. Besides, multi-point microwave discharge igniters have also been developed to extend the lean ignition limit in ICEs [259]. The basic idea for these ignition enhancement techniques is to generate a large ignition kernel whose size is comparable to or even above the critical ignition radius.

According to the premixed ignition theory, the MIE increases greatly with the Lewis number. Therefore, another way to facilitate ignition is to reduce the Lewis number. For large hydrocarbon fuel burning at fuel-lean conditions, the Lewis number is greater than unity. The simplest way to reduce the Lewis number is to blend hydrogen, which has a large mass diffusivity and thereby a sub-unity Lewis number [260,261]. Since the Lewis number increases with the equivalence ratio, fuel stratification also helps to reduce the Lewis number at the ignition kernel. The relatively high equivalence ratio at the ignition kernel compared to that in the surroundings has been shown to greatly enhance ignition kernel propagation and thereby promote ignition [262]. Besides, active cooling with endothermic hydrocarbon fuel is popularly used in thermal protection. The decomposed small fragments from pyrolysis have a much larger mass diffusivity compared to the original hydrocarbon fuel, so the Lewis number can be greatly reduced. Therefore, fuel decomposition has been shown to greatly promote ignition [263]. Moreover, the combination of fuel decomposition and fuel stratification can further promote premixed flame ignition [263]. The underlined principle for the ignition promotion methods mentioned above is to decrease the Lewis number, which reduces the MIE according to the premixed flame ignition theory.

4.2. Future research directions

Though extensive advances in premixed flame ignition theory have been achieved over the last hundred years, there are still some additional research challenges, as listed below.

4.2.1. Multi-step chemistry

Most of the premixed flame ignition theories consider a one-step global reaction, which can interpret fuel consumption and total heat release. However, practical combustion of hydrocarbon fuels involves

numerous elementary reactions among fuel, oxygen, and reactive intermediate species. Therefore, the premixed flame ignition theory needs to be extended to consider multi-step chemistry so that the effects of transport and reaction of intermediate species and key radicals can be quantified. Usually, it is difficult to consider complicated chemistry in theoretical analysis. Besides the modified Zel'dovich-Liñán model proposed by Dold and coworkers [235,236] (see Section 3.5.2), the simplified chemistry developed by Williams and coworkers (see Ref. [264] and references therein) may be considered in ignition theory. Despite the fact that the integration of multi-step chemistry into the theoretical model results in further complexities in mathematical formulation, the potential further understanding of ignition still merits continued efforts in this direction. Note that for a hydrogen/air mixture, eigenvalue analysis considering detailed chemistry can be conducted to determine the critical ignition conditions [73,265].

4.2.2. Cool flame ignition

Recently, cool flame combustion has attracted increasing interest [266,267]. The fundamental knowledge of the ignition and dynamic propagation of cool flames is helpful for the development of combustion science and advanced technology in clean combustion [266,267]. However, there are only a few numerical or experimental studies [268–272] on cool flame ignition. To the authors' knowledge, there is no theoretical analysis of the ignition of premixed cool flames. Since a cool flame is induced by low-temperature chemistry, in future works, it would be interesting to take into account both low- and high-temperature chemistry in transient ignition theory.

4.2.3. Flowing mixture

The theories reviewed here are for premixed flame ignition in a static mixture. However, in practice premixed flame ignition usually takes place in a flowing mixture. The presence of laminar or turbulent flow enhances the heat transfer from the ignition kernel to the surrounding mixture and thereby prohibits premixed flame ignition [1,273–275]. Nevertheless, counterintuitive flow-facilitated ignition and turbulence-facilitated ignition (TFI) have been observed in recent simulations [276] and experiments [102,277–279], respectively. Therefore, ignition theory, considering uniform flow or even turbulent transport, would be of great interest. Recently, the authors have conducted theoretical analysis on premixed flame ignition by a moving hot particle [41], which may be extended to ignition in a mixture with uniform flow. Besides, premixed flame ignition in a counterflow configuration [280,281] may be considered in future works since it is a relatively simple flow field.

4.2.4. Autoigniting mixture

The ignition theories have been developed for premixed flame propagation in a mixture at or close to normal temperature and pressure (NTP). At NTP, the ignition delay time is very large, and the unburned mixture can be considered frozen. However, under engine-relevant conditions with high temperature and pressure, the ignition delay time of the fuel/air mixture may be comparable to the flame residence time. The competition between flame propagation and end-gas autoignition determines whether strong pressure oscillation occurs in spark ignition engines [282]. Therefore, it is of interest to understand premixed flame ignition and propagation in such kinds of autoigniting mixtures, which are closely related to engine knock [282]. Moreover, flame propagation and acceleration in auto-igniting mixtures may induce the deflagration-to-detonation transition (DDT). It is of considerable interest to deepen the fundamental understanding of the DDT phenomenon, especially in studies of explosions and high-speed propulsion systems. Currently, there are only a few theoretical studies [283–286] on premixed flame propagation speed in autoigniting mixtures. In future work, premixed flame ignition theory for autoigniting mixtures needs to be developed.

The ignition theory should be generalized and revised in multiple aspects, taking into account the future research directions mentioned above, and as a consequence, it can provide promising insights into a variety of phenomena critical to the development of combustion science technology. Besides, numerical simulation is another powerful tool to understand premixed flame ignition, which is beyond the scope of the current review. The advances in the numerical simulation of premixed flame ignition need to be discussed in future works.

CRediT authorship contribution statement

Dehai Yu: Formal analysis, Investigation, Methodology, Writing – original draft, Writing – review & editing. **Zheng Chen:** Conceptualization, Formal analysis, Funding acquisition, Investigation, Project administration, Supervision, Writing – original draft, Writing – review & editing.

Declaration of competing interest

The authors declare that they have no known competing financial interests or personal relationships that could have appeared to influence the work reported in this paper.

Data availability

Data will be made available on request.

Acknowledgements

Z.C. wishes to acknowledge Prof. Yiguang Ju and Chung K. Law at Princeton University for their encouragement on this work. Z.C. also thanks his former graduate students, in particular Dr. Wang Han, Dr. Yuan Wang, Dr. Weikuo Zhang, Dr. Yiqing Wang, Dr. Xinyi Chen, and Mr. Shumeng Xie for their work on ignition. Financial support on this work has been provided by National Natural Science Foundation of China (Nos. 52176096, 52006001, 51861135309, and 51322602).

References

[1] Pouech P, Duchaine F, Poinsot T. Premixed flame ignition in high-speed flows over a backward facing step. Combust Flame 2021;229:111398.
[2] Mastorakos E. Ignition of turbulent non-premixed flames. Prog Energy Combust Sci 2009;35:57–97.
[3] Mastorakos E. Forced ignition of turbulent spray flames. Proc Combust Inst 2017;36:2367–83.
[4] Ronney PD, Wu M-S, Pearlman HG, Weiland KJ. Experimental study of flame balls in space: Preliminary results from STS-83. AIAA J 1998;36:1361–8.
[5] Beduneau J-L, Kim B, Zimmer L, Ikeda Y. Measurements of minimum ignition energy in premixed laminar methane/air flow by using laser induced spark. Combust Flame 2003;132:653–65.
[6] Li F, Zhao Z, Wang B, Wang Z. Experimental study of pre-chamber jet ignition in a rapid compression machine and single-cylinder natural gas engine. Int J Engine Res 2021;22:1342–56.
[7] Buckmaster J, Joulin G, Ronney P. The structure and stability of nonadiabatic flame balls. Combust Flame 1990;79:381–92.
[8] He L. Critical conditions for spherical flame initiation in mixtures with high Lewis numbers. Combust Theor Model 2000;4:159.
[9] Kurdyumov V, Sánchez A, Linan A. Heat propagation from a concentrated external energy source in a gas. J Fluid Mech 2003;491:379–410.
[10] Kravchik T, Sher E. Numerical modeling of spark ignition and flame initiation in a quiescent methane-air mixture. Combust Flame 1994;99:635–43.
[11] Wu M-S, Ronney PD, Colantonio RO, VanZandt DM. Detailed numerical simulation of flame ball structure and dynamics. Combust Flame 1999;116:387–97.
[12] Chen Z, Burke MP, Ju Y. On the critical flame radius and minimum ignition energy for spherical flame initiation. Proc Combust Inst 2011;33:1219–26.
[13] Lacaze G, Richardson E, Poinsot T. Large eddy simulation of spark ignition in a turbulent methane jet. Combust Flame 2009;156:1993–2009.
[14] Law CK. Combustion physics. Cambridge University Press; 2010.
[15] Dale JD, Checkel M, Smy P. Application of high energy ignition systems to engines. Prog Energy Combust Sci 1997;23:379–98.
[16] Tsuboi S, Miyokawa S, Matsuda M, Yokomori T, Iida N. Influence of spark discharge characteristics on ignition and combustion process and the lean operation limit in a spark ignition engine. Appl Energy 2019;250:617–32.

[17] Zhao H, Zhao N, Zhang T, Wu S, Ma G, Yan C, Ju Y. Studies of multi-channel spark ignition of lean n-pentane/air mixtures in a spherical chamber. Combust Flame 2020;212:337–44.
[18] Zhang A, Scarcelli R, Lee S-Y, Wallner T, Naber J. Numerical investigation of spark ignition events in lean and dilute methane/air mixtures using a detailed energy deposition model. Argonne, IL (United States): Argonne National Lab. (ANL); 2016.
[19] Xu G, Hanauer C, Wright YM, Boulouchos K. CFD-simulation of ignition and combustion in lean burn gas engines. 2016. Report No. 0148-7191, SAE Technical Paper.
[20] Li F, Zhao Z, Wang Z, Wang B. Experimental and numerical study of a methane-fueled pre-chamber system in rapid compression machine. Combust Sci Technol 2021;193:1463–94.
[21] Zhou Z, Shoshin Y, Hernández-Pérez FE, van Oijen JA, de Goey LP. Effect of pressure on the lean limit flames of H2-CH4-air mixture in tubes. Combust Flame 2017;183:113–25.
[22] Han X, Yu S, Tjong J, Zheng M. Study of an innovative three-pole igniter to improve efficiency and stability of gasoline combustion under charge dilution conditions. Appl Energy 2020;257:113999.
[23] Shen H, Hinze PC, Heywood JB. A model for flame initiation and early development in SI engine and its application to cycle-to-cycle variations. SAE Trans 1994:1808–19.
[24] Biswas S, Tanvir S, Wang H, Qiao L. On ignition mechanisms of premixed CH4/air and H2/air using a hot turbulent jet generated by pre-chamber combustion. Appl Therm Eng 2016;106:925–37.
[25] Qin F, Shah A, Huang Z-w, Peng L-n, Tunestal P, Bai X-S. Detailed numerical simulation of transient mixing and combustion of premixed methane/air mixtures in a pre-chamber/main-chamber system relevant to internal combustion engines. Combust Flame 2018;188:357–66.
[26] Toulson E, Schock HJ, Attard WP. A review of pre-chamber initiated jet ignition combustion systems. SAE International; 2010.
[27] Read RW. Experimental investigations into high-altitude relight of a gas turbine. University of Cambridge; 2008.
[28] Read R, Rogerson J, Hochgreb S. Flame imaging of gas-turbine relight. AIAA J 2010;48:1916–27.
[29] Han W, Chen Z. Effects of finite-rate droplet evaporation on the ignition and propagation of premixed spherical spray flame. Combust Flame 2015;162:2128–39.
[30] Segal C. The scramjet engine: processes and characteristics. Cambridge University Press; 2009.
[31] Curran E, Heiser W, Pratt D. Fluid phenomena in scramjet combustion systems. Annu Rev Fluid Mech 1996;28:323–60.
[32] Seleznev R, Surzhikov S, Shang J. A review of the scramjet experimental data base. Prog Aero Sci 2019;106:43–70.
[33] Hammack SD, Ombrello TM. Spatio-temporal evolution of cavity ignition in supersonic flow. Proc Combust Inst 2021;38:3845–52.
[34] An B, Yang L, Wang Z, Li X, Sun M, Zhu J, Yan W. Characteristics of laser ignition and spark discharge ignition in a cavity-based supersonic combustor. Combust Flame 2020;212:177–88.
[35] Ochs BA, Ranjan R, Ranjan D, Menon S. Topology and flame speeds of turbulent premixed flame kernels in supersonic flows. Combust Flame 2019;210:83–99.
[36] Urzay J. Supersonic combustion in air-breathing propulsion systems for hypersonic flight. Annu Rev Fluid Mech 2018;50:593–627.
[37] Chen Z. Studies on the initiation, propagation, and extinction of premixed flames. Princeton University; 2009.
[38] Kobes M, Helsloot I, De Vries B, Post JG. Building safety and human behaviour in fire: a literature review. Fire Saf J 2010;45:1–11.
[39] Lennon T, Moore D. The natural fire safety concept—full-scale tests at Cardington. Fire Saf J 2003;38:623–43.
[40] Davis SG, Engel D, van Wingerden K. Complex explosion development in mines: case study—2010 upper big branch mine explosion, Process. Saf. Prog 2015;34:286–303.
[41] Yu D, Chen Z. Theoretical analysis on the ignition of a combustible mixture by a hot particle. J Fluid Mech 2022;936:A22.
[42] Hemmatian B, Planas E, Casal J. Fire as a primary event of accident domino sequences: the case of BLEVE. Reliab Eng Syst Saf 2015;139:141–8.
[43] Sun P, Bisschop R, Niu H, Huang X. A review of battery fires in electric vehicles. Fire Technol 2020;56:1361–410.
[44] Wang Q, Mao B, Stoliarov SI, Sun J. A review of lithium ion battery failure mechanisms and fire prevention strategies. Prog Energy Combust Sci 2019;73:95–131.
[45] Suzuki S, Manzello SL. Characteristics of firebrands collected from actual urban fires. Fire Technol 2018;54:1533–46.
[46] Flannigan MD, Stocks BJ, Wotton BM. Climate change and forest fires. Sci Total Environ 2000;262:221–9.
[47] Liu N, Lei J, Gao W, Chen H, Xie X. Combustion dynamics of large-scale wildfires. Proc Combust Inst 2021;38:157–98.
[48] Guibaud A, Legros G, Consalvi J-L, Torero J. Fire safety in spacecraft: past incidents and Deep Space challenges. Acta Astronaut 2022.
[49] Nakamura Y, Aoki A. Irradiated ignition of solid materials in reduced pressure atmosphere with various oxygen concentrations–for fire safety in space habitats. Adv Space Res 2008;41:777–82.
[50] Troitzsch JH. Fires, statistics, ignition sources, and passive fire protection measures. J Fire Sci 2016;34:171–98.
[51] Yu D, Chen X, Chen Z. Analysis on ignition kernel formation in a quiescent mixture: different characteristic time scales and critical heating powers. Combust Flame 2022;245:112336.
[52] Fendell FE. Ignition and extinction in combustion of initially unmixed reactants. J Fluid Mech 1965;21:281–303.
[53] Linan A. The asymptotic structure of counterflow diffusion flames for large activation energies. Acta Astronaut 1974;1:1007–39.
[54] Glassman I, Yetter RA, Glumac NG. Combustion. Academic Press; 2014.
[55] Hanson RK, Davidson DF. Recent advances in laser absorption and shock tube methods for studies of combustion chemistry. Prog Energy Combust Sci 2014;44:103–14.
[56] Sung C-J, Curran HJ. Using rapid compression machines for chemical kinetics studies. Prog Energy Combust Sci 2014;44:1–18.
[57] Goldsborough SS, Hochgreb S, Vanhove G, Wooldridge MS, Curran HJ, Sung C-J. Advances in rapid compression machine studies of low-and intermediate-temperature autoignition phenomena. Prog Energy Combust Sci 2017;63:1–78.
[58] Chen X, Zhao P, Dai P, Chen Z. On the prediction of hot spot induced ignition by the Livengood-Wu integral. Proc Combust Inst 2021;38:4709–16.
[59] Gu X, Emerson D, Bradley D. Modes of reaction front propagation from hot spots. Combust Flame 2003;133:63–74.
[60] Opacich KC, Ombrello TM, Heyne JS, Lefkowitz JK, Leiweke RJ, Busby K. Analyzing the ignition differences between conventional spark discharges and nanosecond-pulsed high-frequency discharges. Proc Combust Inst 2021;38:6615–22.
[61] Jo S, Gore JP. Laser induced spark ignition for laminar premixed hydrogen air jets. AIAA Scitech 2021 Forum; 2021. p. 681.
[62] Wawrzak A, Tyliszczak A. A spark ignition scenario in a temporally evolving mixing layer. Combust Flame 2019;209:353–6.
[63] Kawahara N, Hashimoto S, Tomita E. Spark discharge ignition process in a spark-ignition engine using a time series of spectra measurements. Proc Combust Inst 2017;36:3451–8.
[64] Ono R, Oda T. Spark ignition of hydrogen-air mixture. In: J Phys Conf ser. IOP Publishing; 2008, 012003.
[65] Kravchik T, Sher E, Heywood J. From spark ignition to flame initiation. Combust Sci Technol 1995;108:1–30.
[66] Sher E, Ben-Ya'ish J, Kravchik T. On the birth of spark channels. Combust Flame 1992;89:186–94.
[67] Bradley D, Lung F-K. Spark ignition and the early stages of turbulent flame propagation. Combust Flame 1987;69:71–93.
[68] Sher E, Keck JC. Spark ignition of combustible gas mixtures. Combust Flame 1986;66:17–25.
[69] Ballal D, Lefebvre A. The influence of spark discharge characteristics on minimum ignition energy in flowing gases. Combust Flame 1975;24:99–108.
[70] Maly R. Ignition model for spark discharges and the early phase of flame front growth. Proc Combust Inst 1981;18:1747–54.
[71] Hwang J, Kim W, Bae C. Influence of plasma-assisted ignition on flame propagation and performance in a spark-ignition engine. Applications in Energy and Combustion Science 2021;6:100029.
[72] Collin-Bastiani F, Vermorel O, Lacour C, Lecordier B, Cuenot B. DNS of spark ignition using Analytically Reduced Chemistry including plasma kinetics. Proc Combust Inst 2019;37:5057–64.
[73] Wang Y, Li S, Wang Y, Yu D, Zhang H, Chen Z. Analysis of the ignition of hydrogen/air mixtures induced by a hot particle. Phys Chem Chem Phys 2022;24:21188–97.
[74] Liang W, Law CK. An analysis of the explosion limits of hydrogen/oxygen mixtures with nonlinear chain reactions. Phys Chem Chem Phys 2018;20:742–51.
[75] Endo T, Kuwamoto K, Kim W, Johzaki T, Shimokuri D, Namba S-i. Comparative study of laser ignition and spark-plug ignition in high-speed flows. Combust Flame 2018;191:408–16.
[76] Kobayashi Y, Nakaya S, Tsue M. Laser-induced spark ignition for DME–air mixtures with low velocity. Proc Combust Inst 2019;37:4127–35.
[77] Endo T, Takenaka Y, Sako Y, Johzaki T, Namba S-i, Shimokuri D. An experimental study on the ignition ability of a laser-induced gaseous breakdown. Combust Flame 2017;178:1–6.
[78] Ronney PD. Laser versus conventional ignition of flames. Opt Eng 1994;33:510–21.
[79] Phuoc TX. Laser-induced spark ignition fundamental and applications. Opt Laser Eng 2006;44:351–97.
[80] Phuoc TX. An experimental and numerical study of laser-induced spark in air. Opt Laser Eng 2005;43:113–29.
[81] Srivastava DK, Weinrotter M, Iskra K, Agarwal AK, Wintner E. Characterisation of laser ignition in hydrogen–air mixtures in a combustion bomb. Int J Hydrogen Energy 2009;34:2475–82.
[82] Alger T, Mehta D, Chadwell C, Roberts C. Laser ignition in a pre-mixed engine: the effect of focal volume and energy density on stability and the lean operating limit. 2005. Report No. 0148-7191, SAE Technical Paper.
[83] Morsy MH. Review and recent developments of laser ignition for internal combustion engines applications. Renew Sustain Energy Rev 2012;16:4849–75.
[84] Law C, Ishizuka S, Cho P. On the opening of premixed Bunsen flame tips. Combust Sci Technol 1982;28:89–96.
[85] Buckmaster J. Edge-flames. Prog Energy Combust Sci 2002;28:435–75.
[86] Matalon M. Flame dynamics. Proc Combust Inst 2009;32:57–82.
[87] Shepherd JE. Detonation in gases. Proc Combust Inst 2009;32:83–98.
[88] Lee JH. The detonation phenomenon. Cambridge University Press; 2008.
[89] Clarke JF, Kassoy DR, Riley N. On the direct initiation of a plane detonation wave. Proc. Math. Phys. 1986;408:129–48.

[90] Lee J, Higgins A. Comments on criteria for direct initiation of detonation. Philos. Trans. Royal Soc. A . 1999;357:3503–21.
[91] Oran ES, Gamezo VN. Origins of the deflagration-to-detonation transition in gas-phase combustion. Combust Flame 2007;148:4–47.
[92] Liberman M, Ivanov M, Kiverin A, Kuznetsov M, Chukalovsky A, Rakhimova T. Deflagration-to-detonation transition in highly reactive combustible mixtures. Acta Astronaut 2010;67:688–701.
[93] Zeldovich YB. Regime classification of an exothermic reaction with nonuniform initial conditions. Combust Flame 1980;39:211–4.
[94] Bartenev A, Gelfand B. Spontaneous initiation of detonations. Prog Energy Combust Sci 2000;26:29–55.
[95] Lee J, Knystautas R, Yoshikawa N. Photochemical initiation of gaseous detonations. Acta Astronaut 1978;5:971–82.
[96] Clavin P, Searby G. Combustion waves and fronts in flows: flames, shocks, detonations, ablation fronts and explosion of stars. Cambridge University Press; 2016.
[97] Clavin P. Quasi-isobaric ignition near the flammability limits. Flame balls and self-extinguishing flames. Combust Flame 2017;175:80–90.
[98] Zhang A. Combustion initiation by electrical-discharge-induced plasma in lean and dilute methane-air mixture: experimental and modeling investigation. 2014.
[99] Lee J, Moen I. The mechanism of transition from deflagration to detonation in vapor cloud explosions. Prog Energy Combust Sci 1980;6:359–89.
[100] Ciccarelli G, Dorofeev S. Flame acceleration and transition to detonation in ducts. Prog Energy Combust Sci 2008;34:499–550.
[101] Tse S, He L, Law CK. A computational study of the transition from localized ignition to flame ball in lean hydrogen/air mixtures. Proc Combust Inst 2000;28:1917–24.
[102] Shy SS. Spark ignition transitions in premixed turbulent combustion. Prog Energy Combust Sci 2023;98:101099.
[103] Babrauskas V. Ignition: a century of research and an assessment of our current status. J Fire Protect Eng 2007;17:165–83.
[104] Patane P, Nandgaonkar M. Multipoint laser ignition system and its applications to IC engines. Opt Laser Technol 2020;130:106305.
[105] Starikovskiy A, Aleksandrov N. Plasma-assisted ignition and combustion. Prog Energy Combust Sci 2013;39:61–110.
[106] Ju Y, Sun W. Plasma assisted combustion: dynamics and chemistry. Prog Energy Combust Sci 2015;48:21–83.
[107] Li M, Wang Z, Xu R, Zhang X, Chen Z, Wang Q. Advances in plasma-assisted ignition and combustion for combustors of aerospace engines. Aero Sci Technol 2021;117:106952.
[108] Yu S, Zheng M. Future gasoline engine ignition: a review on advanced concepts. Int J Engine Res 2021;22:1743–75.
[109] Yu D, Chen Z. Theoretical analysis on the transient ignition of a premixed expanding flame in a quiescent mixture. J Fluid Mech 2021;924:A22.
[110] Seers P. Spark ignition: an experimental and numerical investigation. The University of Texas at Austin; 2003.
[111] Bane SPM. Spark ignition: experimental and numerical investigation with application to aviation safety. California Institute of Technology; 2010.
[112] Kassoy D. Non-diffusive ignition of a gaseous reactive mixture following time-resolved, spatially distributed energy deposition. Combust Theor Model 2014;18:101–16.
[113] Lian H, Martz J, Maldonado B, Stefanopoulou A, Zaseck K, Wilkie J, Nitulescu O, Ehara M. Prediction of flame burning velocity at early flame development time with high exhaust gas recirculation and spark advance. J Eng Gas Turbines Power 2017;139.
[114] Lewis B, Von Elbe G. Combustion, flames and explosions of gases. Elsevier; 2012.
[115] Maly R, Vogel M. Initiation and propagation of flame fronts in lean CH4-air mixtures by the three modes of the ignition spark. Proc Combust Inst 1979;17:821–31.
[116] Kono M, Hatori K, Iinuma K. Investigation on ignition ability of composite sparks in flowing mixtures. Proc Combust Inst 1985;20:133–40.
[117] Bane SP, Ziegler JL, Shepherd JE. Investigation of the effect of electrode geometry on spark ignition. Combust Flame 2015;162:462–9.
[118] Tropina AA, Uddi M, Ju Y. On the effect of nonequilibrium plasma on the minimum ignition energy—Part 1: discharge model. IEEE Trans Plasma Sci 2010;39:615–23.
[119] Tropina AA, Uddi M, Ju Y. On the effect of nonequilibrium plasma on the minimum ignition energy: Part 2. IEEE Trans Plasma Sci 2011;39:3283–7.
[120] Han J, Yamashita H. Numerical study of the effects of non-equilibrium plasma on the ignition delay of a methane–air mixture using detailed ion chemical kinetics. Combust Flame 2014;161:2064–72.
[121] Willems H, Sierens R. Modeling the initial growth of the plasma and flame kernel in SI engines. J Eng Gas Turbines Power 2003;125:479–84.
[122] Kolacinski Z. Modelling of short arc re-ignition. J Phys D 1993;26:1941.
[123] Pashley N, Stone R, Roberts G. Ignition system measurement techniques and correlations for breakdown and arc voltages and currents. 2000. Report No. 0148-7191, SAE Technical Paper.
[124] Korolev YD, Frants OB, Landl NV, Geyman VG, Matveev IB. Glow-to-spark transitions in a plasma system for ignition and combustion control. IEEE Trans Plasma Sci 2007;35:1651–7.
[125] Crispim LW, Hallak PH, Benilov MS, Ballester MY. Modelling spark-plug discharge in dry air. Combust Flame 2018;198:81–8.
[126] Kono M, Niu K, Tsukamoto T, Ujiie Y. Mechanism of flame kernel formation produced by short duration sparks. Proc Combust Inst 1989;22:1643–9.
[127] Liou D, Santavicca DA. A model for flame kernel growth at aircraft relight conditions. Proc Combust Inst 1994;25:261–8.
[128] Song J, Sunwoo M. Flame kernel formation and propagation modelling in spark ignition engines. P I MECH ENG D-J AUT 2001;215:105–14.
[129] Eisazadeh-Far K, Parsinejad F, Metghalchi H, Keck JC. On flame kernel formation and propagation in premixed gases. Combust Flame 2010;157:2211–21.
[130] Reddy H, Abraham J. Ignition kernel development studies relevant to lean-burn natural-gas engines. Fuel 2010;89:3262–71.
[131] Liu J, Wang F, Li G, Kuthi A, Gutmark EJ, Ronney PD, Gundersen MA. Transient plasma ignition. IEEE Trans Plasma Sci 2005;33:326–7.
[132] Arpacı VS, Ko Y, Lim MT, Lee HS. Spark kernel development in constant volume combustion. Combust Flame 2003;135:315–22.
[133] Arpacı VS, Lee HS, Zeng P. On inductive ignition. Combust Flame 2005;141:180–5.
[134] Lee JH. The gas dynamics of explosions. Cambridge University Press; 2016.
[135] Bradley D, Sheppard C, Suardjaja I, Woolley R. Fundamentals of high-energy spark ignition with lasers. Combust Flame 2004;138:55–77.
[136] MacArt JF, Wang JM, Popov PP, Freund JB. Detailed simulation of laser-induced ignition, spherical-flame acceleration, and the origins of hydrodynamic instability. Proc Combust Inst 2021;38:2341–9.
[137] Ghosh S, Mahesh K. Numerical simulation of the fluid dynamic effects of laser energy deposition in air. J Fluid Mech 2008;605:329–54.
[138] Takita K, Shishido K, Kurumada K. Ignition in a supersonic flow by a plasma jet of mixed feedstock including CH4. Proc Combust Inst 2011;33:2383–9.
[139] Lin B, Wu Y, Zhang Z, Bian D, Jin D. Ignition enhancement of lean propane/air mixture by multi-channel discharge plasma under low pressure. Appl Therm Eng 2019;148:1171–82.
[140] Kobtsev VD, Kostritsa SA, Pelevkin AV, Smirnov VV, Starik AM, Titova NS, Torokhov SA, Vereshchagin KA, Volkov SY. Ignition and early stage combustion of H2–O2 mixture upon the photodissociation of O2 molecules by UV laser radiation: experimental and numerical study. Combust Flame 2019;200:32–43.
[141] Ko Y, Arpaci VS, Anderson R. Spark ignition of propane-air mixtures near the minimum ignition energy: Part II. A model development. Combust Flame 1991;83:88–105.
[142] Ko Y, Anderson R, Arpaci VS. Spark ignition of propane-air mixtures near the minimum ignition energy: Part I. An experimental study. Combust Flame 1991;83:75–87.
[143] Wang F, Liu J, Sinibaldi J, Brophy C, Kuthi A, Jiang C, Ronney P, Gundersen MA. Transient plasma ignition of quiescent and flowing air/fuel mixtures. IEEE Trans Plasma Sci 2005;33:844–9.
[144] Chen Z, Ju Y. Theoretical analysis of the evolution from ignition kernel to flame ball and planar flame. Combust Theor Model 2007;11:427–53.
[145] Bergman TL. Fundamentals of heat and mass transfer. John Wiley & Sons; 2011.
[146] Weinrotter M, Ast G, Kopecek H, Wintner E. An extensive comparison of laser-induced plasma ignition and conventional spark plug ignition of lean methane-air mixtures under engine-like conditions. Report No. 0148-7191, SAE Technical Paper 2005.
[147] Tanoff MA, Smooke MD, Teets RE, Sell JA. Computational and experimental studies of laser-induced thermal ignition in premixed ethylene-oxidizer mixtures. Combust Flame 1995;103:253–80.
[148] Wu M-S, Ronney P, Ju Y. Numerical simulation of flame balls with radiative reabsorption effects. 38th Aerospace Sciences Meeting and Exhibit 2000:851.
[149] Ju Y, Masuya G, Ronney PD. Effects of radiative emission and absorption on the propagation and extinction of premixed gas flames. Proc Combust Inst 1998;27:2619–26.
[150] Pitaevskii LP, Lifshitz E. Physical kinetics, vol. 10. Butterworth-Heinemann; 2012.
[151] Vazquez-Espi C, Linan A. Thermal-diffusive ignition and flame initiation by a local energy source. Combust Theor Model 2002;6:297.
[152] Vázquez-Espí C, Liñán A. Fast, non-diffusive ignition of a gaseous reacting mixture subject to a point energy source. Combust Theor Model 2001;5:485.
[153] Poludnenko AY, Gardiner TA, Oran ES. Spontaneous transition of turbulent flames to detonations in unconfined media. Phys Rev Lett 2011;107:054501.
[154] Oran ES. Understanding explosions–From catastrophic accidents to creation of the universe. Proc Combust Inst 2015;35:1–35.
[155] Zhou Z. Flame balls at earth gravity. Technische Universiteit Eindhoven; 2017. Ph. D. diss.
[156] Daou J, Daou R. Flame balls in mixing layers. Combust Flame 2014;161:2015–24.
[157] Chen Z, Burke MP, Ju Y. Effects of Lewis number and ignition energy on the determination of laminar flame speed using propagating spherical flames. Proc Combust Inst 2009;32:1253–60.
[158] Nakaya S, Hatori K, Tsue M, Kono M, Segawa D, Kadota T. Numerical analysis on flame kernel in spark ignition methane/air mixtures. J Propul Power 2011;27:363–70.
[159] Kassoy D. The response of a compressible gas to extremely rapid transient, spatially resolved energy addition: an asymptotic formulation. J Eng Math 2010;68:249–62.
[160] Akindele O, Bradley D, Mak P, McMahon M. Spark ignition of turbulent gases. Combust Flame 1982;47:129–55.
[161] Champion M, Deshaies B, Joulin G, Kinoshita K. Spherical flame initiation: theory versus experiments for lean propane-air mixtures. Combust Flame 1986;65:319–37.
[162] Zhou Z, Shoshin Y, Hernández-Pérez FE, van Oijen JA, de Goey LP. Effect of Lewis number on ball-like lean limit flames. Combust Flame 2018;188:77–89.
[163] Tromans P, Furzeland R. An analysis of Lewis number and flow effects on the ignition of premixed gases. Proc Combust Inst 1988;21:1891–7.
[164] Kelley AP, Jomaas G, Law CK. Critical radius for sustained propagation of spark-ignited spherical flames. Combust Flame 2009;156:1006–13.
[165] Peters N. Turbulent combustion. Meas Sci Technol 2001;12:2022. 2022.

[166] Katta VR, Bonebrake JM, Blunck DL, Ombrello TM. Propagation of ignition kernel in CO2-diluted, CH4/air mixtures. Combust Flame 2021;229:111380.
[167] Bonebrake JM, Blunck DL, Lefkowitz JK, Ombrello TM. The effect of nanosecond pulsed high frequency discharges on the temperature evolution of ignition kernels. Proc Combust Inst 2019;37:5561–8.
[168] Lefkowitz JK, Ombrello T. An exploration of inter-pulse coupling in nanosecond pulsed high frequency discharge ignition. Combust Flame 2017;180:136–47.
[169] Shy SS, Chen YR, Lin B-L, Maznoy A. Ignition enhancement and deterioration by nanosecond repetitively pulsed discharges in a randomly-stirred lean n-butane/air mixture at various inter-electrode gaps. Combust Flame 2021;231:111506.
[170] Nguyen M, Shy S, Chen Y, Lin B, Huang S, Liu C. Conventional spark versus nanosecond repetitively pulsed discharge for a turbulence facilitated ignition phenomenon. Proc Combust Inst 2021;38:2801–8.
[171] Kondo S, Takahashi A, Tokuhashi K. Calculation of minimum ignition energy of premixed gases. J Hazard Mater 2003;103:11–23.
[172] Frendi A, Sibulkin M. Dependence of minimum ignition energy on ignition parameters. Combust Sci Technol 1990;73:395–413.
[173] Kumamoto A, Iseki H, Ono R, Oda T. Measurement of minimum ignition energy in hydrogen-oxygen-nitrogen premixed gas by spark discharge. In: J Phys Conf ser. IOP Publishing; 2011, 012039.
[174] Ono R, Oda T. Measurement of OH density and gas temperature in incipient spark-ignited hydrogen–air flame. Combust Flame 2008;152:69–79.
[175] Ono R, Nifuku M, Fujiwara S, Horiguchi S, Oda T. Minimum ignition energy of hydrogen–air mixture: effects of humidity and spark duration. J Electrost 2007;65:87–93.
[176] Kurdyumov V, Blasco J, Sánchez Pérez AL, Liñán Martínez A. On the calculation of the minimum ignition energy. Combust Flame 2004;136:394–7.
[177] De Soete G. Effects of geometrical and aerodynamic induced flame stretch on the propagation of spark fired premixed flames in early stages. Proc Combust Inst 1985;20:161–8.
[178] Adelman HG. A time dependent theory of spark ignition. Proc Combust Inst 1981;18:1333–42.
[179] Sloane TM, Ronney PD. A comparison of ignition phenomena modelled with detailed and simplified kinetics. Combust Sci Technol 1993;88:1–13.
[180] Essmann S, Markus D, Maas U. Investigation of the spark channel of electrical discharges near the minimum ignition energy. Plasma Sci Technol 2016;3:116–21.
[181] Kim HH, Won SH, Santner J, Chen Z, Ju Y. Measurements of the critical initiation radius and unsteady propagation of n-decane/air premixed flames. Proc Combust Inst 2013;34:929–36.
[182] Yu D, Chen Z. Theoretical analysis on the forced ignition of a quiescent mixture by repetitive heating pulse. Proc Combust Inst 2023;39:1881–91.
[183] Ng HD, Lee JH. Comments on explosion problems for hydrogen safety. J Loss Prev Process Ind 2008;21:136–46.
[184] Liñán A, Williams FA. Fundamental aspects of combustion. Oxford University Press; 1993.
[185] Williams FA. Combustion theory. CRC Press; 2018.
[186] Law C. Transient ignition of a combustible by stationary isothermal bodies. Combust Sci Technol 1979;19:237–42.
[187] Law CK. Heat and mass transfer in combustion: fundamental concepts and analytical techniques. Prog Energy Combust Sci 1984;10:295–318.
[188] Livengood JC, Wu PC. Correlation of autoignition phenomena in internal combustion engines and rapid compression machines. Proc Combust Inst 1955;5:347–56.
[189] Khaled F, Badra J, Farooq A. Ignition delay time correlation of fuel blends based on Livengood-Wu description. Fuel 2017;209:776–86.
[190] Miyoshi A. Kinetics of autoignition: a simple intuitive interpretation and its relation to the Livengood–Wu integral. Phys Chem Chem Phys 2018;20:10762–9.
[191] Heywood JB. Internal combustion engine fundamentals. McGraw-Hill Education; 2018.
[192] Yates A, Bell A, Swarts A. Insights relating to the autoignition characteristics of alcohol fuels. Fuel 2010;89:83–93.
[193] Hernández JJ, Lapuerta M, Sanz-Argent J. Autoignition prediction capability of the Livengood–Wu correlation applied to fuels of commercial interest. Int J Engine Res 2014;15:817–29.
[194] Pan J, Zhao P, Law CK, Wei H. A predictive Livengood–Wu correlation for two-stage ignition. Int J Engine Res 2016;17:825–35.
[195] Tao M, Han D, Zhao P. An alternative approach to accommodate detailed ignition chemistry in combustion simulation. Combust Flame 2017;176:400–8.
[196] Zeldovich I, Barenblatt GI, Librovich V, Makhviladze G. Mathematical theory of combustion and explosions. 1985.
[197] Williams F. Theory of combustion in laminar flows. Annu Rev Fluid Mech 1971;3:171–88.
[198] Zhang W, Gou X, Chen Z. Effects of water vapor dilution on the minimum ignition energy of methane, n-butane and n-decane at normal and reduced pressures. Fuel 2017;187:111–6.
[199] Deshaies B, Joulin G. On the initiation of a spherical flame kernel. Combust Sci Technol 1984;37:99–116.
[200] Zeldovich YB. The theory of combustion and detonation. Academy of Sciences; 1944.
[201] Kurdyumov VN, Jiménez C, Sánchez-Sanz M. Flame initiation near a cold isothermal wall: ignition by an instantaneous thermal dipole. Combust Flame 2021;234:111643.
[202] Fernández-Tarrazo E, Sánchez AL, Liñán A, Williams F. The structure of lean hydrogen-air flame balls. Proc Combust Inst 2011;33:1203–10.
[203] Buckmaster J, Joulin G, Ronney P. The structure and stability of nonadiabatic flame balls: II. Effects of far-field losses. Combust Flame 1991;84:411–22.
[204] Buckmaster J, Weeratunga S. The stability and structure of flame-bubbles. Combust Sci Technol 1983;35:287–96.
[205] Ronney PD. Near-limit flame structures at low Lewis number. Combust Flame 1990;82:1–14.
[206] Ronney P, Whaling K, Abbud-Madrid A, Gatto J, Pisowicz V. Stationary premixed flames in spherical and cylindrical geometries. AIAA J 1994;32:569–77.
[207] Shah A, Thatcher R, Dold J. Stability of a spherical flame ball in a porous medium. Combust Theor Model 2000;4:511.
[208] Lee C, Buckmaster J. The structure and stability of flame balls: a near-equidiffusional flame analysis. SIAM J Appl Math 1991;51:1315–26.
[209] Ronney PD. Effect of chemistry and transport properties on near-limit flames at microgravity. Combust Sci Technol 1988;59:123–41.
[210] Daou J, Al-Malki F, Ronney P. Generalized flame balls. Combust Theor Model 2009;13:269–94.
[211] Joulin G. Point-source initiation of lean spherical flames of light reactants: an asymptotic theory. Combust Sci Technol 1985;43:99–113.
[212] Champion M, Deshaies B, Joulin G. Relative influences of convective and diffusive transports during spherical flame initiation. Combust Flame 1988;74:161–70.
[213] Herweg R, Maly R. A fundamental model for flame kernel formation in SI engines. SAE Trans 1992:1947–76.
[214] Hernández-Pérez FE, Oostenrijk B, Shoshin Y, van Oijen JA, de Goey LP. Formation, prediction and analysis of stationary and stable ball-like flames at ultra-lean and normal-gravity conditions. Combust Flame 2015;162:932–43.
[215] Joulin G. Preferential diffusion and the initiation of lean flames of light fuels. SIAM J Appl Math 1987;47:998–1016.
[216] Buckmaster J, Joulin G. Radial propagation of premixed flames and t behavior. Combust Flame 1989;78:275–86.
[217] He L, Law C. On the dynamics of transition from propagating flame to stationary flame ball. 37th Aerospace Sciences Meeting and Exhibit 1999:325.
[218] Han W, Chen Z. Effects of Soret diffusion on spherical flame initiation and propagation. Int J Heat Mass Tran 2015;82:309–15.
[219] Li C, Wu Y, Chen Z. Effects of reaction reversibility on ignition and flame propagation. J Math Chem 2015;53:386–401.
[220] Chen Z. On the accuracy of laminar flame speeds measured from outwardly propagating spherical flames: methane/air at normal temperature and pressure. Combust Flame 2015;162:2442–53.
[221] Egolfopoulos FN, Hansen N, Ju Y, Kohse-Höinghaus K, Law CK, Qi F. Advances and challenges in laminar flame experiments and implications for combustion chemistry. Prog Energy Combust Sci 2014;43:36–67.
[222] Faghih M, Chen Z. The constant-volume propagating spherical flame method for laminar flame speed measurement. Sci Bull 2016;61:1296–310.
[223] Han W, Dai P, Gou X, Chen Z. A review of laminar flame speeds of hydrogen and syngas measured from propagating spherical flames. Applications in Energy and Combustion Science 2020;1:100008.
[224] Lai CC, Charonko JJ, Prestridge K. A Kármán–Howarth–Monin equation for variable-density turbulence. J Fluid Mech 2018;843:382–418.
[225] Yu D, Zhang P. Circulation-controlled firewhirls with differential diffusion. Combust Flame 2018;189:288–99.
[226] Liang W, Law CK, Chen Z. Ignition of hydrogen/air mixtures by a heated kernel: role of Soret diffusion. Combust Flame 2018;197:416–22.
[227] Chen Z. On the extraction of laminar flame speed and Markstein length from outwardly propagating spherical flames. Combust Flame 2011;158:291–300.
[228] Clavin P. Dynamic behavior of premixed flame fronts in laminar and turbulent flows. Prog Energy Combust Sci 1985;11:1–59.
[229] Markstein GH. Experimental and theoretical studies of flame-front stability. Dynamics of curved fronts. Elsevier; 1988. p. 413–23.
[230] Kelley AP, Law CK. Nonlinear effects in the extraction of laminar flame speeds from expanding spherical flames. Combust Flame 2009;156:1844–51.
[231] Wu F, Liang W, Chen Z, Ju Y, Law CK. Uncertainty in stretch extrapolation of laminar flame speed from expanding spherical flames. Proc Combust Inst 2015;35:663–70.
[232] Kelley AP, Bechtold JK, Law CK. Premixed flame propagation in a confining vessel with weak pressure rise. J Fluid Mech 2012;691:26–51.
[233] Liang W, Wu F, Law CK. Extrapolation of laminar flame speeds from stretched flames: role of finite flame thickness. Proc Combust Inst 2017;36:1137–43.
[234] Westbrook CK. Chemical kinetics of hydrocarbon ignition in practical combustion systems. Proc Combust Inst 2000;28:1563–77.
[235] Dold J, Thatcher R, Omon-Arancibia A, Redman J. From one-step to chain-branching premixed flame asymptotics. Proc Combust Inst 2002;29:1519–26.
[236] Dold J. Premixed flames modelled with thermally sensitive intermediate branching kinetics. Combust Theor Model 2007;11:909–48.
[237] Zhang H, Chen Z. Spherical flame initiation and propagation with thermally sensitive intermediate kinetics. Combust Flame 2011;158:1520–31.
[238] Zhang H, Guo P, Chen Z. Critical condition for the ignition of reactant mixture by radical deposition. Proc Combust Inst 2013;34:3267–75.
[239] Wang Y, Guo P, Chen H, Chen Z. Numerical modeling of ignition enhancement by repetitive nanosecond discharge in a hydrogen/air mixture II: forced ignition. J Phys D 2020;54:065502.
[240] Li H, Zhang H, Chen Z. Effects of endothermic chain-branching reaction on spherical flame initiation and propagation. Combust Theor Model 2019;23:496–514.
[241] Aggarwal SK. Single droplet ignition: theoretical analyses and experimental findings. Prog Energy Combust Sci 2014;45:79–107.

[242] Aggarwal SK. A review of spray ignition phenomena: present status and future research. Prog Energy Combust Sci 1998;24:565–600.
[243] Sirignano WA. Fluid dynamics and transport of droplets and sprays. Cambridge university press; 2010.
[244] Yu D, Chen Z. Theoretical analysis on droplet vaporization at elevated temperatures and pressures. Int J Heat Mass Tran 2021;164:120542.
[245] Li Q, Shu C, Zhang H. On the evolution of fuel droplet evaporation zone and its interaction with flame front in ignition of spray flames. Combust Theor Model 2022;26:1131–58.
[246] Zhuang Y, Zhang H. Effects of water droplet evaporation on initiation, propagation and extinction of premixed spherical flames. Int J Multiphas Flow 2019;117:114–29.
[247] Zhuang Y, Zhang H. On flame bifurcation and multiplicity in consistently propagating spherical flame and droplet evaporation fronts. Int J Multiphas Flow 2020;125:103220.
[248] Crowe C, Sommerfeld M, Tsuji Y. Multiphase flows with droplets and particles. second ed. CRC Press; 2011.
[249] Li Q, Liu C, Zhang H, Wang M, Chen Z. Initiation and propagation of spherical premixed flames with inert solid particles. Combust Theor Model 2020;24:606–31.
[250] Singh G, Clarke JF. Transient phenomena in the initiation of a mechanically driven plane detonation. Proc. Math. Phys. 1992;438:23–46.
[251] Linan A, Sánchez AL, Jimenez-Alvarez JL. The coupling of motion and conductive heating of a gas by localized energy sources. SIAM J Appl Math 2003;63:937–61.
[252] Fernandez-Tarrazo E, Sanchez-Sanz M, Sánchez AL, Williams FA. Minimum ignition energy of methanol–air mixtures. Combust Flame 2016;171:234–6.
[253] Yu D, Chen Z. Theoretical analysis on the forced ignition of a quiescent mixture by repetitive heating pulse. Proc Combust Inst 2022.
[254] Xu D, Shneider M, Lacoste D, Laux C. Thermal and hydrodynamic effects of nanosecond discharges in atmospheric pressure air. J Phys D 2014;47:235202.
[255] Lefkowitz JK, Hammack SD, Carter CD, Ombrello TM. Elevated OH production from NPHFD and its effect on ignition. Proc Combust Inst 2021;38:6671–8.
[256] Castela M, Stepanyan S, Fiorina B, Coussement A, Gicquel O, Darabiha N, Laux CO. A 3-D DNS and experimental study of the effect of the recirculating flow pattern inside a reactive kernel produced by nanosecond plasma discharges in a methane-air mixture. Proc Combust Inst 2017;36:4095–103.
[257] Lin B-x, Wu Y, Zhang Z-b, Chen Z. Multi-channel nanosecond discharge plasma ignition of premixed propane/air under normal and sub-atmospheric pressures. Combust Flame 2017;182:102–13.
[258] Zheng M, Yu S, Xie K. Multi-coil spark ignition system. Patent 9 2016;441:604. USA.
[259] Nishiyama A, Ikeda Y, Serizawa T. Lean Limit Expansion up to Lambda 2 by Multi-Point Microwave Discharge Igniter, Ignition Systems for Gasoline Engines: Internationale Tagung Zündsysteme für Ottomotoren. 2018. p. 247.
[260] Li Z, Han W, Liu D, Chen Z. Laminar flame propagation and ignition properties of premixed iso-octane/air with hydrogen addition. Fuel 2015;158:443–50.
[261] Iafrate N, Matrat M, Zaccardi J-M. Numerical investigations on hydrogen-enhanced combustion in ultra-lean gasoline spark-ignition engines. Int J Engine Res 2021;22:375–89.
[262] Wang Y, Han W, Chen Z. Effects of fuel stratification on ignition kernel development and minimum ignition energy of n-decane/air mixtures. Proc Combust Inst 2019;37:1623–30.
[263] Chen X, Peng W, Gillard P, Courty L, Sankhe ML, Bernard S, Wu Y, Wang Y, Chen Z. Effects of fuel decomposition and stratification on the forced ignition of a static flammable mixture. Combust Theor Model 2021;25:813–31.
[264] Sánchez AL, Williams FA. Recent advances in understanding of flammability characteristics of hydrogen. Prog Energy Combust Sci 2014;41:1–55.
[265] Li S, Liang W, Yao Q, Law CK. An analysis of the ignition limits of premixed hydrogen/oxygen by heated nitrogen in counterflow. Combust Flame 2018;198:230–9.
[266] Ju Y, Reuter CB, Yehia OR, Farouk TI, Won SH. Dynamics of cool flames. Prog Energy Combust Sci 2019;75:100787.
[267] Ju Y. Understanding cool flames and warm flames. Proc Combust Inst 2021;38:83–119.
[268] Zhang W, Faqih M, Gou X, Chen Z. Numerical study on the transient evolution of a premixed cool flame. Combust Flame 2018;187:129–36.
[269] Yang Q, Zhao P. Minimum ignition energy and propagation dynamics of laminar premixed cool flames. Proc Combust Inst 2021;38:2315–22.
[270] Wang Y, Zhang H, Zirwes T, Zhang F, Bockhorn H, Chen Z. Ignition of dimethyl ether/air mixtures by hot particles: impact of low temperature chemical reactions. Proc Combust Inst 2021;38:2459–66.
[271] Zhang T, Susa AJ, Hanson RK, Ju Y. Two-dimensional simulation of cool and double flame formation induced by the laser ignition under shock-tube conditions. Proc Combust Inst 2023;39:2017–25.
[272] Wang Y, Han W, Zirwes T, Zhang F, Bockhorn H, Chen Z. Effects of low-temperature chemical reactions on ignition kernel development and flame propagation in a DME-air mixing layer. Proc Combust Inst 2022.
[273] Ballal DR, Lefebvre AH. The influence of flow parameters on minimum ignition energy and quenching distance. Proc Combust Inst 1975;15:1473–81.
[274] Jo S, Gore JP. Laser ignition energy for turbulent premixed hydrogen air jets. Combust Flame 2022;236:111767.
[275] Baum M, Poinsot T. Effects of mean flow on premixed flame ignition. Combust Sci Technol 1995;106:19–39.
[276] Chen X, Xie S, Böttler H, Scholtissek A, Han W, Yu D, Hasse C, Chen Z. Effects of electrodes and imposed flow on forced ignition in laminar premixed hydrogen/air mixtures with large Lewis number. Proc Combust Inst 2022.
[277] Wu F, Saha A, Chaudhuri S, Law CK. Facilitated ignition in turbulence through differential diffusion. Phys Rev Lett 2014;113:024503.
[278] Shy SS, Nguyen MT, Huang S-Y, Liu C-C. Is turbulent facilitated ignition through differential diffusion independent of spark gap? Combust Flame 2017;185:1–3.
[279] Saha A, Yang S, Law CK. On the competing roles of turbulence and differential diffusion in facilitated ignition. Proc Combust Inst 2019;37:2383–90.
[280] Yu C, Markus D, Schießl R, Maas U. Numerical study on spark ignition of laminar lean premixed methane-air flames in counterflow configuration. Combust Sci Technol 2021:1–25.
[281] Xie S, Chen X, Böttler H, Scholtissek A, Hasse C, Chen Z. Forced ignition of a rich hydrogen/air mixture in a laminar counterflow: a computational study. Flow, Turbul Combust 2023;110:441–56.
[282] Wang Z, Liu H, Reitz RD. Knocking combustion in spark-ignition engines. Prog Energy Combust Sci 2017;61:78–112.
[283] Clarke JF. On changes in the structure of steady plane flames as their speed increases. Combust Flame 1983;50:125–38.
[284] Kagan L, Sivashinsky G. Hydrodynamic aspects of end-gas autoignition. Proc Combust Inst 2013;34:857–63.
[285] Zhang T, Ju Y. Structures and propagation speeds of autoignition-assisted premixed n-heptane/air cool and warm flames at elevated temperatures and pressures. Combust Flame 2020;211:8–17.
[286] Yang L, Wang Y, Chen Z. Comparison of combustion duration and end-gas autoignition in inwardly and outwardly propagating flames induced by different ignition configurations. Combust Theor Model 2022:1–15.

Dehai Yu is an associate professor at Institute of Mechanics, Chinese Academy of Sciences. He received his bachelor's degree from Harbin Institute of Technology, and Ph.D. degree from The Hong Kong Polytechnic University. After that, he was a postdoc fellow and an associate researcher at Peking University. Dr. Yu's research focuses on theoretical studies of fundamental combustion processes, including premixed flame ignition, dynamics of premixed and non-premixed flames, and droplet vaporization and combustion. His work on premixed flame ignition theory has been published on *Journal of Fluid Mechanics*, *Combustion and Flame*, and *Proceedings of the Combustion Institute*.

Zheng Chen is a professor at Peking University. He obtained his bachelor's and master's degrees from Tsinghua University, and completed his Ph.D. at Princeton University. Dr. Chen's research focuses on the flame dynamics of fundamental combustion processes. He was awarded the Bernard Lewis Fellowship and Hiroshi Tsuju Early Career Researcher Award from the Combustion Institute. Additionally, he received the Distinguished Paper Award of the 39th International Symposium on Combustion. He is a fellow of the Combustion Institute, and currently serves on the Board of Directors of both the Combustion Institute and the Institute for Dynamics of Explosions and Reactive Systems. He also serves as the associate editor for Combustion and Flame.